Physics – Uspekhi **69** (4) 311 – 343 (2026)

REVIEWS OF TOPICAL PROBLEMS

PACS numbers: 42.25.Ja, 42.65.Ky, 42.65.Re, **42.65. – k**

Atom in intense laser fields: from the generation of coherent short-wavelength radiation to the nonlinear properties of a gas medium

K.V. Lvov, S.Yu. Stremoukhov

DOI: https://doi.org/10.3367/UFNe.2025.09.040041

Contents

Abstract. The interaction of intense laser fields with matter is accompanied by a multitude of phenomena, ranging from the generation of coherent radiation across various spectral ranges (from terahertz to soft X-rays) to the creation of beams of accelerated charged particles and micromodification of the volume and surface of various samples. To describe this diversity of phenomena, several theoretical approaches have been developed to date. These approaches utilize different approximations to address this complex nonlinear problem, allowing for the explanation of specific aspects of such interactions. The developed theoretical frameworks consider the interaction at both microscopic and macroscopic levels; at the microscopic level, they investigate the characteristics of single atoms interacting with laser fields, while at the macroscopic level, they analyze nonlinear susceptibilities that describe the nonlinear polarization of the medium during the propagation of laser radiation through it. This work presents an overview of methods describing some of the most commonly employed theoretical approaches to model the response of a medium at a microscopic (quantum-mechanical) level, as well as various methods for controlling the properties of generated coherent radiation. A model for the gas medium is described that accounts for both the response characteristics of individual atoms and allows for consideration of phase and quasi-phase matching effects during radiation generation. The influence of medium parameters on the efficiency of generation and polarization properties of generated radiation is analyzed under both phase and quasi-phase matching conditions. A detailed description of an analytical method for calculating the nonlinear susceptibility of a gas medium is provided. The obtained values of nonlinear susceptibility for arbitrary orders may be useful in numerical calculations concerning the propagation of laser radiation in matter. Various channels for radiation generation are analyzed as parameters of the laser field are varied.

Keywords: interaction of intense laser radiation with matter, high-order harmonic generation, phase synchronization, nonperturbative theory, nonlinear susceptibility of the medium

K.V. Lvov[(1,2)], **S.Yu. Stremoukhov**[(1,2,3,*)]

[(1)] Lomonosov Moscow state University, Faculty of Physics, Leninskie gory 1, str. 2, 119991 Moscow, Russian Federation

[(2)] National Research Center 'Kurchatov Institute', pl. Akademika Kurchatova 1, 123182 Moscow, Russian Federation

[(3)] Lebedev Physical Institute, Russian Academy of Sciences, Leninskii prosp. 53, 119991 Moscow, Russian Federation

E-mail: [(*)] sustrem@gmail.com

Received 11 July 2025, revised 23 September 2025

Uspekhi Fizicheskikh Nauk **196** (4) 333 – 368 (2026)

Translated by the authors

1. Introduction

With the development of methods for generating intense laser pulses [1], scientists have gained the ability to experimentally study the nonlinear interaction of radiation with matter, creating a powerful impetus for research in this area of physics. The peak laser field strength of such pulses is no longer small compared to the intra-atomic field strength ($E_{\text{at}} = e/a_{\text{B}}^2 \simeq 5 \times 10^9$ V cm^{-1}), the response of the medium becomes significantly nonlinear, and nonlinear polarization can no longer be considered a small perturbation.

Improvements in mode-locking techniques have led to the production of ultrashort (femtosecond, attosecond) and extremely short (single-cycle and half-cycle) laser pulses, which have significantly expanded the practical applications of laser physics, laying the foundation for attosecond spectroscopy of atoms, molecules, and solids [2], petahertz electronics [3], and the creation of dynamic gratings and microresonators in a medium [4]. The transition to ultrashort and extremely short laser pulses requires abandoning the traditional method of slowly varying field amplitudes and phases [5], calculating the evolution of the field itself in the medium rather than its envelope, and accounting for the multilevel structure of the medium. The spectrum of phenomena and effects that must be considered in developing a modern theoretical framework is extremely broad [6–10].

Infinitely short laser pulses can have intensities comparable to subatomic values. Therefore, there is need for developing new methods for describing the interaction of such radiation with matter that takes into account both the strong dispersion of the medium and the significantly nonlinear interaction regime. Quantum-mechanical nonperturbative methods, which consider the interaction of radiation with matter at the microscopic level, have become widespread [7, 8, 11–13].

Approaches to describing the transition region from weak to extremely strong light fields have been little studied theoretically; however, the development of such an approach is of interest from several perspectives. First, it will enable a unified understanding of the phenomena occurring in an atom during its interaction with an electromagnetic field. Second, it will enable a qualitative understanding of experimentally observed effects that cannot be explained by theoretical approaches that have proven successfully in describing interactions with weak and extremely strong fields. Therefore, interest has remained strong for several decades in studying the interaction of atoms with near-atom laser fields. During this time, a huge number of papers have been published. Their systematization is ongoing (see, for example, books [12, 13, 14–21] and reviews [22–27]).

Among the phenomena accompanying the interaction of matter with intense laser fields, the generation of terahertz radiation [28–35] and the generation of high-order harmonics [36–45] are intensively studied. Interest in the study of these phenomena is driven not only by their fundamental nature, but also by the possibility of creating compact and more accessible (compared to such megascience-class setups as synchrotrons and free-electron lasers) sources of coherent radiation in the THz, ultraviolet, and X-ray spectral regions. The ability to control the polarization state (from linear to circular) of the radiation from such sources opens up an additional 'degree of freedom' in their application. Thus, using circularly polarized radiation, it is possible to study the chiral properties of molecules and nanoparticles, the magnetic properties of matter, and other properties [46–48].

High-order harmonic generation was first observed in dense laser plasma, which emerges when focusing high-power laser radiation of pico- and nanosecond duration onto a laser target [49–51]. High-order harmonic generation is possible in various media, each of which differs from the others by process efficiency and experimental conditions. A classic and still popular medium is an inert gas [40, 52, 53]. A disadvantage of generation in gaseous media is low conversion efficiency due to the low concentration of atoms in the gas, while an undoubted advantage is the relatively simple experimental setup. Another promising medium is plasma specially prepared from solids [41, 54, 55]. In a number of studies presented in the review [55], the target is preheated by a laser pulse (laser ablation method), a plasma column is formed above the target, through which the control laser radiation is passed. A higher concentration of particles in the plasma compared to a gas increases the efficiency of harmonic generation. However, the complexity of controlling the plasma parameters makes this method more labor-intensive from an experimental point of view. Another method is the generation of harmonics in the bulk of solids [56, 57] and on their surface [58]. Generation in the bulk of a crystal up to the 25th harmonic was first observed in 2010 in a ZnO crystal under the action of femtosecond laser pulses in the mid-IR range [56]. A feature of generation in crystals is that the cutoff frequency depends on the field strength not quadratically, but linearly [56]. Compared to gases, the concentration of atoms is significantly higher, which increases the efficiency of harmonic generation. However, these advantages are offset by a serious drawback: strong absorption of the generated radiation, as well as a limitation on the laser intensity a crystal can withstand without failure. Therefore, generation in gaseous media and plasma appears to be the most promising.

The development of methods for increasing the spectrum width of high-order harmonics opens up new areas of application of such radiation for studying the structure of matter. Thus, to study the inner shells of industrially important materials (Fe, Co, Ni), it is necessary to use X-ray radiation with a photon energy of ~ 1 keV [59]. To obtain it by the method of generating high-order harmonics, it is necessary to use laser systems with a lower radiation frequency (for example, mid-IR range [60]), which increases the cutoff frequency by increasing the maximum ponderomotive energy, which is proportional to the square of the wavelength of the laser source. However, this significantly reduces the efficiency of the harmonic generation process, which scales with the wavelength of the laser source (λ) as $\lambda^{-5.5}$ [61–63]. In addition, when using laser sources in the mid- and far-IR range, the influence of the magnetic field becomes significant due to a decrease in the magnitude of the relativistic intensity, which also limits the efficiency of high-order harmonic generation [24, 64–68].

Adding the second harmonic to the fundamental laser frequency improves the generation efficiency — a second set of variable parameters appears (polarization, duration, and intensity of the second harmonic), as well as the delay between pulses and the angle between their polarization vectors. For example, it has been shown that adjusting the time delay between the fundamental and second harmonic pulses can increase the intensity of the generated harmonics by more than an order of magnitude [69]. The use of ion and atomic resonances [41, 70, 71], additional laser fields [72], and focusing the laser beam to a point slightly offset from the jet center [73, 74] also improves the generation efficiency.

Quasi-phase matching is an another mechanism of high-order harmonic generation, which utilizes a periodic structure in the medium for phase matching. The effects of quasi-phase matching have been extensively studied in waveguides [75], gas sequences [76], gas mixtures [77], gas media with pressure gradients [78], and gas jets [79, 80]. Some recent advances in this field are systematized in the review [81].

The generation of harmonics with arbitrary, including circular, polarization is of interest not only from a fundamental but also from a practical standpoint. For example, the X-ray magnetic circular dichroism (XMCD) method, which allows for the measurement of the magnetic moments of atomic elements and the recording of the magnetization dynamics of individual components of matter, requires circularly polarized X-ray radiation [82, 83]. The study of magnetization dynamics is also possible using linearly polarized VUV or soft X-ray harmonic radiation using the Faraday resonance effect [84]. This stimulated the development of methods for generating high-order harmonics in elliptically polarized laser fields and controlling the polarization characteristics of the generated radiation by adjusting the degree of ellipticity of the laser field, both in monatomic inert gases [85, 86], and in molecules [87, 88], and in solids [89]. The dependence of the harmonic generation efficiency on the magnitude of the laser field ellipticity has been extensively studied by various researchers [90–95]. As a rule, this dependence has a similar character regardless of the harmonic number [90–92]. Although there are exceptions to this rule, manifested in the detection of an anomalous dependence for specific harmonics [93–95].

Another sub-direction, more important from the applied point of view, is the stable production of harmonics with a high degree of ellipticity. Currently, there are several effective schemes for producing intense harmonics with a high degree of ellipticity [82, 96, 97]. The first scheme uses two-frequency elliptically polarized fields with opposite helicity (the polarization vectors of the components of the two-frequency field rotate towards each other) [96]. This scheme is distinguished by complete control over the polarization of the harmonic radiation and makes it possible to generate even circularly polarized harmonics. Another approach, using atomic and continuum resonances in a single-frequency elliptically polarized field, makes it possible to produce low-order quasi-circular harmonics, but does not have such good control over the polarization as in the first scheme, and, in addition, requires the use of only certain gases to obtain high ellipticity [97]. The third method operates with a dual-frequency laser field, with the laser carrier frequency and its second harmonic having linear polarizations oriented orthogonally with respect to each other [82]. It is simpler from an experimental view, as it does not require a large number of optical elements.

A consideration of the interaction of laser radiation with matter is, generally speaking, incomplete until the effects of radiation propagation in matter are also described. In this case, the nonlinear properties of the medium are specified by nonlinear susceptibility tensors of various ranks, which are expansions of the nonlinear polarization in powers of the laser field. For example, third harmonic generation is a process of four-wave mixing:

$$P_i(3\omega) = \chi^{(3)}_{ijkl}(3\omega;\omega,\omega,\omega)E_j(\omega)E_k(\omega)E_l(\omega)\,.$$

The nonlinear susceptibility of a medium is typically determined phenomenologically, by matching a theoretical model with the experimental data obtained. For example, [98–100] present values for the third-order nonlinear susceptibility of atomic hydrogen, noble gases, and diatomic molecules in various spectral ranges, obtained by measuring the third harmonic signal, the spectral broadening of the fundamental harmonic, and other experimental techniques.

In addition to purely experimental methods for determining nonlinear susceptibility, several theoretical approaches have also been developed. The classical anharmonic oscillator model was used in early fundamental studies [101–103]. However, its use also requires determining parameters such as the relaxation time and oscillator strength in some other ways. A similar idea of an anharmonic oscillator is used in [103], where the inertialess nonlinear response of dielectric media is calculated in the approximation of a three- and four-level energy structure of the medium. The dispersion law for the nonlinear refractive index is presented, and numerous experimental data on the measurement of the nonlinear refractive index of various dielectric media are collected. In the terahertz spectral range, extremely high vibrational contributions of molecules to the nonlinear refractive index have been theoretically predicted and experimentally recorded [104, 105].

By measuring two-photon absorption and using the Kramers–Kronig relations, it is possible to determine the dispersion of the nonlinear refractive index [106], which is in full agreement with the experimental data.

A widely used method for calculating the nonlinear susceptibility of free atoms is perturbation theory, where an external electric field is considered as a perturbation. The dispersion relations for H and He calculated using perturbation theory are presented in [107] and [108], respectively. However, the applicability limits of this approach and the conditions for the convergence of perturbation theory generally remain beyond the scope of research.

Furthermore, at laser radiation intensities comparable to the atomic intensity, the series expansion of the nonlinear polarization in powers of the laser field, the validity of which was due to the smallness of the laser field, can be called into question. Thus, in [109], the nonlinear susceptibility was calculated using perturbation theory and by numerically solving the nonstationary Schrödinger equation. A significantly nonperturbative regime of nonlinear susceptibility formation was observed at laser radiation intensities higher than 1–10 TW cm^{-2} (for the hydrogen atom). At laser radiation intensities greater than 40 TW cm^{-2} (for the hydrogen atom), saturation is first observed, followed by a decrease in nonlinear susceptibility, which is confirmed by experimental data [106]. This fact indicates the need to abandon the series expansion of nonlinear polarization in powers of the laser field and use more accurate approaches.

Section 2 presents a more detailed discussion of the main, frequently used theoretical approaches to describing the interaction of atoms with a laser field, developed to date. Their advantages, disadvantages, and applicability limits are discussed. Section 3 presents the results of a study of the characteristics of high-order harmonic generation in gaseous media, obtained using a nonperturbative approach. This study describes the properties of radiation (spectrum, polarization) generated by both a single atom and a set of gas jets, where the quasi-phase matching regime of harmonic radiation is realized. Section 4 presents the results of applying the nonperturbative theory of the single atom response to a laser field to the analytical calculation of the nonlinear susceptibility of a gaseous medium. Analytical formulas are derived for the nonlinear susceptibility of an arbitrary order and the value of the laser field intensity at which the series expansion of the nonlinear polarization in powers of the laser field becomes incorrect.

2. General theoretical approaches to the study of laser field interaction with an atom

Following numerous studies, we will consider the interaction of an atom with a laser field in the single-electron approximation and focus on finding the wavefunction of a single (valence) electron located in the Coulomb potential, as well as in an external laser field. We will consider gaseous media in which the influence of other atoms on electron movement can be neglected due to their large distance from it. The wavefunction ψ of a valence electron in an atom located in the laser field is the solution of the nonstationary Schrödinger equation:

$$\mathrm{i}\hbar\frac{\partial}{\partial t}\psi=\hat{H}\psi=\left[\frac{1}{2m}\left(\hat{\mathbf{p}}-\frac{q}{c}\mathbf{A}\right)^2+q\varphi+V\right]\psi\,, \tag{1}$$

where $\hat{H}$ is the Hamiltonian, V is the Coulomb potential, $\mathbf{p}=-\mathrm{i}\hbar\nabla$ is the momentum operator, $\hbar$ is the Plank constant, c is the speed of light in vacuum, q and m are the electron charge and the electron mass correspondingly, $\mathbf{A}$ and φ are the vector and scalar potential of the laser field $\{\mathbf{E},\mathbf{B}\}$.

Vector and scalar potentials are not uniquely defined, since they satisfy the equalities:

$$\mathbf{E}=-\frac{1}{c}\frac{\partial}{\partial t}\mathbf{A}-\nabla\varphi\,,\quad \mathbf{B}=\nabla\times\mathbf{A}\,, \tag{2}$$

and therefore can be simultaneously changed as follows:

$$\mathbf{A}\to\mathbf{A}'=\mathbf{A}+\nabla\Lambda(\mathbf{r},t),\quad \varphi\to\varphi'=\varphi-\frac{1}{c}\frac{\partial}{\partial t}\Lambda(\mathbf{r},t)\,, \tag{3}$$

where $\Lambda(\mathbf{r},t)$ is an arbitrary function of the coordinates and time.

When transforming (3), the wavefunction satisfying (1) changes in the following way:

$$\psi\to\psi'=\hat{U}\psi\,,\quad \hat{U}=\exp\left(\frac{\mathrm{i}q\Lambda(\mathbf{r},t)}{\hbar c}\right). \tag{4}$$

As a rule, when solving the Schrödinger equation (1), the full Hamiltonian of the problem is represented as the sum of the Hamiltonian of the problem in the absence of the laser field and the interaction Hamiltonian:

$$\hat{H}=\hat{H}_0+\hat{H}_{\mathrm{int}}\,,\quad \hat{H}_0=\frac{\hat{p}^2}{2m}+V\,,$$
$$\hat{H}_{\mathrm{int}}=\frac{1}{2m}\left(-\frac{q}{c}(\hat{\mathbf{p}}\mathbf{A}+\mathbf{A}\hat{\mathbf{p}})+\frac{q^2}{c^2}A^2\right)+q\varphi\,. \tag{5}$$

Two different gauges of laser field potentials are most commonly used. In the length gauge (LG), it is assumed that $\mathbf{A}=0$, while in the velocity gauge (VG) $\varphi=0$, and therefore

$$\hat{H}_{\mathrm{int}}^{\mathrm{LG}}=q\varphi,\quad \hat{H}_{\mathrm{int}}^{\mathrm{VG}}=\frac{1}{2m}\left(-\frac{q}{c}(\hat{\mathbf{p}}\mathbf{A}+\mathbf{A}\hat{\mathbf{p}})+\frac{q^2}{c^2}A^2\right). \tag{6}$$

The total mechanical energy operator $\hat{\mathcal{E}}=(1/2m)(\hat{\mathbf{p}}-(q/c)\mathbf{A})^2+V$, unlike the Hamiltonian $\hat{H}$, is an observable quantity, since this operator is gauge-invariant. Also observable quantities are the total mechanical momentum $\hat{\mathbf{p}}-(q/c)\mathbf{A}$ and the radius vector $\mathbf{r}$.

The wavefunction ψ, defined by equation (1), can be determined at each instant of time through the evolution operator $\hat{U}$: $\psi(t)=\hat{U}(t,t')\psi(t')$. In the long-wave approximation (the vector potential is only a function of time $\mathbf{A}=\mathbf{A}(t)$), there is a formal implicit solution for the evolution operator [110], which is verified by direct substitution into equation (1):

$$\hat{U}(t,t')=\hat{U}_1(t,t')-\frac{\mathrm{i}}{\hbar}\int_{t'}^{t}\mathrm{d}\tau\hat{U}(t,\tau)q\left(\varphi(\tau)+\frac{\mathbf{r}}{c}\frac{\partial\mathbf{A}(\tau)}{\partial\tau}\right)\hat{U}_1(\tau,t'), \tag{7}$$

where $\hat{U}_1(\tau,t')$ is the evolution operator, defined as:

$$\mathrm{i}\hbar\frac{\partial}{\partial t}\hat{U}_1(t,t')=\left(\hat{\mathcal{E}}(t)-\frac{q\mathbf{r}}{c}\frac{\partial\mathbf{A}(t)}{\partial t}\right)\hat{U}_1(t,t')\,. \tag{8}$$

The solution given by formula (7) uses only the long-wavelength and single-electron approximations and is gauge-invariant. Note that in the length gauge (6), the interaction Hamiltonian is represented as $\hat{H}_{\mathrm{int}}^{\mathrm{LG}}=-q\mathbf{r}\mathbf{E}(t)$, which means that the atom-field interaction is taken into account in the dipole approximation. This is precisely the case when the long-wavelength approximation is used, which implies spatial homogeneity of the field and the complete absence of any multipole moments. Similarly, in the velocity gauge, the problem of the atom-laser field interaction is solved in the dipole approximation as soon as the long-wavelength approximation is applied. A more detailed discussion of the use of various gauges and approximations can be found in [111]. Differences in the results obtained in different gauges are explained solely by the use of additional approximations, which destroy the gauge-invariance of expression (7).

The choice of a particular gauge is motivated by the convenience of solving the problem. For example, when studying the properties of radiation generated by an atom, the microscopic current density is simpler in the velocity gauge: $\hat{\mathbf{j}}=q/m\,(\hat{\mathbf{p}}-(q/c)\mathbf{A})$. On the contrary, for the ionization probability of an atom, it is more convenient to use the length gauge, since in this case expressions (7) and (8) are significantly simplified. When numerically solving the nonstationary Schrödinger equation (1), in addition to the convenience of the analytical form of the equations, the computational efficiency of the numerical methods used is also important. In [112], it was shown that at high laser radiation intensities (more than 3×10^{14} W cm^{-2}), it is more efficient (in terms of computational complexity) to use the velocity gauge, while at low intensities both gauges are comparable (Fig. 1).

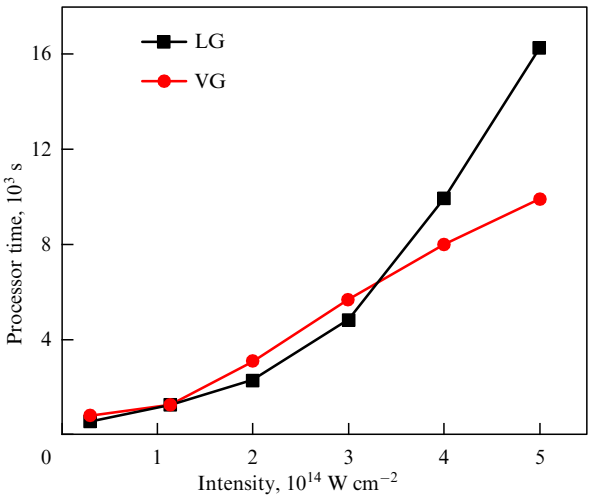

Figure 1. Processor time required to calculate the response of an atom to a laser field of different intensities using length gauge (black curve with squares) and velocity gauge (red curve with circles) [112].

Below we present a brief summary of the main methods for calculating the interaction of a laser field with an atom and the approximations used. Note that all approaches described below are nonrelativistic, and therefore neglect the influence of an external magnetic field on the atom. However, it is worth noting that the transition from the nonrelativistic to the relativistic regime is determined by the quantity $I\lambda^2$ [μm]/1.3×10^{18} W cm^{-2} (I is the radiation intensity, λ is the wavelength in microns), which must be much less than 1 in the nonrelativistic regime. Therefore, increasing the wavelength of laser radiation can significantly reduce the limit on the radiation intensity at which a relativistic approach to the problem is required.

2.1 Analytical methods

Photoionization is one of the most important processes that occurs during the interaction of a single atom with a laser field, which has been studied for many decades. Pioneering works in this field were primarily devoted to studying the probability of tunneling through a potential barrier: both in atoms [113, 114] and in semiconductors [115–117], as well as issues of multiphoton ionization [118–120]. In a 1964 paper [120], L.V. Keldysh succeeded in combining the tunneling and multiphoton mechanisms of photoionization within a single theory.

Keldysh's theory considers the ionization of an atom from its hydrogen-like ground state

$$\psi_0(\mathbf{r}) = \frac{1}{\sqrt{\pi a_\mathrm{B}^3}} \exp\left(-\frac{r}{a}\right), \tag{9}$$

where $a_\mathrm{B} = \hbar^2/me^2$ is the Bohr radius, into a free state modulated by a harmonic electric field (Volkov state [121])

$$\psi_\mathbf{p}(\mathbf{r},t) = \exp\left[\frac{\mathrm{i}\mathbf{r}}{\hbar}\left(\mathbf{p}-\frac{q}{c}\,\mathbf{A}(\mathbf{r},t)\right) - \frac{\mathrm{i}}{2m\hbar}\int_0^t\left(\mathbf{p}-\frac{q}{c}\,\mathbf{A}(\mathbf{r},t')\right)^2 \mathrm{d}t'\right]. \tag{10}$$

The field's interaction with the atom is described in the dipole approximation in the length gauge $\hat{H}_\mathrm{int} = q\mathbf{r}\mathbf{E}_0\cos(\omega t)$. The expression for the photoionization rate $w_\mathbf{p}(t) = \int \psi_\mathbf{p}^*(\mathbf{r},t)\hat{H}_\mathrm{int}\,\psi_0(\mathbf{r})\,\mathrm{d}\mathbf{r}$ is averaged over the field period and the free electron momentum, yielding the expression:

$$w_\mathrm{K} = \frac{2\pi}{\hbar}\int |L(\mathbf{p})|^2 \sum_n \delta\left(I_0 + \frac{p^2}{2m} + \frac{e^2E_0^2}{4m\omega^2} - n\hbar\omega\right)\frac{\mathrm{d}\mathbf{p}}{(2\pi\hbar)^3}, \tag{11}$$

where I_0 is the ionization potential of an atom, δ is the Delta-function,

$$L(\mathbf{p}) = \frac{1}{2\pi}\oint \mathrm{d}x W\left(\mathbf{p}+\frac{q\mathbf{E}_0}{\omega}\,x\right) \times \exp\left[\frac{\mathrm{i}}{\hbar\omega}\int_0^x\left(I_0 + \frac{1}{2m}\left(\mathbf{p}+\frac{q\mathbf{E}_0}{\omega}\,u\right)^2\right)\frac{\mathrm{d}u}{\sqrt{1-u^2}}\right], \tag{12}$$

$$W(\mathbf{s}) = \frac{q}{\sqrt{\pi a^3}}\int \mathbf{r}\mathbf{E}\,\exp\left(-\frac{r}{a}-\frac{\mathrm{i}\mathbf{s}\mathbf{r}}{\hbar}\right)\mathrm{d}\mathbf{r}, \tag{13}$$

and the integral in $L(\mathbf{p})$ is calculated over the closed contour surrounding a segment $[-1, 1]$.

Since $L(\mathbf{p})$ contains a rapidly oscillating exponential, the main contribution to the integral in expression (11) is given by the saddle points determined by the equation:

$$I_0 + \frac{1}{2m}\left(\mathbf{p}+\frac{q\mathbf{E}_0}{\omega}\sin(\omega t)\right)^2 = 0. \tag{14}$$

By calculating the integral (12) using the saddle-point method, one can obtain the Keldysh formula for the photoionization rate:

$$w_\mathrm{K} = Q(\gamma, I_0, \omega)\,\exp\left[-\Phi(\gamma, I_0, \omega)\right], \tag{15}$$

where Q is a multiplier,

$$\Phi(\gamma, I_0, \omega) = \frac{2I_0}{\hbar\omega}\left(1+\frac{1}{2\gamma^2}\right)\left(\sinh^{-1}\gamma - \gamma\,\frac{\sqrt{1+\gamma^2}}{1+2\gamma^2}\right), \tag{16}$$

$$\gamma = \frac{\omega\sqrt{2mI_0}}{qE_0}. \tag{17}$$

The Keldysh parameter γ determines the characteristic photoionization regime: at $\gamma \gg 1$, multiphoton ionization predominates, while at $\gamma \ll 1$, tunneling ionization does. It also simultaneously measures the adiabatic nature of the photoionization process [27] and is essentially the ratio of the subbarrier transit time $\tau = d/v$ ($d = I_0/qE_0$ is the characteristic barrier width, $v = \sqrt{2I_0/m}$ is the particle velocity) to the electric field period $T = 2\pi/\omega$.

Keldysh theory has found wide application in describing the results of experiments on the interaction of atoms with laser pulses. However, it only takes into account ionization from the ground level, neglecting the influence of excited discrete levels. Furthermore, it does not take into account the influence of the Coulomb potential on the wavefunction of the free state. Therefore, for many years, experimental verification of the pre-exponential factor has been conducted, and the limits of applicability of the Keldysh formula have been discussed [122–125]. Another natural limitation of the applicability of the Keldysh formula is related to the duration of the laser pulse. Since the formula was derived by averaging over the laser field period, the pulse must contain many field periods.

Subsequently, in the works of Nikishov and Ritus [126], Perelomov, Popov, and Terentyev [127–129], and Ammosov, Delone, and Krainov [130], analytical expressions for the energy and momentum spectrum of photoelectrons, as well as the exact form of the pre-exponential factor, were obtained. The results presented in these works are valid for arbitrary values of the Keldysh parameter γ and pertain to the ionization of a state bound by a short-range potential (e.g., in the case of ionization of singly charged negative ions). For example, for the tunnel ionization regime ($\gamma \ll 1$), the following expression was obtained for the pre-exponential factor for the case of ionization from the state with orbital angular momentum l and projection m by linearly polarized laser field:

$$Q = \frac{2I_0}{\hbar}\sqrt{\frac{3}{\pi}}(2l+1)\,\frac{(l+m)!}{2^m m!(l-m)!}\,C_{kl}^2\,2^{2n^*-m} \times \left(\frac{q\hbar}{\sqrt{m(2I_0)^3}}\,E_0\right)^{m+1.5-2n^*}, \tag{18}$$

$$C_{kl}^2 = \frac{2^{2n^*-2}}{n^*(n^*+l)!(n^*-l-1)!}, \tag{19}$$

where $n^* = Z\sqrt{mq^4/2I_0\hbar^2}$ is the effective main quantum number, Z is the charge of the remaining atom.

Further development of the theory of atomic ionization by a strong electromagnetic field involved taking into account the multiple valence states in the discrete spectrum, rather than simply ionization from the ground state alone, and the abandonment of the saddle-point method for calculating the probability of transition from a bound to a free state — the Keldysh–Faisal–Rees (KFR) method in the strong-field approximation [131–133]. In this case, the exact solution given by formula (7) makes the assumption that the wavefunction of the free state is the Volkov wavefunction (10), which violates the gauge invariance of the solution. In the length gauge, a simple expression for the photoionization probability is obtained:

$$w_{\mathrm{KFR}} = \mathrm{i}q \int_{-\infty}^{\infty} \mathrm{d}\tau \int \psi_{\mathbf{p}}^{*}(\mathbf{r},\tau)\, \mathbf{r}\mathbf{E}\,(\tau)\psi_0(\mathbf{r},\tau)\,\mathrm{d}\mathbf{r}\,. \qquad (20)$$

The development of the Keldysh theory for the case of ultrashort laser pulses is carried out in the work [27], in which the integration over the momenta of the expression for the photoionization rate within the framework of the Keldysh theory is carried out, but averaging over the period of the laser field is omitted. The ionization probability in the case of ultrashort laser pulses with a duration of several half-periods is presented in the work [134].

2.2 Semiclassical approach

When an atom (or gaseous medium) is exposed to high-intensity (more than 10^{12}–10^{13} W cm^{-2}) laser radiation, two nonlinear effects are clearly manifested: high-order harmonic generation (HHG) and above-threshold ionization. Both effects are associated with the absorption of a large number of laser photons by the atom. In the first effect, the absorbed energy is released as a quantum of harmonic radiation, while in the second, the atom is ionized. A semiclassical model of HHG generation was proposed in [36, 37, 39, 70, 135] and was subsequently called a three-stage model. In the first stage, the atom is ionized, i.e., its valence electron is removed, under the influence of laser radiation. In the second stage, the free electron is accelerated by the laser field. Finally, in the third stage, the electron recombines with the HHG radiation.

The maximum energy of the emitted photon $\hbar\omega_{\mathrm{HHG}}$ is equal to the sum of the maximum kinetic energy $K_{\max}$, which an electron accelerated by an oscillating laser field $E(t) = E_0 \sin(\omega_0 t)$ will have upon collision with the parent ion, and the ionization potential of the atom I_0: $\hbar\omega_{\mathrm{HHG}} = K_{\max} + I_0$.

Consider an electron at the bound state which at time t_i transitioned to a free state with zero coordinates and velocity. The electron's subsequent trajectory is found by solving classical equation of motion for a free electron:

$$x(t) = \frac{qE_0}{m\omega_0^2}\left(\sin\omega_0(t-t_i) - \omega_0(t-t_i)\right). \qquad (21)$$

The electron's trajectory depends crucially on the phase of the laser field $\phi = \omega_0 t_i$ at which the atom is ionized. If $0 \leqslant \phi \leqslant \pi/2$ or $\pi \leqslant \phi \leqslant 3\pi/2$, the electron will never pass through the initial coordinate, i.e., it will not reach the parent ion, while if $\pi/2 \leqslant \phi \leqslant \pi$ or $3\pi/2 \leqslant \phi \leqslant 2\pi$, the electron returns to the parent ion one or more times (Fig. 2a). The moment of return t_r and the time of free motion $\tau = t_r - t_i$ are

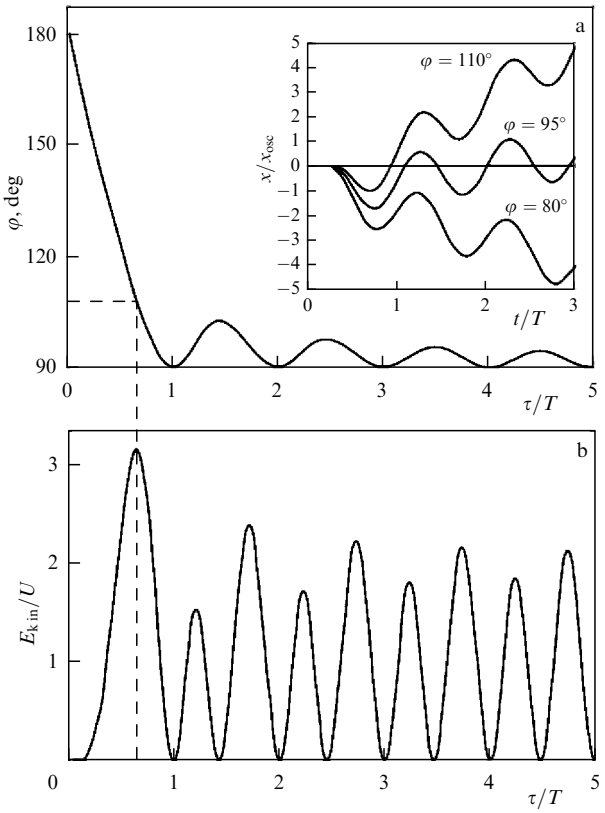

Figure 2. (a) The relationship between the field phase at the moment of electron detachment and the time of its free motion before returning to the parent ion. The inset shows the trajectories of electrons that began free motion at different field phases. (b) The dependence of the kinetic energy of the electron upon returning to the parent ion on the time of its free motion. (The figure is taken from [136].)

related as [26]:

$$\tan\phi = \frac{\omega_0\tau - \sin(\omega_0\tau)}{\cos(\omega_0\tau) - 1}\,, \qquad (22)$$

and the kinetic energy of the electron at the moment of return is equal to:

$$K = 2U_p\,\frac{C^2\omega_0\tau}{\omega_0\tau - \sin(\omega_0\tau) - C}\,, \qquad (23)$$

where $U_p = q^2E_0^2/4m\omega_0^2$ is the ponderomotive (oscillatory) energy, and $C = \sin(\omega_0\tau) - 2(1 - \cos(\omega_0\tau)/\omega_0\tau)$. The maximum value of kinetic energy (23) is $K_{\max} \approx 3.17U_p$, which corresponds to the values $\phi = 1.88$, $\omega_0\tau = 4.09$. Therefore, the maximum energy of the HHG photon is:

$$\hbar\omega_{\mathrm{HHG}} = I_0 + 3.17U_p\,, \qquad (24)$$

which is consistent with numerous experimental data on the generation of HHG in gaseous media [26, 39, 52, 53]. In a periodic laser field, the three-step process described above is repeated at each half-period of the field, therefore the HHG spectrum is discrete, and only odd harmonics are present.

The three-step model became a unique platform for the development of a whole spectrum of semiclassical theories of high-order harmonic generation. One of the first such theories was the theory developed by Levenshtein et al.

[137]. The main contribution to the generation of high-order harmonics comes from electron transitions between free and bound states, while the contribution of intermediate bound states is neglected, which is justified in the tunnel ionization regime. The electron wavefunction is represented as a superposition of the ground bound state ψ_0 and a set of free states $\psi_{\mathbf{p}}$:

$$\psi(\mathbf{r},t)=\left(a(t)\psi_0(\mathbf{r})+\int b(\mathbf{p},t)\psi_{\mathbf{p}}(\mathbf{r})\,\mathrm{d}\mathbf{p}\right)\exp\left(\mathrm{i}I_0t\right), \quad (25)$$

where the population amplitude of the ground state is considered to be approximately equal to unity $a(t)\approx 1$ (the case of weak ionization is considered), and the free states are written in the plane-wave approximation. In the indicated approximations, the following expression was obtained for the dipole moment of an atom [137]:

$$\begin{aligned}\boldsymbol{\mu}(t)=\mathrm{i}\int_0^t \mathrm{d}t'\int \mathrm{d}\mathbf{p}\mathbf{E}(t')\,\mathbf{d}\left(\mathbf{p}-\frac{q}{c}\,\mathbf{A}(t')\right)\\ \times\exp\left(-\frac{\mathrm{i}S\left(\mathbf{p},t,t'\right)}{\hbar}\right)\mathbf{d}^*\left(\mathbf{p}-\frac{q}{c}\,\mathbf{A}(t')\right)+\text{c.c.}\,,\end{aligned} \quad (26)$$

where $\mathbf{d}(\mathbf{p})=-q\int\psi_{\mathbf{p}}^*\mathbf{r}\,\psi_0\,\mathrm{d}^3\mathbf{r}$ is the dipole moment of the transition between exited and ground states, and $S(\mathbf{p},t,t')$ is the quasiclassical action:

$$S(\mathbf{p},t,t')=\int_{t'}^{t}\left[\frac{1}{2m}\left(\mathbf{p}-\frac{q}{c}\,\mathbf{A}(t'')\right)^2+I_0\right]\mathrm{d}t''. \quad (27)$$

The largest contribution to integral (27) comes from stationary action points, for which $\nabla_{\mathbf{p}}S(\mathbf{p},t,t')=0$. As is readily apparent, this condition implies the equality of the initial and final coordinates of the electron, i.e., its return to the parent ion. Therefore, as in the semiclassical theory, the largest contribution to the HHG comes from electrons that, after tunneling away from the atom and moving in the oscillating laser field, return to the parent ion.

The presented quantum-mechanical approach also allows us to analyze the phase matching of the generated harmonics. For a sufficiently large harmonic number, the main contribution to the harmonic signal comes from just two trajectories, called 'short' (electron return time $\tau_1<0.65T$, where T is the laser field period) and 'long' (electron return time $\tau_1>0.65T$) [138]. Moreover, as detailed quantum-mechanical calculations of the dipole moment spectrum (26) show, for example, in [139, 140], the phase of the signal introduced by the n-th trajectory, often called the 'atomic phase,' is proportional to the intensity I of the laser radiation:

$$\Phi_n=-\alpha_n I. \quad (28)$$

Moreover, the dependence of the atomic phase on the laser radiation intensity is several tens of times stronger for the 'long' trajectory compared to the 'short:' $\alpha_2/\alpha_1\approx 27$ [139].

The stationary phase method has also been used in other studies that developed similar quantum mechanical approaches [26, 36, 85, 141–143]. The response of an atom at a given frequency is composed of various terms, each of which has the meaning of a quantum trajectory (quantum orbit) of an electron from the initial state to the final one. The HHG spectrum was also calculated in terms of Feynman path integrals [144]. The probability of an electron transition from the initial state to the final one can be represented as a sum:

$$M=\sum_n a_n\exp\left[\frac{\mathrm{i}S\left(\mathbf{r}_n(t)\right)}{\hbar}\right], \quad (29)$$

where $\mathbf{r}_n(t)$ is the nth classical trajectory of the electron, a_n are the trajectory amplitudes, S is the total action, consisting of the sum of the action of the initial bound state $S_{i,n}=-I_0t_i$ (I_0 where is the energy of this state), the action of the free state $S_{f,n}$ (27), and the action of the final bound state $S_{r,n}=(\hbar\omega_s+I_0)t_r$ (where s is the harmonic number). In this case, the quantities t_i, $\mathbf{p}$ and t_r are determined by the saddle-point method, i.e., by solving the following equations:

$$\left(\mathbf{p}-\frac{q}{c}\,\mathbf{A}(t_i)\right)^2=2mI_0\,, \quad (30a)$$

$$\mathbf{p}(t_r-t_i)=\frac{q}{c}\int_{t_i}^{t_r}\mathbf{A}(t')\,\mathrm{d}t'\,, \quad (30b)$$

$$\left(\mathbf{p}-\frac{q}{c}\,\mathbf{A}(t_r)\right)^2=2m(\hbar\omega_s+I_0)\,. \quad (30c)$$

The three-step model was further developed in [145] as a four-step model, which proposes dividing the electron recombination step into two steps. In the first, the electron is assumed to be captured by the autoionization state of the ion. In the second, the electron transitions to the ground state with the emission of light at the harmonic frequency. However, during the 'step' of the electron's motion in the laser pulse field, classical equations are still used.

2.3 Numerical solution methods

The method of direct numerical solution (*ab-initio*) of the nonstationary Schrödinger equation was first used in [146] to study the multiphoton ionization of the hydrogen atom by a low-frequency laser field. In this work, only the ground state of the discrete spectrum was taken into account and the cylindrical symmetry of the Hamiltonian was used, so the dimension of the numerical problem was equal to $2\mathrm{D}+1$ (two spatial dimensions and time). Subsequently, the method of direct numerical solution of the nonstationary Schrödinger equation was developed to solve three-dimensional problems and was used to study the ionization of various quantum systems (atoms, ions, etc.) during their interaction with fields of both linear [147, 148] and circular polarization [149]. Subsequent work focused on studying the physics of interactions between atoms and ions and intense laser fields: the generation of high-order harmonics by molecular hydrogen ions [150–152], the generation of harmonics by lithium and rubidium in the field of elliptically polarized radiation [153]; and the improvement of numerical schemes: the suppression of reflections at the boundary of the computational grid [154].

On of the widely used method is to represent the wavefunction of an electron as an expansion in the basis of eigenfunctions:

$$\psi(\mathbf{r},t)=\sum_n a_n(t)\,\psi_n(\mathbf{r})\,. \quad (31)$$

The resulting expansion is substituted into the nonstationary Schrödinger equation (1), reducing the problem to solving a system of equations for the expansion coefficients $a_n(t)$.

Among the expansion bases, various analytical bases have been used, such as the Roothaan–Hartree–Fock basis [155], which is convinient for atoms and ions of chemical elements from H to Xe, or the B-spline basis [156], which was successfully applied to calculate above-threshold ionization [157]. In addition, numerical bases, calculated by preliminary numerically solving the eigenvalue problem of the Hamiltonian operator unperturbed by the field, have become widely used. As emphasized in [158], one of the advantages of the numerical basis is the ability to take into account highly excited bound states of the atom.

All of the above-mentioned studies used the Coulomb potential of the electron-nucleus interaction. This imposed a certain limitation on the spatial step of the numerical grid both in the vicinity of $r = 0$ and at large values of r. In order to overcome these limitations, a smoothed Coulomb potential $U(r) = -q/\sqrt{a^2 + r^2}$ was used in [159–161], which made it possible to study the photoionization processes of both the Rydberg states of the atom [161] and the effects of ionization stabilization [160].

The analytical methods presented in the previous sections often treat the interaction Hamiltonian $\hat{H}_{\text{int}}$ as a small addition to the Hamiltonian in the absence of an external field $\hat{H}_0$ and employ perturbation theory, retaining only the first or second order of smallness, i.e., only the term linear in the field ($\sim E_0$) or, rather rarely, the quadratic term ($\sim E_0^2$).

Generally speaking, this approach is justified when the external laser field is significantly smaller than the intra-atomic field: $E_0 \ll E_{\text{at}} = e/a_{\text{B}}^2 \simeq 5 \times 10^9$ V cm^{-1}, which corresponds to an intensity of $I \ll I_{\text{at}} \simeq 3.5 \times 10^{16}$ W cm^{-2}. However, for highly excited bound states, whose orbital radii are several units or even tens of Bohr radii, the intra-atomic field is reduced, and even at significantly lower external field intensities, there is not sufficient to use only the first-order perturbation theory. This is especially evident when calculating the nonlinear susceptibility of an atom, since its presence is determined, among other things, by the form of the radial part of the wavefunction of excited states.

Numerical methods for solving the nonstationary Schrödinger equation have the advantage of allowing one to go beyond perturbation theory with relative ease and not impose restrictions on the intensity of the laser field. The authors of [109], by comparing the results of calculations carried out using perturbation theory and those obtained by directly solving the nonstationary Schrödinger equation, came to the conclusion that even at intensity 5×10^{13} W cm^{-2}, the series expansion in powers of the laser field becomes incorrect, since terms of higher order become comparable in value to terms of lower order (Fig. 3).

Another powerful method for calculating the response of atoms to a high-intensity laser field, operating outside the framework of perturbation theory, is an approach developed at Lomonosov Moscow State University in the group of A.V. Andreev [162]. This approach uses velocity gauge and retains both terms in the interaction Hamiltonian $\hat{H}_{\text{int}}^{\text{VG}} = 1/m\,(-(q/c)\mathbf{A}\hat{\mathbf{p}} + (q^2/2c^2)A^2)$. This approach has been successfully applied to the analysis of polarization and spectral features of coherent radiation generated by an atom (both high-order harmonics and terahertz radiation) [163–165], as well as to the search for new methods of phase matching of high-order harmonic radiation in gas media [166]. In the next section, the more detailed examination of this approach is presented.

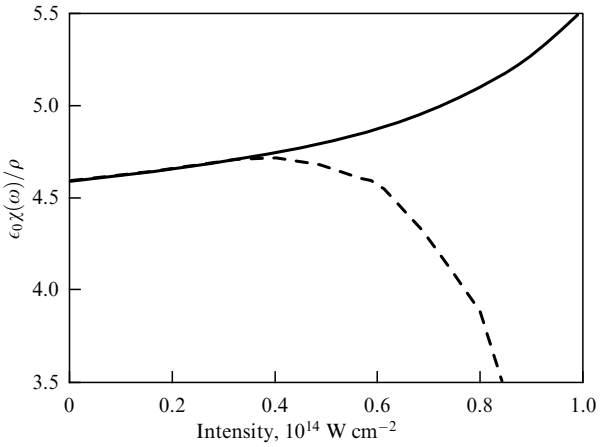

Figure 3. Susceptibility of a gas medium as a function of the peak intensity of an exciting 10-cycle laser pulse with the wavelength of 800 nm, calculated using perturbation theory (solid line) and by numerically solving the Schrödinger equation [109].

2.4 Nonperturbative approach

The wavefunction $\psi(\mathbf{r}, t)$ can be expanded in the basis of eigenfunctions $\{u_n(\mathbf{r})\}$ of the stationary Schrödinger equation, written for an electron located in the Coulomb potential (the 'free atom' problem):

$$\psi(\mathbf{r}, t) = \sum_n a_n(t)\, u_n(\mathbf{r})\,. \tag{32}$$

$$\hat{H}_0 u_n(\mathbf{r}) = \left(\frac{\hat{p}^2}{2m} - \frac{q}{r}\right) u_n(\mathbf{r}) = E_n u_n(\mathbf{r})\,. \tag{33}$$

Wavefunctions $\{u_n(\mathbf{r})\}$ have a well-known analytical form, presented, for example, in [167]. For atoms with high atomic numbers, corrections to the atomic core potential are required. In this case, wavefunctions $\{u_n(\mathbf{r})\}$ and level energies E_n can be calculated approximately (the Roothaan–Hartree–Fock analytical basis [155], the numerical basis [158]) or can be estimated from spectroscopic data [168].

Consider the operator

$$\hat{V}(\mathbf{r}, t) = \exp\left(-\mathrm{i}\,\frac{q}{\hbar c}\,\mathbf{A}(t)\mathbf{r}\right) \tag{34}$$

and the states $|\varphi_n\rangle = \hat{V}^{-1}|u_n\rangle$. They are the solution of the boundary-value problem 'an atom in a field' of the form:

$$\left[\frac{1}{2m}\left(\mathbf{p} - \frac{q}{c}\,\mathbf{A}(t)\right)^2 + U(\mathbf{r})\right]\varphi_n(\mathbf{r}, t) = E_n\varphi_n(\mathbf{r}, t) \tag{35}$$

with boundary conditions coinciding with the boundary conditions of the problem (33) in the limit $\mathbf{A}(t) \to 0$.

As noted above, the total energy operator $\hat{\mathcal{E}} = (1/2m)(\hat{\mathbf{p}} - (q/c)\,\mathbf{A})^2 + V$ is gauge-invariant. In the velocity gauge, it is a Hamiltonian $\hat{H}$ in the presence of a laser field, and in the length gauge, it is a Hamiltonian $\hat{H}_0$ in the absence of a laser field. Therefore,

$$\langle\varphi_n|\hat{H}|\varphi_n\rangle = \langle u_n|\hat{H}_0|u_n\rangle = E_n\,. \tag{36}$$

Thus, the states $|\varphi_n\rangle$ are eigenfunctions of the operator $\hat{H}$ with the same eigenvalues E_n as the eigenvalues of the operator $\hat{H}_0$. It is easy to show that the states $|\varphi_n\rangle$ form the orthogonal basis in Hilbert space. In the coordinate repre-

sentation, the wavefunctions $\{\varphi_n(\mathbf{r},t)\}$ and $\{u_n(\mathbf{r})\}$ are related as follows:

$$\varphi_n(\mathbf{r},t)=\sum_m (V^{-1})_{nm}(t)u_m(\mathbf{r})\,, \tag{37a}$$

$$u_n(\mathbf{r})=\sum_m V_{nm}(t)\varphi_m(\mathbf{r},t)\,, \tag{37b}$$

$$V_{nm}(t)=\int u_n^*(\mathbf{r})\exp\left(-\mathrm{i}\,\frac{q}{\hbar c}\,\mathbf{A}(t)\mathbf{r}\right)u_m(\mathbf{r})\,\mathrm{d}^3\mathbf{r}\,. \tag{37c}$$

When solving equation (1) with the basis $\{\varphi_n(\mathbf{r},t)\}$ the terms $\psi(\mathbf{r},t)$ will arise that are, generally speaking, no longer orthogonal to the function $\varphi_n(\mathbf{r},t)$. Therefore, it is most convenient to expand $\psi(\mathbf{r},t)$ in the basis $\{u_n(\mathbf{r})\}$. After setting in equation (1), we obtain a system of first-order ordinary differential equations for the population amplitudes:

$$\frac{\mathrm{d}a_n}{\mathrm{d}t}=-\frac{\mathrm{i}}{\hbar}\sum_{m,p}V_{nm}^{-1}(t)E_mV_{mp}(t)\,a_p(t)\,. \tag{38}$$

In the case of strong excitation of atoms, when it is necessary to also take into account the transitions of electrons to levels from the continuous spectrum, the expansion of the wavefunction in the basis $\{u_n(\mathbf{r})\}$ should be supplemented by a linear combination of wavefunctions from the continuous spectrum (l is the angular momentum):

$$\psi(\mathbf{r},t)=\sum_n a_n(t)u_n(\mathbf{r})+\sum_l\int a\,(k,l,t)\,u\,(k,l,\mathbf{r})\,\mathrm{d}k\,. \tag{39}$$

In this case, the system of ordinary differential equations for the population amplitudes $a_n(t)$ becomes more complicated:

$$\begin{aligned}\frac{\mathrm{d}a_n}{\mathrm{d}t}=&-\frac{\mathrm{i}}{\hbar}\sum_{m,p}V_{nm}^{-1}(t)\,E_mV_{mp}\,(t)a_p(t)-\frac{\mathrm{i}}{\hbar}\sum_{m,l}\int\mathrm{d}kV_{nm}^{-1}(t)\\&\times E_mV_{m(kl)}(t)\,a\,(k,l,t)-\mathrm{i}\sum_{p,l}\int\mathrm{d}kV_{n(kl)}^{-1}(t)\,\frac{\hbar k^2}{2m_e}\\&\times V_{(kl)p}(t)\,a_p(t)-\mathrm{i}\sum_{l_1,l_2}\int\mathrm{d}k_1\int\mathrm{d}k_2V_{n(k_1l_1)}^{-1}(t)\,\frac{\hbar k_1^2}{2m_e}\\&\times V_{(k_1l_1)(k_2l_2)}(t)\,a(k_2,l_2,t)\,.\end{aligned} \tag{40}$$

Here, various combinations of transitions are taken into account (D is the discrete level, C is the continuum level): D–D–D (the first term on the right-hand side), D–D–C (the second term), D–C–D (the third term), D–C–C (the fourth term). Similarly, the equations for the population amplitudes $a\,(k,l,t)$ of the continuum levels are written (the transitions C–D–D, C–D–C, C–C–D, and C–C–C are taken into account):

$$\begin{aligned}\frac{\mathrm{d}a\,(k,l,t)}{\mathrm{d}t}=&-\frac{\mathrm{i}}{\hbar}\sum_{m,p}V_{(kl)m}^{-1}(t)E_mV_{mp}(t)a_p(t)\\&-\frac{\mathrm{i}}{\hbar}\sum_{m,l_1}\int\mathrm{d}k_1V_{(kl)m}^{-1}(t)E_mV_{m(k_1l_1)}(t)a\,(k_1,l_1,t)\\&-\mathrm{i}\sum_{l_1,p}\int\mathrm{d}k_1V_{(kl)(k_1l_1)}^{-1}(t)\,\frac{\hbar k_1^2}{2m_e}\,V_{(k_1l_1)p}(t)\,a_p(t)\\&-\mathrm{i}\sum_{l_1,l_2}\int\mathrm{d}k_1\int\mathrm{d}k_2V_{(kl)(k_1l_1)}^{-1}(t)\,\frac{\hbar k_1^2}{2m_e}V_{(k_1l_1)(k_2l_2)}(t)\\&\times a(k_2,l_2,t)\,.\end{aligned} \tag{41}$$

Note that the system of equations (40) and (41) generally contains an infinite number of equations defining the dynamics of the population amplitudes of both the discrete and continuum levels. Of course, to numerically solve the resulting system, the number of equations must be limited. The number of states that must be considered depends both on the parameters of the laser field and on the energy structure of the atom itself. Limiting the number of levels naturally makes the basis $\{u_n(\mathbf{r})\}$ incomplete. However, there is a way to determine how complete the remaining, truncated basis is.

Consider the quantity

$$S_n^{(N)}=\sum_{m=1}^{N}|V_{nm}|^2\,. \tag{42}$$

If we consider the entire infinite set of eigenfunctions, then, as follows from the definition of matrix elements V_{nm}, the value of (42) must be equal to unity: $S_n^{(\infty)}=1$. Restricting the basis $\{u_n(\mathbf{r})\}$ leads to a decrease in $S_n^{(N)}$. Therefore, by adding additional levels to the analysis and achieving a small deviation of $S_n^{(N)}$ from unity for all levels under consideration, we can consider the truncated basis complete.

Note also that the quantum-mechanical approach presented above makes it possible to take into account the multi-quantum nature of the process of excitation of an atom by a laser field. Indeed, series expansion of the operator $\hat{V}(\mathbf{r},t)$ in powers of the field, we obtain an infinite sum of increasing orders of multi-quantum nature (for a small interaction between the electron and the laser field):

$$\hat{V}(\mathbf{r},t)=\exp\left(-\mathrm{i}\,\frac{q}{\hbar c}\,\mathbf{A}(t)\,\mathbf{r}\right)=\sum_{k=0}^{\infty}\frac{1}{k!}\left(-\mathrm{i}\,\frac{q}{\hbar c}\,\mathbf{A}(t)\,\mathbf{r}\right)^k. \tag{43}$$

Consider the generation of radiation by an excited atom. The dynamics of the population amplitudes of energy levels forms the microscopic current density of the atom:

$$\begin{aligned}\mathbf{j}\,(\mathbf{r},t)=\frac{q}{2m}\,\Bigg[&\psi^*(\mathbf{r},t)\left(\mathbf{p}-\frac{q}{c}\,\mathbf{A}(t)\right)\psi(\mathbf{r},t)\\&+\psi(\mathbf{r},t)\left(\left(\mathbf{p}-\frac{q}{c}\,\mathbf{A}(t)\right)\psi(\mathbf{r},t)\right)^*\Bigg]\,,\end{aligned} \tag{44}$$

which, taking into account (39) and (37), is reduced to a quadruple sum (for simplicity, we will consider only bound states):

$$\mathbf{j}\,(\mathbf{r},t)=\frac{q}{m_e}\sum_{n,k,p,m}a_n^*(t)V_{nk}^{-1}(t)u_k^*(\mathbf{r})\,\mathbf{p}u_p(\mathbf{r})V_{pm}(t)\,a_m(t)\,. \tag{45}$$

The microscopic current of an atom is the source of electric and magnetic fields. In the far zone, the spectral density of the radiation intensity will be equal to [167]:

$$\frac{\mathrm{d}I}{\mathrm{d}\omega\,\mathrm{d}\sigma}\,(\mathbf{r})=\frac{\omega^2}{4c^3}\left|\int\left[\mathbf{j}\,(\mathbf{r}',\omega)\times\frac{\mathbf{r}}{r}\right]\exp\left(-\mathrm{i}\mathbf{k}\mathbf{r}\right)\mathrm{d}V'\right|^2, \tag{46}$$

where k is the wave vector of the radiation field. In the case where $ka_0\ll 1$ (a_0 is the amplitude of electron oscillations in

the laser field) for all frequencies of the generated field, the spectral intensity of the radiation is proportional to the macroscopic current of the atom:

$$\frac{\mathrm{d}I}{\mathrm{d}\omega\,\mathrm{d}\sigma}(\mathbf{r}) = \frac{\omega^2}{4c^3}\left|\left[\mathbf{J}(\omega)\times\frac{\mathbf{r}}{r}\right]\right|^2, \tag{47}$$

$$\mathbf{J}(\omega) = \int \mathrm{d}V\int \mathbf{j}(\mathbf{r},t)\exp(\mathrm{i}\omega t)\,\mathrm{d}t = \frac{q}{m}\sum_{n,k,p,m}\mathbf{p}_{kp} \times \int a_n^*(t)V_{nk}^{-1}(t)V_{pm}(t)\,a_m(t)\exp(\mathrm{i}\omega t)\,\mathrm{d}t\,. \tag{48}$$

In the long-wave approximation, the matrix elements $\mathbf{p}_{kp}$ are linearly related to the matrix elements of the coordinate operator [169]: $\mathbf{p}_{nm} = \mathrm{i}m_e\omega_{nm}\mathbf{r}_{nm}$, where $\omega_{nm} = (E_n - E_m)/\hbar$.

In addition to calculating the frequency spectrum of the radiation generated by an atom, the approach presented also allows for analyzing the angular spectrum of the radiation. The exponential $\exp(\mathrm{i}(q/\hbar c)\mathbf{A}(t)\mathbf{r})$ can be expanded into a series of spherical harmonics:

$$\exp\left(\mathrm{i}\frac{q}{\hbar c}\mathbf{A}(t)\mathbf{r}\right) = 4\pi\sum_{l=0}^{\infty}\sum_{m=-l}^{l}\mathrm{i}^l j_l\left(\frac{q}{\hbar c}A(t)r\right)Y_{lm}^*(\mathbf{e}(t))\,Y_{lm}(\mathbf{n}), \tag{49}$$

where $\mathbf{e}(t) = \mathbf{A}(t)/A(t)$, $\mathbf{n} = \mathbf{r}/r$, Y_{lm}, is the spherical function, j_l is the spherical Bessel function. Let us expand the matrix elements $V^{-1}_{(n_1,l_1,m_1)(n_2,l_2,m_2)}$ in a series of spherical functions. Taking into account the rules for summing angular momenta [167], one can obtain:

$$V^{-1}_{(n_1,l_1,m_1)(n_2,l_2,m_2)} = \sum_{l=|l_1-l_2|}^{l_1+l_2}\left\langle n_1 l_1\left|\left| j_l\left(\frac{q}{\hbar c}A(t)r\right)\right|\right| n_2 l_2\right\rangle \times \sum_{m=-l}^{l}Y_{lm}^*(\mathbf{e}(t))\,C(lm\,|\,l_1m_1,l_2m_2), \tag{50a}$$

$$\left\langle n_1 l_1\left|\left| j_l\left(\frac{q}{\hbar c}A(t)r\right)\right|\right| n_2 l_2\right\rangle = \int_0^{\infty}R_{n_1l_1}(r)\,j_l\left(\frac{q}{\hbar c}A(t)r\right) \times R_{n_2l_2}(r)r^2\,\mathrm{d}r\,, \tag{50b}$$

$$C\left(lm|l_1m_1,l_2m_2\right) = (-1)^{m_1}\,\mathrm{i}^{2l-l_1+l_2}\sqrt{4\pi(2l+1)(2l_1+1)(2l_2+1)} \times \begin{pmatrix} l_1 & l & l_2\\ -m_1 & m & m_2\end{pmatrix}\begin{pmatrix} l_1 & l & l_2\\ 0 & 0 & 0\end{pmatrix}. \tag{50c}$$

and $R_{n_1l_1}(r)$ is the radial part of the hydrogen-like wavefunction.

Similarly, expand the matrix element $\mathbf{r}_{(n_1,l_1,m_1)(n_2,l_2,m_2)}$ in a series of the spherical functions:

$$\mathbf{r}_{(n_1,l_1,m_1)(n_2,l_2,m_2)} = \langle n_1l_1||r||n_2l_2\rangle(-1)^{m_1}\mathrm{i}^{l_2-l_1} \times \sqrt{(2l_1+1)(2l_2+1)}\sum_{m=-1}^{1}\mathbf{n}^{(m)} \times \begin{pmatrix} l_1 & 1 & l_2\\ -m_1 & m & m_2\end{pmatrix}\begin{pmatrix} l_1 & 1 & l_2\\ 0 & 0 & 0\end{pmatrix}. \tag{51}$$

After substituting expressions (50) and (51) into (48) one can obtain the angular spectrum of the matrix element of the current density:

$$\begin{aligned}\mathbf{J}_{(n_1,l_1,m_1)(n_2,l_2,m_2)} &= 4\pi q\mathrm{i}^{1-l_1+l_2}\sqrt{(2l_1+1)(2l_2+1)}\\ &\times\sum_{n_3l_3}\sum_{n_4l_4}(\omega_{n_3l_3}-\omega_{n_4l_4})(2l_3+1)(2l_4+1)\\ &\times\sum_{l=|l_1-l_3|}^{l_1+l_3}\sum_{l'=|l_2-l_4|}^{l_2+l_4}\sqrt{(2l+1)(2l'+1)}\\ &\times\langle n_1l_1||j_l||n_3l_3\rangle\langle n_3l_3||r||n_4l_4\rangle\langle n_4l_4||j_{l'}||n_2l_2\rangle\\ &\times\begin{pmatrix} l_1 & l & l_3\\ 0 & 0 & 0\end{pmatrix}\begin{pmatrix} l_3 & 1 & l_4\\ 0 & 0 & 0\end{pmatrix}\begin{pmatrix} l_4 & l' & l_2\\ 0 & 0 & 0\end{pmatrix}\\ &\times\sum_{m=-1}^{1}\sum_{m_3=-l_3}^{l_3}(-1)^{l'-m_2+m_3}Y_{l(m_3-m_1)}(\mathbf{e})\,\mathbf{n}^{(m)}\\ &\times Y_{l'(m_3-m_2-m)}(\mathbf{e})\\ &\times\begin{pmatrix} l_1 & l & l_3\\ -m_1 & m_1-m_3 & m_3\end{pmatrix}\begin{pmatrix} l_3 & 1 & l_4\\ -m_3 & m & m_4\end{pmatrix}\\ &\times\begin{pmatrix} l_4 & l & l_2\\ -m_4 & m_2-m_3+m & m_2\end{pmatrix},\end{aligned} \tag{52}$$

where it is used for brevity: $j_l = j_l((q/\hbar c)A(t)r)$.

Thus, the quantum-mechanical approach presented above allows one to calculate the frequency-angular spectrum of radiation generated by an atom placed in a laser field. This approach is beyond the scope of perturbation theory and remains valid up to relativistic limit of laser field intensities $I \ll 1.3\times10^{18}/\lambda^2[\mu\mathrm{m}]$ W cm^{-2}. It utilizes the long-wavelength approximation, i.e., the spatial inhomogeneity of the beam intensity is not considered. The nonperturbative nature of the approach and the possibility of studying the response of atoms to high-intensity fields are due to the special choice of the basis of the electron wavefunctions (35), (36). The matrix elements $V_{nm}(t)$ can be calculated analytically for the hydrogen atom and hydrogen-like atoms, or numerically for a model atom for any given vector potential $\mathbf{A}(t)$ of the laser field, making the nonperturbative approach a unique analytical and numerical method for studying the interaction of atoms with laser radiation. The following sections present results from some applications of this approach.

3. Harmonic generation in gases as the atom response in the far-field

3.1 Excitation by a single-frequency laser field

It is appropriate to begin a discussion of the results of numerical calculations obtained within the framework of nonperturbative quantum mechanical theory [162] with a description of the response of a single atom to a single-frequency femtosecond laser pulse. We will describe the influence of laser field parameters on the harmonic generation efficiency.

Consider the response of a hydrogen-like atom interacting with a single-frequency Ti:Sa laser pulse (wavelength 800 nm, Gaussian profile with a duration of 27 fs, transform-limited pulse).

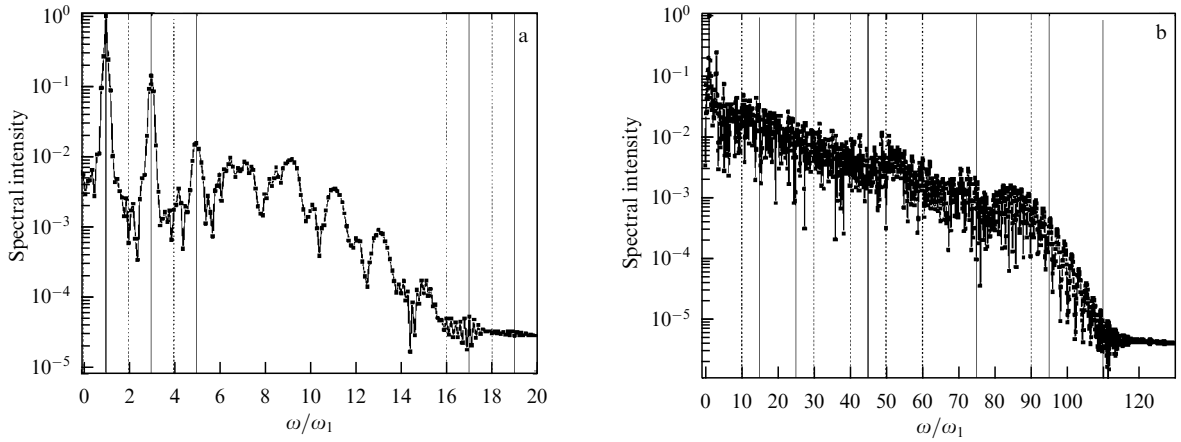

Figure 4. Spectrum of the hydrogen-like atom response (the Ag atom as an example) on the laser field: (a) $\mu_0 = 0.025$, (b) $\mu_0 = 0.08$. The frequency on the horizontal axis is given in units of the laser field frequency ω_1. Spectral intensity is given here and below in relative units [170].

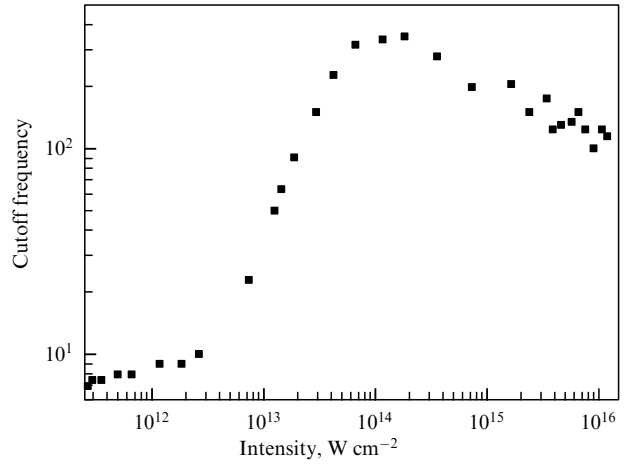

Figure 5. The cutoff frequency in the dependence of the laser radiation intensity, calculated for the silver atom [170].

For further consideration, it is convenient to introduce the parameter μ_0, which relates the laser intensity and the wavelength:

$$\mu_0 = \frac{qE_0 a_B}{\hbar\omega_0} . \qquad (53)$$

The parameter μ_0 can be represented as the ratio of the force acting on the electron from the external field, $F_0 = qE_0$, and the 'intra-atomic force' $F_{at} = \hbar\omega_0/a_B$. Note also that, as follows from (17), for the hydrogen atom, the parameter μ_0 is inversely proportional to the Keldysh parameter γ: $\mu_0 = 1/\gamma$.

In fields of substantially subatomic strength $\mu_0 \ll 10^{-4}$, the spectrum of the response field contains only a component at the frequency of the applied pulse; i.e., the atomic response is linear and does not contain harmonics of the laser pulse carrier frequency. As the laser pulse field strength increases, odd harmonics of the laser pulse frequency appear in the response spectrum, the amplitude of which drops sharply with increasing harmonic number — a perturbative harmonic generation regime. At the laser pulse field strength $\mu_0 \approx 10^{-2}$, the profile of the atomic response spectrum begins to change. The width of the spectrum increases, and a plateau with a pronounced cutoff frequency appears (Fig. 4a). A further increase in field strength leads to an increasingly clear manifestation of these trends: the width of the plateau increases significantly, and the cutoff frequency becomes more contrasting (Fig. 4b).

The dependence of the cutoff frequency on the laser radiation intensity (i.e., actually μ_0^2) is not a monotonically increasing function, but saturates at an intensity of approximately 10^{14} W cm^{-2} (Fig. 5).

3.2 Excitation by a dual-frequency linearly-polarized laser field

Let us now turn to a discussion of the response of a single atom to a dual-frequency laser field represented by the fundamental and second harmonics of a Ti:Sa laser with the following parameters: intensity of the components $\mu_{01} = 0.1$, $\mu_{02} = 0.1$, pulse duration $\tau = \tau_2 = 26.6$ fs, angle between components' polarization and pulse time delay $t_{12} = 0$. The influence of the main parameters of such a field (component intensity, duration, polarization angle, and pulse time delay) on the atomic response spectrum is shown in Fig. 6. In each of the presented comparative spectra, one field parameter is varied while the other parameters remain constant.

Figure 6a shows the spectra calculated for three values of the second harmonic amplitude: $\mu_{02}=0$ (black curve with squares), $\mu_{02} = 0.01$ (red curve with circles), and $\mu_{02} = 0.1$ (blue curve with triangles). The spectrum calculated $\mu_{02} = 0$ for consists of odd harmonics of the field. The even harmonics of the spectrum calculated for $\mu_{02} = 0.01$ are smaller than the odd harmonics. The intensities of the even and odd field harmonics become comparable with further increase in the field (see the blue curve with triangles in Fig. 6a). It is important to note that the spectral width in the latter case is larger (compared to the previous cases). This is due both to the additional field symmetry violation, which typically occurs in dual-frequency laser fields and is the cause of the generation of even field harmonics, and to the increase in the overall nonlinearity of the atomic response due to the higher laser field energy. This dynamics of the relative intensities of the even and odd harmonics is quite predictable.

The effect of the time delay between pulses on the atomic response spectra is shown in Fig. 6b, which compares the spectra obtained with a delay of $t_{12} = 13.3$ fs (red curve with circles) and $t_{12} = 0$ fs (black curve with squares). Calculations show that the time delay between pulses changes the shape of the spectrum only slightly if the delay time is less than the pulse duration (there is only a small difference in the region of high harmonics, $N \geqslant 20$).

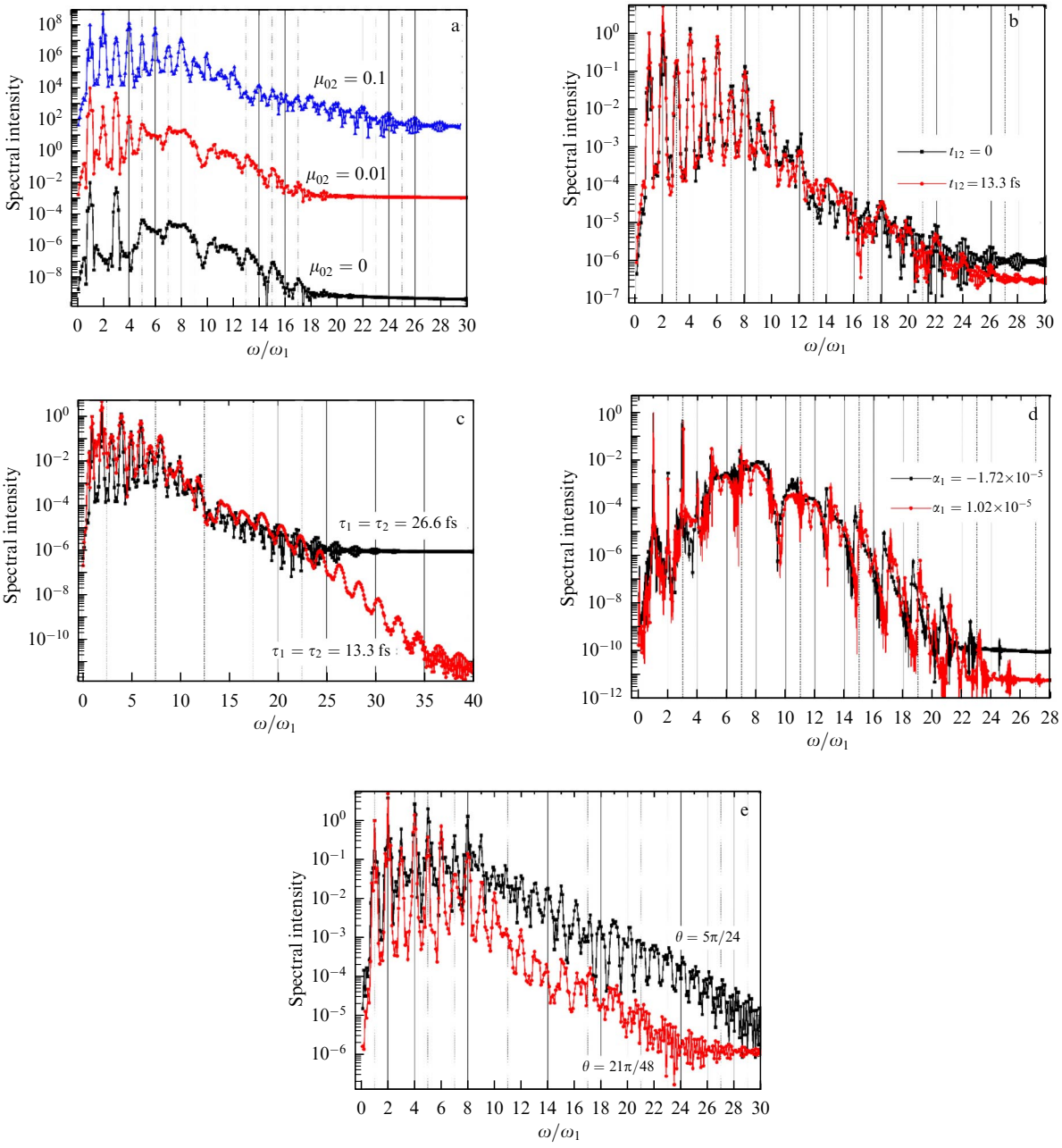

Figure 6. Spectra of an argon atoms' response to the dual-frequency laser field generated by linearly polarized first and second harmonics of a Ti:Sa laser: (a) $\mu_{02} = 0$ (black curve with squares), $\mu_{02} = 0.01$ (red curve with circles), $\mu_{02} = 0.1$ (blue curve with triangles); (b) $t_{12} = 13.3$ fs (red curve with circles) and $t_{12} = 0$ fs (black curve with squares); (c) $\tau_1 = \tau_2 = 26.6$ fs (black curve with squares), $\tau_1 = \tau_2 = 13.3$ fs (red curve with circles); (d) $\alpha_1 = 1.02 \times 10^{-5}$ (red curve with circles), $\alpha_1 = -1.72 \times 10^{-5}$ (black curve with squares); (e) $\theta = 5\pi/24$ (black curve with squares), $\theta = 21\pi/48$ (red curve with circles). The remaining parameters have the values: $\mu_{01} = 0.1$, $\mu_{02} = 0.1$, $\tau_1 = \tau_2 = 26.6$ fs, $\theta = \pi/2$, $t_{12} = 0$ fs, $\alpha_1 = \alpha_2 = 0$ [171].

The effect of pulse duration on the atomic response spectra is shown in Fig. 6c: the black curve with squares denotes the response spectrum calculated for $\tau_1 = \tau_2 = 26.6$ fs, and the red curve with circles denotes the response spectrum for $\tau_1 = \tau_2 = 13.3$ fs. It can be seen that, due to the larger spectral width at shorter pulse durations, the harmonic widths calculated for $\tau_1 = \tau_2 = 13.3$ fs are larger than those calculated for $\tau_1 = \tau_2 = 26.6$ fs. Due to the large spectral width, even and odd harmonics appear in the high-frequency part of the atomic response spectra, forming a supercontinuum-like spectrum. However, for longer laser pulses, even and odd harmonics can be spectrally resolved over the entire spectral range observed.

The effect of chirp on the atomic response spectrum is shown in Fig. 6d: the red curve with circles corresponds to a positive chirp of the fundamental harmonic $\alpha_1 = 1.02 \times 10^{-5}$, and the black curve with squares — to a negative chirp $\alpha_1 = -1.72 \times 10^{-5}$. The second harmonic of the dual-frequency field was assumed to be unchirped. Calculations show that the effect of the field chirp is strongest in the high-frequency part of the atomic response spectrum and consists of a slight change in the harmonic frequency.

Figure 6e shows the atomic response spectra calculated for two different angles between the polarization directions of the incident fundamental and second harmonic laser pulses:

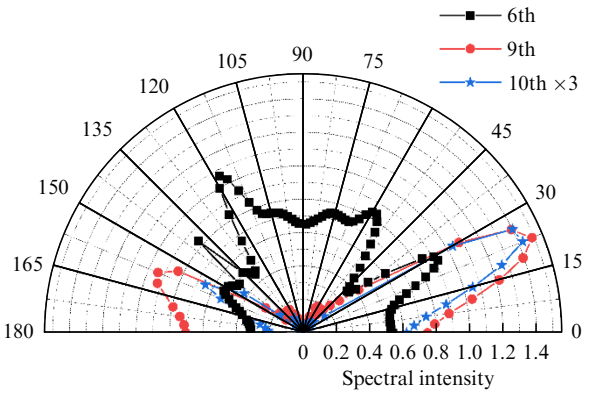

Figure 7. Generation efficiency of the 6th (black curve with squares), 9th (red curve with circles), and 10th harmonics (blue curve with asterisks) as a function of the angle between the polarization vectors of the fundamental and second harmonics of a Ti:Sa laser. Field parameters: $\mu_{01} = 0.1$, $\mu_{02} = 0.1$, $\tau_1 = \tau_2 = 26.6$ fs, $t_{12} = 0$ fs, $\alpha_1 = \alpha_2 = 0$. The intensity of the 10th harmonic is multiplied by a factor of 3 for a clearer representation [171].

$\theta = 5\pi/24$ (black curve with squares) and $\theta = 21\pi/48$ (red curve with circles). Both spectra contain both even and odd harmonics of the laser field. It can be seen that the intensities of the harmonics with $N \geqslant 10$ differ from each other by up to several orders of magnitude. Thus, changing the orientation of the incident pulse polarization vectors is one of the most effective methods for controlling the parameters of high-order harmonics. It is important to note that changing the angle between the components of the dual-frequency field does not change the total energy of the dual-frequency field, but merely redistributes it in the plane of polarization. The reason for such a significant change in the parameters is the dependence of the matrix elements of the operator $\hat{V}$ (50) and the matrix elements of the atomic response current (52) on the angle between the polarizations of the dual-frequency laser field.

An additional illustration of the effectiveness of the polarization control method is shown in Fig. 7, which shows the dependence of the spectral intensity of the 6th (black curve with squares), 9th (red curve with circles), and 10th (blue curve with asterisks) harmonics on the angle between the polarization vectors of the components of a dual-frequency laser field, the parameters of which are similar to those for the results presented in Fig. 6. It is evident that the harmonic intensities depend nonlinearly and nonmonotonically on the angle between the polarization vectors. Consequently, by varying this angle, it is possible to optimize the generation efficiency of selected harmonics or harmonic groups.

As noted in the Section 1, the polarization state of the generated high-order harmonics is of fundamental and practical interest. A nonperturbative approach allows one to obtain the spatial distribution of the HHG amplitude for each harmonic. However, the results presented below assume that the polarization of the fundamental harmonic and the angular momentum of the atom coincide, and the laser field is a plane wave. This means that the polarization of the generated radiation is distributed in the plane xz: $\mathbf{E} = E_{x0} \exp(i\delta_x)\,\mathbf{e}_x + E_{z0} \exp(i\delta_z)\,\mathbf{e}_z$. Let us denote $\chi = E_{x0}/E_{z0} \exp(i(\delta_x - \delta_z))$, then the ellipticity ε of the radiation and the inclination angle of the ellipse can be calculated using the following formulas:

$$\varepsilon = \tan\left[\frac{1}{2}\arcsin\left(2\,\frac{E_{x0}}{E_{zo}}\,\frac{\sin(\delta_x - \delta_z)}{1 + |E_{x0}/E_{z0}|^2}\right)\right], \tag{54}$$

$$\tan(2\theta) = 2\,\frac{E_{x0}}{E_{z0}}\,\frac{\cos(\delta_x - \delta_z)}{1 - |E_{x0}/E_{z0}|^2}\,. \tag{55}$$

Let us present some results of numerical studies of the polarization properties of high-order harmonics generated as a result of interaction of the two-frequency orthogonally polarized low-intensity laser field with a neon atom. The corresponding experiment was performed in [172], in which the low intensity of laser radiation ($(I(\omega) \sim I(2\omega) \sim 10^{13}$ W cm^{-2})) was chosen so that the population of the ground state (2p) of the atom did not change significantly during the interaction with the laser field. The result of such interaction should be the generation of harmonics, each of which has a linear polarization (the ellipticity is close to zero), with the polarization of the even harmonics coinciding with the polarization of the second harmonic radiation, and the polarization of the odd harmonics coinciding with the polarization of the fundamental harmonic. The results of numerical studies for the values of the parameters $\tau_1 = \tau_2 = 38$ fs, $\theta = \pi/2$, $t_{12} = 0$ fs are presented in Fig. 8. Even at the maximum of the laser field envelope, the population of the ground state is much greater than the population of all excited states (not shown in the figure). The atomic response spectrum contains linearly polarized odd and even harmonics. The results of numerical calculations demonstrate good agreement with experimental studies [172].

Now we turn to intense dual-frequency (fundamental and second harmonics of a Ti:Sa laser) orthogonally polarized laser fields and study the generation of high-order harmonics (spectral intensity and ellipticity) in this case. In the experimental setup [165] corresponding to this numerical calculation, dual-frequency (fundamental and second harmonics of a Ti:Sa laser) linearly polarized laser field with the pulse duration $\tau_1 = \tau_2 = 42$ fs is used. Polarizations of the compo-

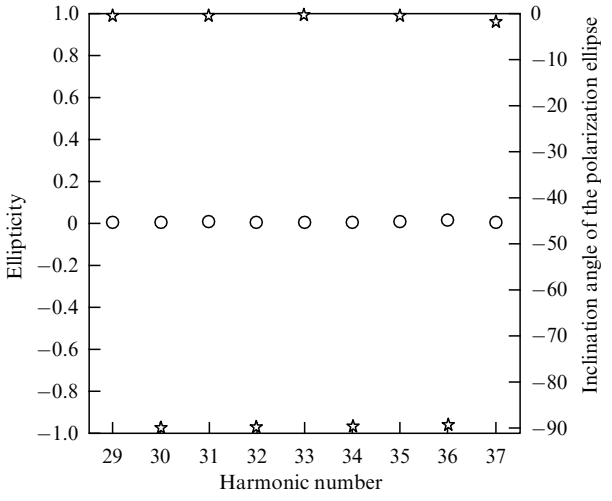

Figure 8. Ellipticity of high-order harmonics at low excitation of an atom by the laser field [165]. The parameters of the dual-frequency laser field correspond to the experimental work [172].

nents form an angle $\theta = \pi/2$, possessing a phase shift $\Delta\varphi = \pi/2$ relative to each other and a nonzero time delay $t_{12} = 14$ fs and $t_{12} = 42$ fs. The laser field was focused into a 5 mm long gas jet under a pressure of 40 mbar. A BBO crystal (of two different thicknesses: 100 μm and 250 μm) was placed directly within the laser beam after the lens. Different thicknesses of the BBO crystal used lead to different absolute and relative intensities of the fundamental and second harmonic fields due to different nonlinear interaction lengths: $I(\omega) = 1.5 \times 10^{14}$ W cm^{-2} and $I(2\omega) = 1.3 \times 10^{13}$ W cm^{-2} for 100 μm; and $I(\omega) = 3 \times 10^{14}$ W cm^{-2} and $I(2\omega) = 0.4 \times 10^{14}$ W cm^{-2} for 250 μm.

Figure 9 shows the results of numerical calculations of the response spectra of a neon atom (dots) and experimental measurements of the main harmonic characteristics (lines). For each characteristic, odd and even harmonics are presented separately for clarity. The solid black curves and black squares correspond to a BBO crystal thickness of 100 μm, while the dashed red lines and red dots correspond to a thickness of 250 μm. It can be seen that the theoretically calculated and experimentally measured values of the ellipticity of high-order harmonics and their spectral intensities are close to each other. When calculating the harmonic intensities, the phase-matching conditions for the fundamental and second harmonics [173] were taken into account, as well as the transmission of the generated harmonics through the gas and filters 2×10 nm Al_2O_3.

The example of studying the ellipticity of high-order harmonic radiation above demonstrates good agreement between simulation and experimental measurements. Therefore, the nonperturbative theory of the interaction of a single atom with a laser field provides a reliable description of the observed phenomena and can be used to determine the nature of the generation of elliptically polarized harmonics.

According to (52), the direction of the atomic current depends on the orientation of the atom's dipole moment, which is actually the quantum-mechanical average radius-vector of an atomic electron. On the other hand, the matrix elements $V_{nm}(t)$ depend on the relative orientation of the laser pulse field and the angular momentum of the atomic electron. Consequently, the atomic current in tensor form depends on the direction of the laser field polarization and the angular momentum of the atom, the orientation of which determines the orientation of the matrix elements $\mathbf{d}_{nm}$.

In subatomic laser fields, the ground state $|0\rangle$ is the most populated, so the atomic current can be approximately written as follows:

$$\mathbf{J}(t) \approx \langle 0|\mathbf{j}|0\rangle = \mathrm{i} \sum_{n_1 l_1 m_1} \sum_{n_2 l_2 m_2} (\omega_{n_1 l_1 m_1} - \omega_{n_2 l_2 m_2}) \times \langle 0|\hat{V}^{-1}|n_1 l_1 m_1\rangle \langle n_1 l_1 m_1|\mathbf{d}\,|n_2 l_2 m_2\rangle \langle n_2 l_2 m_2|\hat{V}|0\rangle, \quad (56)$$

where it is defined $a_{nlm} \approx \delta_{n0}\delta_{l0}$.

The ground state of the neon atom is $2\mathrm{p} = |0\rangle = |n = 2, l = 1\rangle$, which has three sublevels corresponding to different values of $m = \{0, \pm 1\}$. We will explicitly identify in (56) the dependence of the current on the magnetic quantum number and, for brevity, denote the matrix elements of the current as $\langle m_1|\mathbf{j}|m_2\rangle$:

$$\langle 0|\mathbf{j}|0\rangle = \sum_{m_1 m_2} \langle 2, 1, m_1|\mathbf{j}|2, 1, m_2\rangle = \sum_{m_1 m_2} \langle m_1|\mathbf{j}|m_2\rangle . \quad (57)$$

In the subatomic region of the laser field strength, this dependence has the form $\langle n_1 l_1||j_l||n_2 l_2\rangle \sim \mu_0^{|l_1 - l_2|}$. The rules for selecting dipole matrix elements require that $l_1 - l_2 = \pm 1$. As a result, even in the subatomic region of the laser field strength, where the ground state is predominantly populated, the atomic current (56), due to summation over $(n_1 l_1 m_1)$ and $(n_2 l_2 m_2)$, includes the contributions of all other atomic states. When calculating (56), there are taken into account the contributions of the levels $3\mathrm{s} = |1\rangle$ and $3\mathrm{d} = |2\rangle$ — the lowest levels associated with the ground state $2\mathrm{p} = |0\rangle$ by dipole-allowed transitions.

The sum of the diagonal matrix elements of current (57) is equal to:

$$\sum_{m=-1}^{+1} \langle m|\mathbf{j}|m\rangle = -\frac{2}{5} \times \begin{pmatrix} 5\omega_1 d_{10} \langle 1||j_1(z)||2\rangle \left[\langle 1||j_0(z)||1\rangle - 2\langle 1||j_2(z)||1\rangle\right] \\ +2\omega_2 d_{12} \begin{bmatrix} 5\langle ||j_0(z)||1\rangle \langle 1||j_1(z)||2\rangle \\ -\langle 1||j_2(z)||1\rangle \left(\langle 1||j_1(z)||2\rangle\right. \\ -9\langle 1||j_3(z)||2\rangle\big) \end{bmatrix} \end{pmatrix} \times \left((\mathbf{e}_x \cos\varphi + \mathbf{e}_y \sin\varphi)\sin\theta + \mathbf{e}_z \cos\theta\right), \quad (58)$$

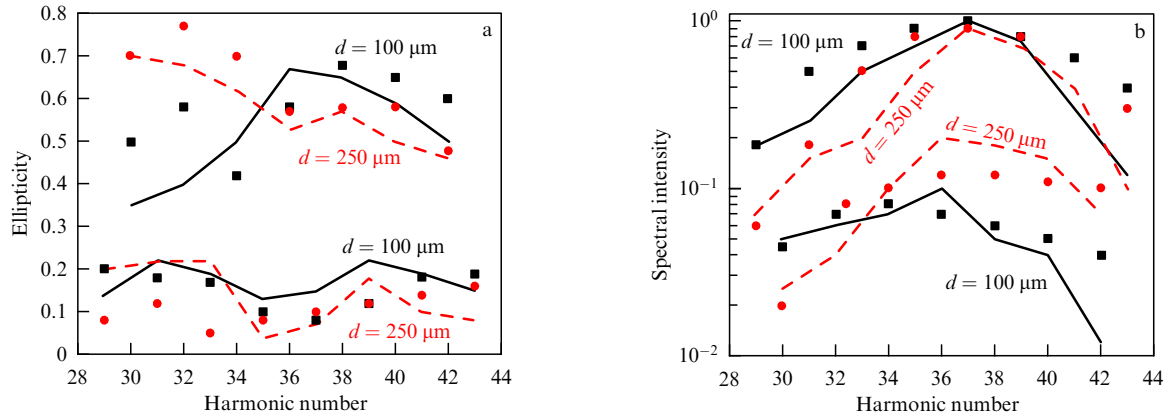

Figure 9. Measured (solid lines) and numerically calculated (squares and dots) ellipticity (a) and spectral intensity (b) of odd- and even-order harmonics for a 100-μm-thick (black solid curves and black squares) and 250-μm-thick (red dashed curves and red dots) BBO crystal [165].

where $\mathbf{e}_a$ are the unit vectors in the atomic configuration space, that is, in a Cartesian coordinate system in which the axis z coincides with the direction of the atom's angular momentum. The angles θ and φ determine the orientation of the laser field polarization vector:

$$\mathbf{e}(t) = \frac{\mathbf{A}(t)}{A(t)} \left(\mathbf{e}_x \cos\varphi + \mathbf{e}_y \sin\varphi\right) \sin\theta + \mathbf{e}_z \cos\theta \,. \tag{59}$$

Formulas (58) and (59) clearly show that the atomic current and the harmonic polarization vectors follow the laser field polarization during the laser pulse.

Thus, the polarization properties of the atomic current (56), associated with the diagonal elements of matrix (57), coincide with the polarization properties of the incident laser field. For example, if the incident laser field is two-frequency and consists of orthogonally polarized components $\omega + 2\omega$, then the polarizations of the odd and even harmonics will be mutually orthogonal. The polarization vector of the odd (and, accordingly, even) harmonics will follow the polarization vector of the radiation at the fundamental harmonic (and, accordingly, at the second harmonic). This is due to the fact that the matrix elements of the dipole moment have a nonzero value only for transitions between states of opposite parity. Consequently, the matrix elements of the operator $\hat{V}$ in formula (56), $\langle 0|\hat{V}^{-1}|l_1\rangle$ and $\langle l_2|\hat{V}^{-1}|0\rangle$, are the functions of opposite parity with respect to $A(t)$. As a result, the right-hand side of (56) is the product of $\mathbf{A}(t)$ and an even function of $A(t)$. When $\mathbf{A}(t) = \mathbf{e}_1 A_1(t)\cos\omega t + \mathbf{e}_2 A_2(t)\cos 2\omega t$, $\mathbf{e}_1$ and $\mathbf{e}_2$ are orthogonally polarized, the odd and even harmonics also become orthogonally polarized with respect to each other. Harmonics generated by atoms with the ground s-state (hydrogen, silver, etc.) will have the same polarization properties.

The sum of the matrix elements (57) with $\Delta m = \pm 1$ gives a zero contribution:

$$\langle 1|\mathbf{j}|0\rangle + \langle 0|\mathbf{j}|-1\rangle + \langle 0|\mathbf{j}|1\rangle + \langle -1|\mathbf{j}|0\rangle = 0 \,. \tag{60}$$

It should be noted that, despite the fact that each term in (60) is nonzero and has a polarization dependence different from that presented in (58), their sum is zero. This is due to symmetry reasons, and any symmetry violation, for example by adding additional external fields, will lead to a nonzero influence of the matrix elements with $\Delta m = \pm 1$ and, consequently, to the generation of radiation whose polarization does not coincide with the polarization of the laser field.

The remaining components of matrix (57) have polarization properties that are fundamentally different from those of the incident laser field. Even in the case of the Ne atom, the expressions for these components are very complex, so only the functional dependence of the projection of the sum of these matrix elements onto the x axis in atomic configuration space is presented below:

$$\mathbf{e}_x \left(\langle 1|\mathbf{j}|-1\rangle + \langle -1|\mathbf{j}|1\rangle - \sum_{m=-1}^{+1} \langle m|\mathbf{j}|m\rangle\right) = \sin\theta \Big[\left(f_1(t) + f_2(t)\cos 2\theta\right)\cos\varphi + f_3(t)\cos 3\varphi \sin^2\theta\Big] . \tag{61}$$

Expression (61) includes trigonometric functions of the angles θ, φ, and their product. This leads to a sharp change in the polarization state of the generated harmonics compared to the laser field.

Thus, the above considerations provide a profound understanding of the physics behind the high ellipticity of the generated harmonics. Within the theory of the interaction of light atoms with fields based on the dipole approximation, the atomic response is determined by selection rules for dipole transitions. However, within the framework of nonperturbative theory, the atomic response is determined by the matrix elements of the operator $\hat{V}$, which includes all powers of operator $\mathbf{r}$ (43). Therefore, the initial and final states of cascade transitions do not obey specific selection rules. The ellipticity of the harmonics is primarily due to the matrix elements of the atomic current, which are most unusual for the dipole approximation approach. For example, in the case of the Ne atomic 2p-state, these matrix elements link the sublevels $m = +1$ and $m = -1$. This conclusion is an exact analytical result obtained under the assumption $a_{nlm} \approx \delta_{n0}\delta_{l0}$. At the same time, the numerical simulation results presented above show that when this assumption is not met, harmonics with high ellipticity are generated. Consequently, the nature of harmonic generation in fields of moderate intensity is the same as in subatomic laser fields. Note that the numerically calculated atomic current (56) includes, for example, the following term:

$$(\omega_{2,1,-1} - \omega_{3,0,0})\langle 3,2,-2|\hat{V}^{-1}|2,1,-1\rangle \times \langle 2,1,-1|\mathbf{d}|3,0,0\rangle\langle 3,0,0|\hat{V}|4,1,1\rangle \,. \tag{62}$$

On the one hand, the levels for which the matrix elements of the operators $\hat{V}$ and $\mathbf{d}$ are calculated, are related by dipole-allowed transitions. On the other hand, the resulting matrix element $\langle m_1|\mathbf{j}|m_2\rangle$ is one with $\Delta m = -3$. However, this does not mean that other transitions (even dipole-forbidden ones) are not taken into account when calculating the total atomic response current. All transitions between all states are taken into account with their own weight, which depends nonlinearly on the laser field strength.

We also note that the analysis above was performed for plane waves. Taking into account focusing and the influence of the magnetic field of the electromagnetic wave (especially for intense mid-IR laser fields) can lead to an 'imbalance' in the contributions of the transitions with $\Delta m = -1$ and $\Delta m = +1$, leading to an increase in the ellipticity of the generated radiation.

3.3 Excitation by a dual-frequency circular-polarized laser field

One of the most frequently used experimental methods for generating high-order elliptical harmonics is a method based on the interaction of gas jets with dual-frequency laser fields formed by circularly polarized harmonics at the fundamental and the second harmonic of a Ti:Sa laser, possessing opposite helicities [96].

Figure 10 shows the results of studies of the properties of high-order harmonics generated by a single Ne atom interacting with the laser field described above, the parameters of which were chosen as in [96]. Numerical calculations agree well with the experimentally observed features: the atom response spectrum exhibits the alternation of one low-intensity harmonic (3rd, 6th, 9th, etc.), followed by two more intense ones.

To study the nature of the generation of low-intensity harmonics, we examine the dependence of their spectral intensity on the delay time between the pulses of the

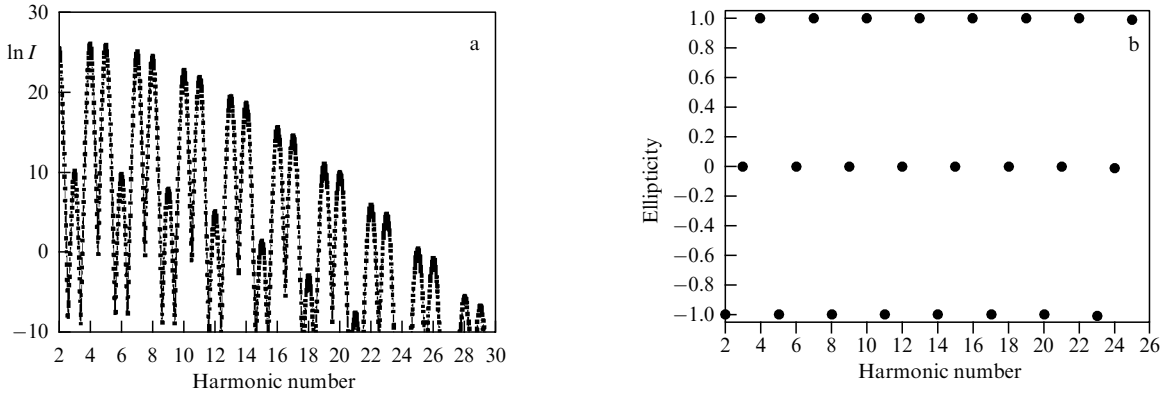

Figure 10. Spectrum of the Ne atom response to the laser field (a) and ellipticity (b) calculated for the dual-frequency laser fields formed by circularly polarized fundamental and second harmonics of a Ti:Sa laser with opposite helicities, for which each component of the laser field has an intensity of $\sim 10^{14}$ W cm^{-2} [174].

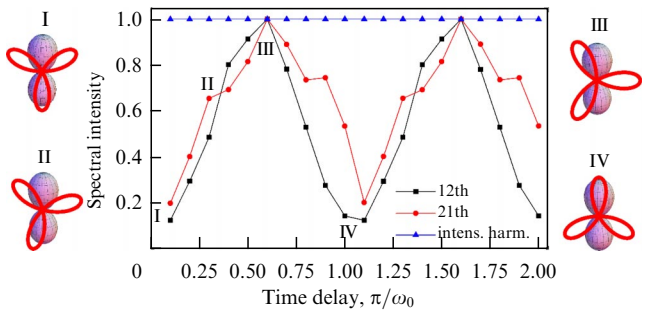

Figure 11. Spectral intensity of the low-intensity 12th (black curve with squares), 21st (red curve with circles) harmonic and high-intensity harmonic (blue curve with triangles) in the dependence on the time delay between fundamental and second harmonics of the laser field. The insets schematically show the relative orientation of the laser field polarization and the *p*-orbital [174].

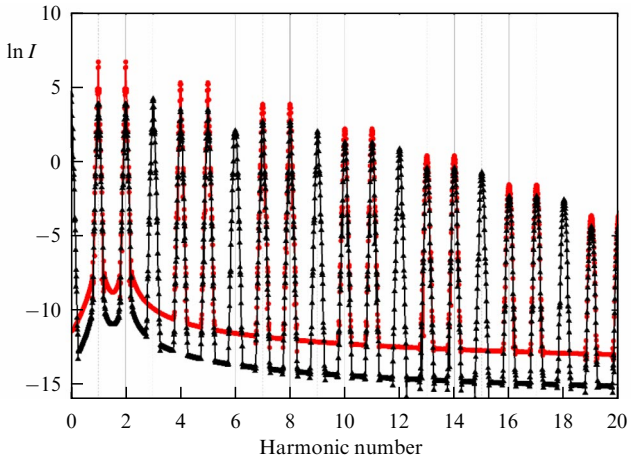

Figure 12. Single-atom response spectra calculated as the sum of the components of the matrix (57) corresponding to cascade transitions with $\Delta m = \pm 2$ (black curve with triangles) and the sum of the remaining seven components of the matrix (57) (red curve with circles) [174].

fundamental and second harmonics of the laser field (Fig. 11). It is clearly seen that the efficiency of generating intense harmonics is independent of the delay time (see the blue curve with triangles in Fig. 11). This is an expected result, since for a dual-frequency laser field formed by circularly polarized fundamental and second harmonics, whose polarization vector rotates in opposite directions, changing the delay time leads to a simple rotation of the field, the polarization vector of which describes a trefoil-shaped curve (see the insets in Fig. 11). As a result, there is no change in the laser field strength (in contrast to the case of a dual-frequency linearly polarized laser field with a change in the delay time). However, a strong dependence of the generation efficiency of low-intensity harmonics is observed with a change in the delay time between the components of the dual-frequency field (see the black curve with squares and the red curve with circles in Fig. 11). This feature is associated with a change in the relative position of the -orbital (the ground state of the neon atom) and the two-frequency field (see the left and right panels in Fig. 11).

In Section 3.2, it was shown that elliptically polarized radiation is generated by cascade transitions with $\Delta m = \pm 2$, and $\Delta m = \pm 1$ that transitions with are very sensitive to the field symmetry, so any modifications of the laser field (i.e., additional external fields, etc.) alter the properties of the generated radiation. In the case of a two-frequency laser field formed by circularly polarized fields whose polarization vectors rotate in opposite directions, the generation of low-intensity harmonics also occurs due to transitions of this kind. This can be easily demonstrated within the framework of the 'single-level' approximation. Figure 12 shows the spectra of the sums of two sets (57): the black curve with triangles shows the sum of the components of the matrix (57) corresponding to cascade transitions with $\Delta m = \pm 2$, the red curve with circles is the sum of the remaining seven components of the matrix (57). The part of the current containing the seven components of the matrix (57) has no signal at the location of low-intensity harmonics, and the spectra of the sum of the other two components contain a signal at the frequencies of all harmonics. Therefore, the nature of the generation of low-intensity harmonics lies in cascade transitions with $\Delta m = \pm 2$. The magnitude of low-intensity harmonics can be changed due to the dynamics of the probability amplitudes of atomic states. The latter is not taken into account within the framework of the 'single-level' approximations, but was taken into account in the calculations of the total atomic current (52) to obtain the results presented in Figs 10 and 11.

The behavior of the two parts of the set (57) explains the dependence of the low-intensity harmonic generation efficiency and the independence of the high-intensity harmonic

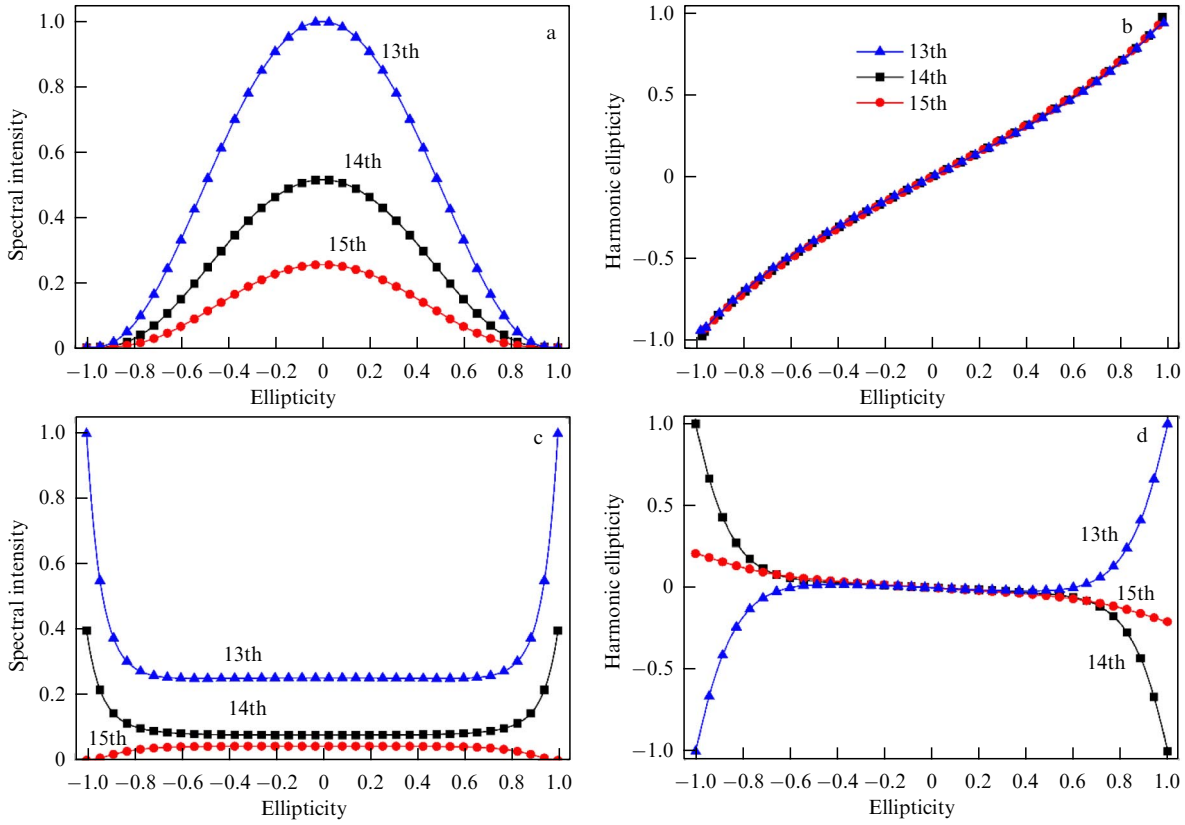

Figure 13. Intensities of harmonics (a, c) and their ellipticities (b, d), calculated for the cases of identical helicities (a, b) and opposite helicities (c, d) of elliptically polarized fundamental and second harmonics of a Ti:Sa laser [174].

generation efficiency on the time delay between the fundamental and second harmonics, shown in Fig. 11. Indeed, while low-intensity harmonics are generated only due to transitions with $\Delta m = \pm 2$, the magnitudes of the corresponding components of the current (57) are very sensitive to the symmetry of the laser field. Changes in the relative position of the p-orbital and the field distribution in the polarization plane with changes in the time delay between pulses are 'transferred' to the dependence of the intensity of low-intensity harmonics. At the same time, the contribution of transitions with $\Delta m = \pm 2$ to the formation of intense harmonics is significantly smaller than the sum of the contributions of all other transitions. Consequently, the generation of such harmonics is not as sensitive to changes in the relative orientation of the wavefunction and the distribution of the polarization vector of the dual-frequency field in the plane of polarization. As a result, the intensity of such harmonics does not change with variations in the time delay between pulses of the dual-frequency field.

Consider also the generation of harmonics in dual-frequency laser fields formed by elliptically polarized fundamental and second harmonics of a Ti:Sa laser with varying ellipticity of the field components for the case of codirectional (Fig. 13a, b) and counterdirectional (Fig. 13c, d) rotation of the polarization vectors of the field components. In the numerical calculations, the ellipticity of the field components varied simultaneously. It is clearly seen that in the case of co-rotating dual-frequency field components (Fig. 13a, b), the maximum harmonic generation efficiency is achieved for linearly polarized components. The ellipticities of the harmonics follow the ellipticities of the component pulses. Circularly polarized harmonics are generated for the case of circularly polarized components of a dual-frequency laser field, but the harmonic intensities are low.

In the case of counter-rotating fundamental and second harmonics (Fig. 13c, d), it is clearly seen that the intensities and ellipticities (the values of which are close to zero) of the generated harmonics vary insignificantly over a wide range of laser field component ellipticities (from -0.7 to 0.7). As the range of laser field component ellipticities changes from -1 to -0.7 and from 0.7 to 1, the parameters of the generated harmonics change significantly: the ellipticities of the two intense harmonics vary from ~ 0 to ± 1, and their intensity increases significantly. Meanwhile, the dynamics of the intensities of the low-intensity harmonics is not as significant. This difference in the nature of the dependence of intense and low-intensity harmonics is associated with their nature, i.e. with which transitions are 'responsible' for their generation.

3.4 High-order harmonic generation in the dual-frequency cross-polarized laser fields

The results described above are presented for the case where the propagation directions of the components of a multi-frequency laser field coincide. In this case, in a nonperturbative interaction regime, it is difficult to isolate a specific harmonic generation channel (how many photons, and of what type, participate in the generation of a given harmonic). When generating a given harmonic, there are many competing channels of generation.

However, in certain cases, conditions exist where the number of photons forming a harmonic can be reliably determined. This occurs in noncollinear laser fields, when, for example, the components of a two-frequency field

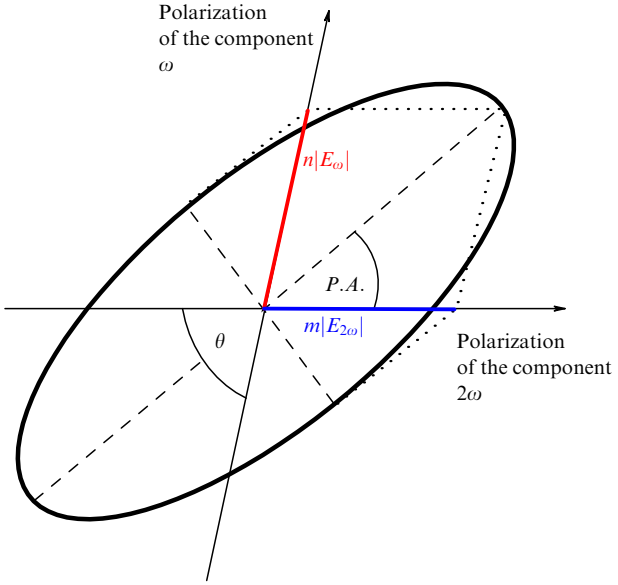

Figure 14. Harmonic polarization ellipse and relative positions of the polarizations of the field components $\omega + 2\omega$. *P.A.* is the inclination angle of the polarization ellipse, θ is the angle between the polarizations of the components, n is the number of photons of radiation at frequency ω, m is the number of photons of radiation at frequency 2ω, participating in the formation of a given harmonic $n + 2m$ [175].

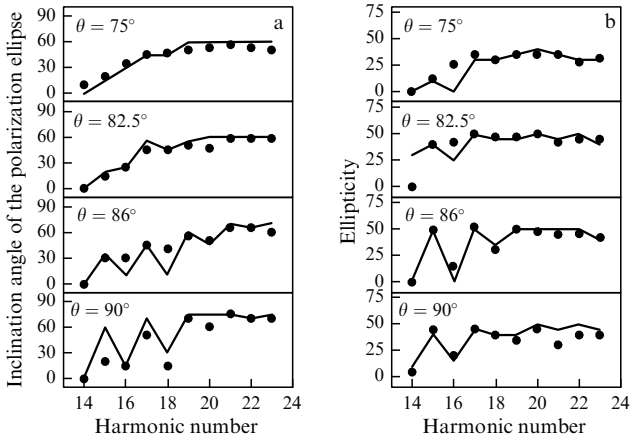

Figure 15. Comparison between experimentally measured (lines) and numerically calculated (dots) polarization characteristics of the generated harmonics: (a) inclination angle of the polarization ellipse, (b) ellipticity. In the numerical calculations, χ was chosen to be equal to 0.2, 0.3, 0.5, and 1.5 for $\theta = 75°$; 82,5°; 86° and 90°, respectively [175].

propagate along crossed directions. In this case, the angular distribution of the harmonics allows one to determine the number of photons forming the harmonic [175], and the polarization characteristics of the generated radiation can be calculated without using a nonperturbative approach.

Consider the generation of harmonics in dual-frequency laser fields formed by linearly polarized fundamental and second harmonics of a Ti:Sa laser, the propagation directions of which are noncollinear, and the polarization directions of the linearly polarized field components form an angle θ. We assume that harmonics with a nonzero ellipticity are generated in a gas interacting with such a field. Then the polarization ellipse can be represented in the plane formed by the polarization vectors of the field components (Fig. 14). We assume that a given harmonic is formed by n photons of radiation at the fundamental frequency ω and m by photons at twice the laser frequency 2ω. Then the field strength of the corresponding harmonic can be represented as the sum of vectors $n\mathbf{E}_\omega + m\mathbf{E}_{2\omega}$, multiplied by a certain coefficient χ, which is associated with the component of the susceptibility tensor at the corresponding harmonic frequency and corresponds to the direction of harmonic propagation. Then, from geometric considerations, one can calculate the inclination angle of the harmonic polarization ellipse (*P.A.*) and its ellipticity ε:

$$P.A. = \arcsin\left(\frac{\sin\theta}{\sqrt{k}}\right), \tag{63}$$

$$\varepsilon = \tan\left[\frac{1}{2}\arcsin\left(\frac{2\zeta k}{\zeta^2 + k^2}\right)\right], \tag{64}$$

where $k = 1 + 2\cos\theta/\eta + 1/\eta^2$, $\zeta = \sin\theta/\eta$, $\eta = \chi(n/m)\times(|E_\omega|/|E_{2\omega}|)$. When deriving these formulas, it was assumed that the phase difference between the radiation at the fundamental and second harmonics is $\pi/2$, which corresponds to the conditions of ideal phase matching in the BBO crystal.

It is useful to compare the above reasoning with the results of an experiment on studying the polarization characteristics of harmonics in crossed fields [175]. Figure 15 shows the experimentally measured (indicated by lines) and numerically calculated (indicated by dots) the inclination angle of the polarization ellipse (Fig. 15a) and the ellipticity of the harmonics (Fig. 15b) for $\theta = 75°$, 82.5°, 86°, 90°. Specific values of n and m were obtained from the experiment. The coupling coefficient χ is set in such a way as to match the calculations and the experiment: its value varies from 0.2 (for $\theta = 75°$) to 1.5 (for $\theta = 90°$).

We also note that in this experiment, a dependence of the harmonic parameters on the angle θ between the polarization directions of the field components is observed; this is an experimental confirmation of the assumption made in [176] regarding the effectiveness of this control parameter (see Section 3.2).

3.5 Interference model of the medium nonlinear response

The spectral and polarization properties of the generated harmonics discussed above relate to individual atoms placed in a laser field. However, in reality, experiments always deal with a medium containing multiple atoms. This raises a number of important issues that complicate the comparison of theoretical calculations with experimental observations. First, since laser beams are confined in a direction perpendicular to the propagation direction, different atoms in the medium experience laser field of varying intensity (higher in the near-axis region, lower at the periphery). However, the nonlinear nature of the interaction between laser radiation and atoms allows us to consider only the near-axis region of the beam, since the interaction at the periphery is significantly weaker (and the higher the order of the generated harmonic). Second, the radiation generated by the atoms generally affects surrounding atoms, altering the populations of their energy states. However, such 'secondary' effects are typically neglected, since the harmonic generation efficiency remains significantly less than unity, and the fixed-field approximation can be used. Third, the generated radiation, propagating from sources (separately located atoms) in the medium, is

subject to changes in its spectral properties due to the material dispersion of the medium, as well as due to the interference of radiation from different atoms.

Atoms of the medium, located at points $\mathbf{r}_i$ and placed in the laser field, create a distribution of electron density $\rho_i(\mathbf{r}', t_i')$ and current density $\mathbf{j}_i(\mathbf{r}', t_i')$ in the space around them, the dynamics of which determine the electric field at the point $\mathbf{r}$ [167]:

$$\mathbf{E}(\mathbf{r}, t) = -\frac{1}{4\pi\varepsilon_0 c^2}\sum_i \int \left[\frac{\partial \mathbf{j}_i(\mathbf{r}', t_i')}{\partial t} - \mathbf{n}_i' \left(\frac{\partial \mathbf{j}_i(\mathbf{r}', t_i')}{\partial t}\,\mathbf{n}_i'\right)\right] \times \frac{\mathrm{d}V'}{|\mathbf{r} - \mathbf{r}_i - \mathbf{r}'|} + \frac{1}{4\pi\varepsilon_0 c}\sum_i \int \mathbf{n}_i' \left(\mathbf{j}_i(\mathbf{r}', t_i')\,\mathbf{n}_i'\right) \times \frac{\mathrm{d}V'}{|\mathbf{r} - \mathbf{r}_i - \mathbf{r}'|^2} + \frac{1}{4\pi\varepsilon_0}\sum_i \int \mathbf{n}_i' \rho_i(\mathbf{r}', t_i') \times \frac{\mathrm{d}V'}{|\mathbf{r} - \mathbf{r}_i - \mathbf{r}'|^2}\,, \tag{65}$$

where $\mathbf{n}_i' = \mathbf{r} - \mathbf{r}_i - \mathbf{r}'/|\mathbf{r} - \mathbf{r}_i - \mathbf{r}'|$, $t_i' = t - |\mathbf{r} - \mathbf{r}_i - \mathbf{r}'|/c$.

In the approximation of the point atom model ($|\mathbf{r} - \mathbf{r}_i| \gg a_\mathrm{B}$), under the assumption of the identity of the atoms ($\rho_i(\mathbf{r}', t_i') = \rho_0(\mathbf{r}', t')$, $\mathbf{j}_i(\mathbf{r}', t_i') = \mathbf{j}_0(\mathbf{r}', t')$) and the constancy of the shape of the laser pulse, in the far-field ($|\mathbf{r} - \mathbf{r}_i| \gg \mathbf{r}'$) there is only a transverse electric field:

$$\mathbf{E}(\mathbf{r}, \omega) = -\frac{\mathrm{i}\omega}{c^2}\sum_i \frac{\exp\left(\mathrm{i}\omega|\mathbf{r} - \mathbf{r}_i|/c\right)}{|\mathbf{r} - \mathbf{r}_i|}\left[\mathbf{n}_i, \left[\mathbf{n}_i, \mathbf{J}(\omega)\right]\right], \tag{66}$$

where $\mathbf{J}(\omega)$ is definded in (48), and $\mathbf{n}_i = \mathbf{r} - \mathbf{r}_i/|\mathbf{r} - \mathbf{r}_i|$.

In the far-field, we can assume that the distance to the observation point is much greater than the linear dimensions of the atomic ensemble. Then, from (66) taking into account $|\mathbf{r}| \gg |\mathbf{r}_i|$, one can obtain:

$$\mathbf{E}(\mathbf{r}, \omega) = -\frac{\mathrm{i}\omega}{rc^2}\exp\left(\frac{\mathrm{i}\omega r}{c}\right)\sum_i \left[\mathbf{n}, \left[\mathbf{n}, \mathbf{J}_i(\omega)\right]\right]\exp\left(\mathrm{i}\mathbf{k}\mathbf{r}_i\right), \tag{67}$$

where $\mathbf{k} = \omega\mathbf{r}/cr$, $\mathbf{n} = \mathbf{r}/r$.

Formula (67) is used to calculate the response of extended gaseous media within the interference model. This model is as follows. The medium is a chain of atoms located on the pulse propagation axis (under the assumption that the laser field intensity rapidly decreases with distance from the axis, see Fig. 16). The atomic response spectrum is calculated using the nonperturbative theory presented above. The spectral components of the radiation generated by single atoms are 'summed' using formula (67), which takes into account the interference of contributions from different field sources in the far field.

The interference model offers a combination of unique advantages: it allows one to calculate the response of a medium by taking into account the responses of single atoms calculated quantum mechanically using a nonperturbative theoretical approach. It makes possible to trace modifications in the response spectra as the laser beam propagates through the medium, while preserving the features of the atomic response spectrum. This becomes critically important in the study of high-order harmonic generation, since the nature of the generation is considered to lie in the response of a single atom. At the same time, the interference model can serve as an alternative to models of

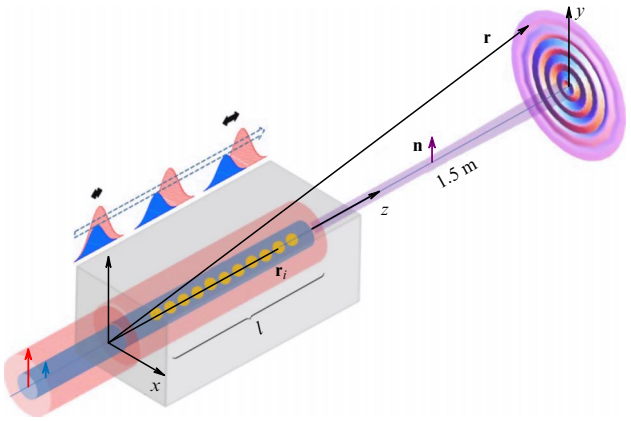

Figure 16. Schematic representation of a one-dimensional interference model: a linearly polarized laser field propagates along a chain of atoms (yellow circles) [177].

media that use nonlinear susceptibility tensors of the medium, typically defined phenomenologically. The advantage of the interference model of a medium is that the nonlinearities of the medium are considered in a quantum-mechanical way.

It should be noted that in extended media, the assumption of an invariant laser pulse shape is never strictly satisfied. In the case of a single-frequency pump field, this is due to the difference in the phase and group velocities of the pulse, leading to a dependence of the pulse time delay on the position of the atom in the ensemble. For example, for a dual-frequency laser pulse generated by radiation at frequencies ω_0 and $2\omega_0$ due to dispersion during propagation in the medium, additional phase shifts arise: $\varphi_1 = \mathbf{k}_1\mathbf{r} = (\omega_0/c)n_1(\omega_0)z$ and $\varphi_2 = \mathbf{k}_2\mathbf{r} = (2\omega_0/c)n_2(2\omega_0)z$, where $n_{1,2}$ are the refractive indices of the atomic medium at the fundamental frequency of the laser pulse and at the second harmonic frequency, respectively. This results in a phase difference that depends on the coordinate in the medium:

$$\Delta\varphi = 2\varphi_1 - \varphi_2 = \frac{2\omega_0}{c}\left(n_1(\omega_0) - n_2(2\omega_0)\right)z\,. \tag{68}$$

The atomic current becomes modulated along the length of the medium with a spatial frequency:

$$\Lambda = \frac{\pi c}{2\omega_0}\frac{1}{n_1(\omega_0) - n_2(2\omega_0)}\,. \tag{69}$$

The response field of an extended atomic medium in the far zone is determined by expression (67), in which $\mathbf{J}(\omega, \mathbf{k}) = \sum_i \mathbf{J}_i(\omega)\exp\left[\mathrm{i}(\Delta\varphi_i - \mathbf{k}\mathbf{r}_i)\right]$. Assuming that the density of atoms within the ensemble is uniform, we obtain:

$$\mathbf{J}(\omega, \mathbf{k}) = \mathbf{J}_0(\omega)\int_0^\infty \mathrm{d}\rho\rho \int_0^{2\pi}\mathrm{d}\varphi \exp\left(-\frac{\rho^2}{d^2}\right) \times \exp\left(\mathrm{i}\Delta\mathbf{k}_\perp\boldsymbol{\rho}\right)\int_{-L/2}^{L/2}\mathrm{d}z f(z)\exp\left(\mathrm{i}\Delta k_\parallel z\right), \tag{70}$$

where $\mathbf{J}_0(\omega)$ is the response current of a single atom located on the axis of the laser beam and with zero time delay of the dual-frequency field, d is the transverse dimension of the laser beam, L is the longitudinal dimension of the atomic medium. Taking into account (68), for $\Delta\mathbf{k}$ we obtain:

$$\Delta\mathbf{k} = 2\mathbf{k}_1 - \mathbf{k}_2 - \mathbf{k}\,. \tag{71}$$

The function $f(z)$ in (70) describes a periodic spatial profile of the response of an atomic medium with a spatial period (69). This profile is well approximated by the following expression:

$$f(z) = \left|\sin(Kz)\right|, \tag{72}$$

where $K = 2\pi/\Lambda$ and Λ is the spatial period of the field. Substituting (72) into (70) and integrating, we obtain:

$$\mathbf{J}(\omega,\mathbf{k}) = \mathbf{J}_0\,\frac{\pi d^2 K}{K^2 - \Delta k_{\parallel}^2}\exp\left(-\frac{\Delta k_{\perp}^2 d^2}{4}\right)\frac{\sin\left(\Delta k_{\parallel}\Lambda(N+1)/2\right)}{\sin\left(\Delta k_{\parallel}\Lambda/2\right)} \times \exp\left(\frac{\mathrm{i}\Delta k_{\parallel}\Lambda N}{2}\right)\left[1+\exp\left(\mathrm{i}\,\frac{\Delta k_{\parallel}\Lambda}{2}\right)\right]^2, \tag{73}$$

where $N = L/\Lambda$.

Due to the transverse confinement of the incident laser beam, the laser field in the region of the atomic medium is a superposition of plane-wave components with a characteristic transverse width $\Delta k_{\perp} = \pi/d$. On the other hand, the longitudinal projection of the wave vector due to the spatial periodicity of the response field of the atomic medium is $k_{\parallel}^{(n)} = k_{\parallel}^{(0)} + 2\pi n/\Lambda$, where $k_{\parallel}^{(0)}$ is the projection of the wavevector of the incident field onto the direction of its propagation. Thus, the resulting angular spectrum of the generated radiation at frequency $\omega = 2\pi c/\lambda$ depends on the ratio of the wavelength λ and the parameters d, and Λ is, in general, a superposition of nested cones. For a one-dimensional chain of atoms, this superposition of nested cones degenerates.

In conclusion of this section, we discuss the validity of the one-dimensional interference model. To this end, we conduct numerical studies of laser radiation propagation in argon using the classical unidirectional propagation model [178], in which the nonlinear properties of the medium are determined by the nonlinear refractive index $n_2 = p \times 10^{-18}$ W^{-1} cm^2 [179] (where p is the gas pressure in bars), and the resulting low-order harmonics are generated as a result of a cascade process of four-wave mixing.

Figure 17 shows the angular spectra of the fifth harmonic at the exit from an argon medium with a length of $L = 7$ mm at different gas pressures. The harmonic radiation has both a collinear and a noncollinear component, with the energy of the latter accounting for no more than 1% of the total harmonic radiation energy. It is also worth noting that the deflection angle of the noncollinear component from the propagation direction increases with increasing gas jet pressure: for $p = 1$ bar, the angle is 4.6°, and for $p = 15$ bar, it is 11.9°. Since the collinear component of the 5th harmonic contains about 99% of the total harmonic energy (over the entire range of pressures studied), when using the quantum mechanical approach to calculate harmonic signals, one can consider only the near-axis region of radiation propagation and use the interference model to calculate the total harmonic signal on the detector located in the far-field zone.

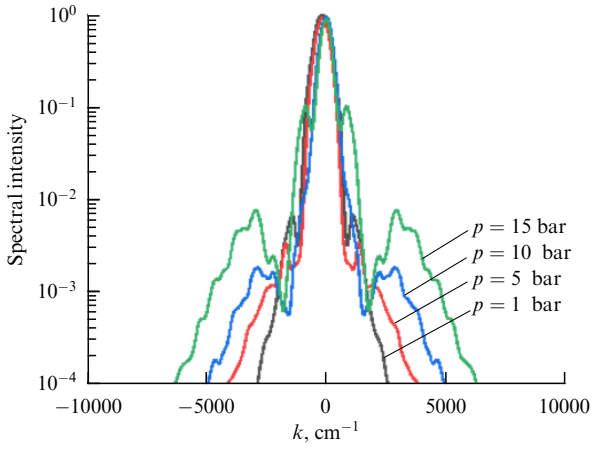

Figure 17. Angular spectrum of the 5th harmonic at the back boundary of an argon medium of length $L = 7$ mm at different gas pressures.

3.6 Phase matching of high-order harmonic radiation

Consider the effects of phase matching of harmonic radiation in gases using the example of atomic argon gas. For this, we will use the interference model described in detail in the previous section. The medium is a chain of atoms, the number of which is determined by the pressure in the medium and its length. Studies of the characteristics of the generated field are conducted in the far-field (at a distance of 1.5 m from the medium) in a plane perpendicular to the direction of radiation propagation.

Refractive index dependences for various wavelengths are available in specialized databases [180]. Figure 18 shows the spatial distribution of electromagnetic radiation in a plane perpendicular to the direction of radiation propagation (on a virtual detector), generated by a gas medium consisting of a chain of atoms of $L = 1$ cm long, calculated for the 5th (a) and 35th (b) harmonics of the incident laser radiation. The calculations were performed for laser radiation formed by the fundamental and second harmonics of a Ti:Sa laser ($\lambda = 800$ nm), the intensity of the field components $\mu_{01} = 0.1$, $\mu_{02} = 0.1$, pulse duration $\tau = 30$ fs, the angle between the polarizations of the field components $\theta = 0$. The figures show the dependences of the radiation intensity on the distance from the detector axis (y). It is evident that at low pressures, the spatial distribution of the harmonics is Gaussian — there is a peak in the center, the radiation intensity decreases as the coordinate moves from the center to the periphery. A similar distribution of the radiation

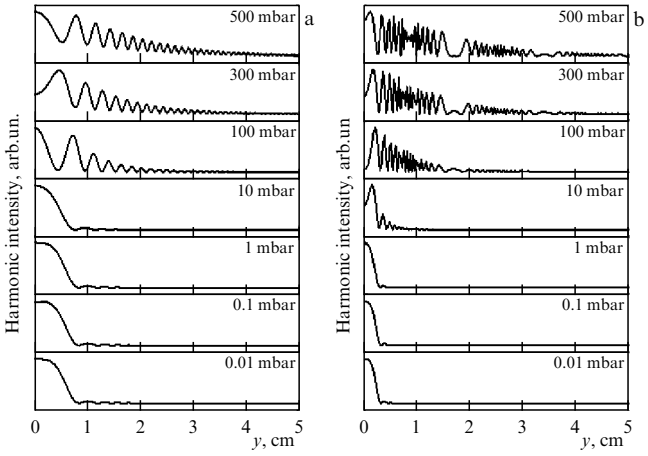

Figure 18. Radial distribution of the 5th (a) and 35th (b) harmonics, calculated for a $L = 1$ cm long argon gas medium for various pressure. The laser field consists of the fundamental and second harmonics of a Ti:Sa laser, the intensity of the field components $\mu_{01} = 0.1$, $\mu_{02} = 0.1$, pulse duration $\tau = 30$ fs, and the angle between the polarizations of the field components $\theta = 0$ [177].

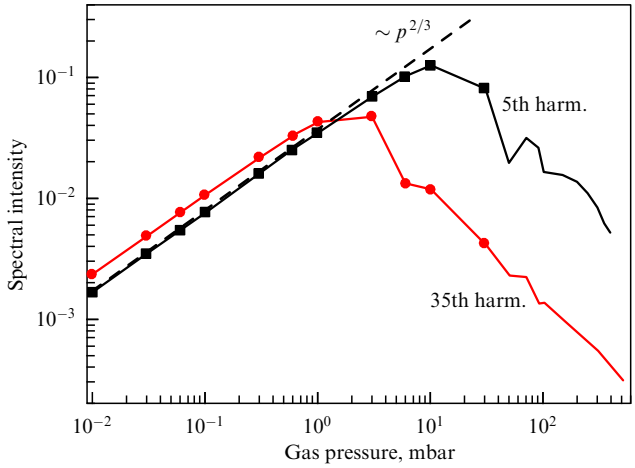

Figure 19. Generation efficiency of the 5th (black curve with squares) and 35th (red curve with dots) harmonics in the dependence of the pressure. The dashed line is the pressure dependence of the square of the number of atoms in the gas. The medium and laser field parameters are similar to those in Fig. 18 [177].

intensity in space is characteristic of both low (Fig. 18a) and high (Fig. 18b) harmonics. With increasing pressure, the spatial distribution changes: radiation propagating at a zero angle to the direction of the wavevector of the laser radiation no longer forms the most intense peak, and conical emission peaks appear in the frequency-angular spectra. Their presence is due to the interference of the contributions of different atoms. A similar angular distribution of harmonics was observed experimentally for both low [181] and high harmonics [182]. The nature of the appearance of additional peaks in the angular spectrum of the medium response is in the constructive and destructive interference of the contributions of different atoms, which depends on the pressure (number of atoms) [183–185].

To study the integral characteristic of the generated radiation, we perform integration of the radial distribution. This results in the dependence of the radiation generation efficiency calculated for a given harmonic at fixed values of the medium parameters. Figure 19 shows the integral generation efficiency of the 5th and 35th harmonics for various pressure of the gas medium. The dependencies show the following features: (1) the spectral intensity of harmonics at low pressures increases proportionally to the square of the number of atoms in the chain that forms it (given the one-dimensionality of the model, the spectral intensity is proportional to the pressure of the gas medium to the power of $2/3$ or to the square of the gas pressure in the capillary); the quadratic increase in the efficiency of harmonic generation indicates that the radiation of different atoms in the chain interferes coherently; (2) with a further increase in pressure, the dependences of the efficiency of harmonic generation are saturated, and the spectral intensity of the harmonics decreases, forming a region of 'optimal' pressure for each harmonic. The presence of 'optimal' pressure p_{opt} has been confirmed by numerous experiments, see, for example, [181].

Comparing Figs 18 and 19, it can be noted that the harmonic generation efficiency ceases to increase when additional components of the angular spectrum increase in the spatial distribution, since the appearance of such ring structures in the spatial distribution indicates destructive interference of the contributions of different atoms, reducing the overall intensity of the generated radiation. This is the nature of the emergence of 'optimal' gas pressure.

The results of numerical studies allow one to propose a simple relationship linking the harmonic number H, the length of the medium L, and the 'optimal' pressure in the medium p_{opt} for the maximum spectral intensity of a given harmonic:

$$LHp_{\text{opt}} = \text{const}\,. \tag{74}$$

This formula agrees well with experimental data [186] and can be used to 'fine-tune' the generation efficiency of a given harmonic (or groups of harmonics) in an experiment. The studies were performed for unfocused beams. In the case of focusing elements in the optical system, the parameter L is the minimal between the total length of the medium and the waist length.

3.7 Quasi-phase matching of high-order harmonic radiation

Consider quasi-phase matching (QPM) effects arising in periodic media, that is, media in which the spatial distribution of emitting particles is not uniform. There are several ways to create such a media: a set of gas jets, a set of plasma clouds, gas-cluster media, or gas mixtures. Density profiling of the medium is the most effective way to create conditions for quasi-phase matching of harmonics [81]. QPM effects can also be observed in continuous gas media interacting with a laser field whose parameters (e.g., intensity) are nonuniformly distributed within the medium.

At first, consider the QPM in a periodic gas medium. As an example, consider a sequence of argon gas jets with width d separated by vacuum gaps of the same length, forming a gas medium of length L. This sequence of gas jets is located along the axis of propagation of the laser radiation. Let us assume that the total length of the medium $L = 0.5$ cm, $d = 0.03$ and 0.08 cm (the parameters of the medium were selected to fit the experimental conditions in [187]). The laser radiation is dual-frequency, consisting of linearly polarized fundamental and second harmonics of a Ti:Sa laser, the angle between the polarization of which $\theta = 0$. Figure 20a shows the 18th harmonic generation efficiency in the dependence of pressure. It is evident that in the case of a spatially profiled medium, after the 'optimal' pressure p_{opt}, there is a pressure region $p_{\text{opt, QPM}}$ where the harmonic generation efficiency is almost an order of magnitude higher. A similar increase in the harmonic generation efficiency was experimentally observed in [187]. This increase arises due to the QPM effect, in which the condition of destructive interference of different atoms is violated in the region of pressures greater than p_{opt}. As a result, conditions are created for a new set of atoms generating radiation of comparable phase. These conditions arise in the region of high pressures (compared to the 'optimal' pressure region) and, consequently, for a larger number of atoms, which leads to an increase in the harmonic generation efficiency.

In the region of the new optimal pressure $p_{\text{opt,QPM}}$, the spatial distribution of radiation generated in a set of gas jets has a Gaussian structure (Fig. 20b, black curve with squares), while the spatial distribution for a continuous gas medium has a ring-shaped structure (Fig. 20b, red curve with dots). A similar change in the spatial distribution was also observed experimentally for a set of plasma plumes in [187]. Note that the higher generation efficiency for a continuous medium, which is observed in the region of low pressures, arises

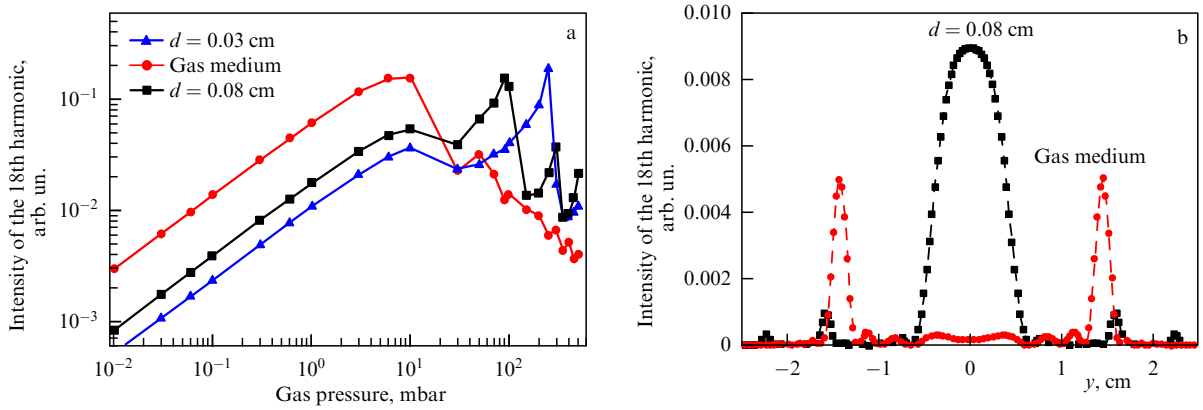

Figure 20. (a) Intensity of the 18th harmonic in the dependence of the gas pressure and (b) the spatial distribution of intensity on the detector at a pressure of 100 mbar, calculated for a set of 3 gas jets with $d = 0.08$ cm (black curve with squares), 8 gas jets with $d = 0.03$ cm (blue curve with triangles) and an extended gas (red curve with dots). The total length of the medium $L = 0.5$ cm [177].

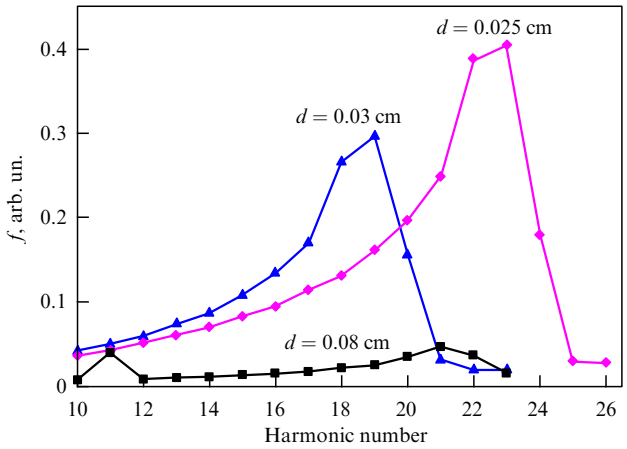

Figure 21. The QPM gain of harmonics, calculated for some harmonics at $p = 250$ mbar, $L = 0.5$ cm and a set of gas jets with widths $d = 0.08$ cm (black curve with squares), $d = 0.03$ cm (blue curve with triangles) and $d = 0.025$ cm (pink curve with diamonds) [177].

because a continuous medium, for a fixed length, contains twice as many atoms as a medium consisting of a set of gas jets. In this regard, in the region where constructive interference from various sources is observed, the generation efficiency is higher.

For further research, it is convenient to introduce a quantity f as the QPM gain, which is equal to the ratio of the response magnitude of the medium to the maximum response of a single atom, calculated for the given parameters of the laser field. The quantity f defined in such a way is close in value to the parameter that is used to study the effects of the QPM in plasma media [188].

Figure 21 shows the QPM gain calculated for a part of the spectrum of gas jets response at a pressure of $p = 250$ mbar (at which the efficiency of generating the 18th harmonic is maximal at $d = 0.03$ cm, see Fig. 20a) and for various values of the jet widths d: from 0.025 to 0.08 cm while maintaining the total length of the medium $L = 0.5$ cm. It is evident that the quasi-phase matching conditions are satisfied not only for a given harmonic, but also for a whole group of harmonics with close numbers (for example, the 18th and 19th harmonics in the case of $d = 0.03$ cm). Moreover, by changing d, one can effectively control the region of harmonics for which the quasi-phase matching conditions are satisfied: as the value of d increases, the region of amplified harmonics shifts toward their lower numbers. Such a dependence is also observed in the experiment [189].

Figure 22 shows the spectral distribution of the QPM gain, calculated for two gas jet widths: $d = 100$ μm (black curve) and $d = 50$ μm (red curve), two wavelengths: (a) $\lambda = 800$ nm and (b) $= 1310$ nm, presented for convenience in eV. As the width of the gas jets decreases, the spectral region for which the QPM effect is manifested shifts toward the long-wavelength region. This trend is also confirmed for other pump wavelengths (see Fig. 22b for $\lambda = 1310$ nm). Numerical calculations allow one to conclude that the number H of the harmonic maximally amplified in the spectrum is inversely proportional to the width d of the gas jet:

$$Hd = \text{const}\,. \tag{75}$$

Thus, varying the jet width allows one to shift the spectral position of the peak of the harmonic amplified by the QPM. Furthermore, it's important to note that as the width of the gas medium decreases, the amplification efficiency increases. The rate of increase in the QPM gain:

$$f \sim d^{-1.5}\,. \tag{76}$$

Note that the calculated spectrum of the QPM gain contains several peaks (Fig. 22a), while in experiment only one peak is usually observed [189]. This may be due to the influence of the uncertainty of gas jet parameters. To test this hypothesis, the study of the influence of the inaccuracy of determining the gas jets width on the distributions of the QPM gain were performed. The gas jets width was set as follows: $d = d_0 + d_1 g$, where $d_0 = 50$ μm, the value d_1 varies within the interval $(0, 0.1d_0)$ and specifies the 'amplitude' of the random variable g, distributed in the interval $(-0.5, 0.5)$ and changing its value during the formation of each jet. Figure 23a shows the spectra of the QPM gain, calculated for d_1 from 0 to $0.1d_0$. It is evident that inaccurate specification of the gas jets width primarily affects the gain of the higher-frequency QPM peaks. Thus, at $d_1 = 0.01d_0$, the gain of the first QPM peak decreases by 5%, while the gain of the second and third QPM peaks decreases by 40% and 60%, respectively (Fig. 23b). A further increase in the d_1 leads to a more significant decrease in the gain of all QPM peaks. Apparently, such a high sensitivity of the QPM gain to the accuracy of determination and regularity of setting the widths of gas jets is an obstacle to the experimental confirmation of the presence of the gain of the high-frequency peaks.

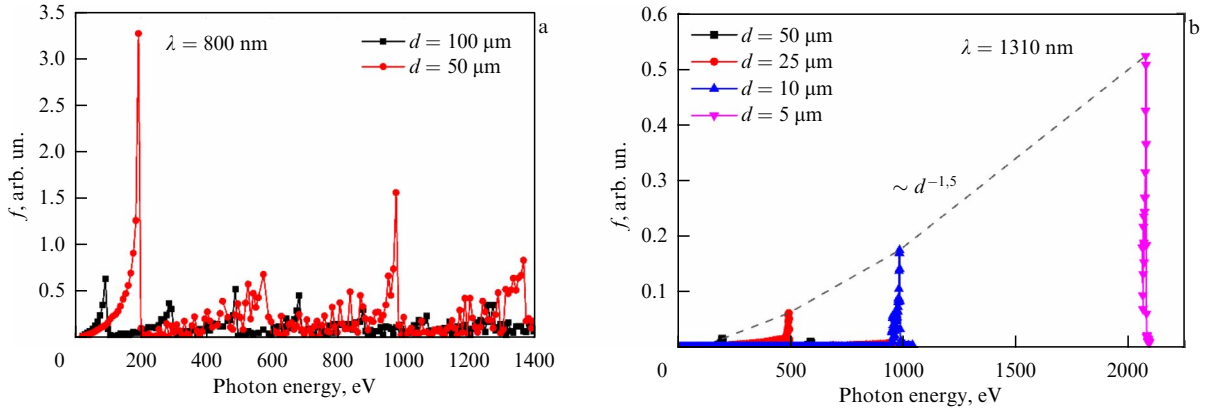

Figure 22. Spectrum of the QPM gain for $p = 230$ mbar, $L = 0.5$ cm. (a) $\lambda = 800$ nm, $d = 100$ μm (black curve with squares), $d = 50$ μm (red curve with dots), (b) $\lambda = 1310$ nm, $d = 50$ μm (black curve with squares), $d = 20$ μm (red curve with dots), $d = 10$ μm (blue curve with triangles), $d = 5$ μm (purple curve with triangles) [166].

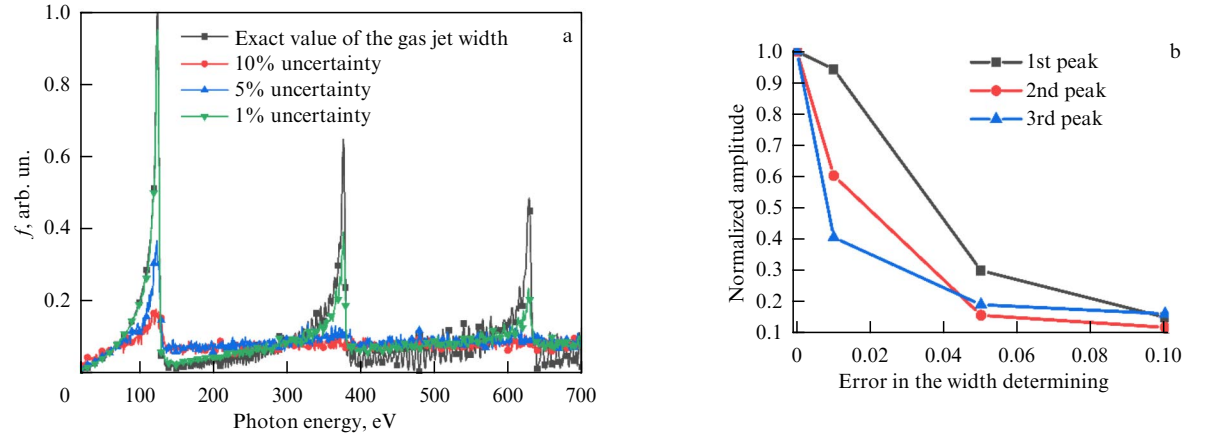

Figure 23. (a) Spectrum of the QPM gain in a medium representing a set of gas jets with $d_0 = 50$ μm and $d_1 = 0$ (black curve with squares), $d_1 = 0.01d_0$ (green curve with triangles), $d_1 = 0.05d_0$ (blue curve with triangles), $d_1 = 0.1d_0$ (red curve with dots). Pressure $p = 230$ mbar, medium length $L = 0.5$ cm, wavelength $\lambda = 800$ nm. (b) Normalized gain of the d_1 QPM peak depending on the [190].

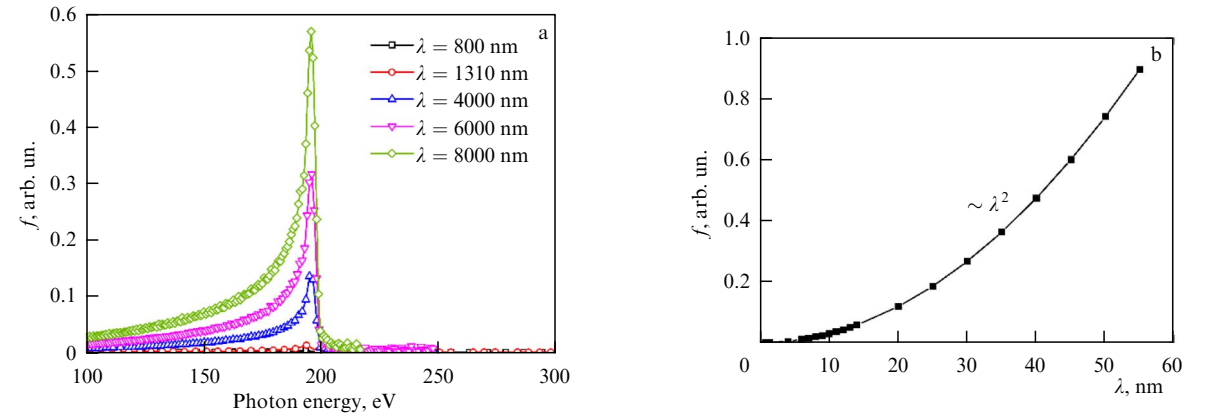

Figure 24. (a) Spectrum of the QPM gain calculated for several laser wavelengths: $\lambda = 800$ nm (black curve with squares), 1310 nm (red curve with dots), 4 μm (blue curve with triangles), 6 μm (purple curve with triangles), 8 μm (green curve with diamonds) at a fixed gas jet width of $d = 50$ μm and gas pressure of $p = 230$ mbar. (b) The QPM gain for the harmonic with a photon energy of ~ 196 eV in the dependence of the laser wavelength [166].

Consider in more detail the influence of the laser radiation wavelength on the magnitude of the harmonic gain. For this, a series of numerical calculations of the response of an extended gas medium to the action of a two-frequency (fundamental and second harmonics) laser field of different wavelengths were performed. The results are shown in Fig. 24a. It can be seen that the photon energy of radiation for which the QPM conditions are best satisfied does not change with laser wavelength (the harmonic number for which the QPM conditions are satisfied increases with laser wavelength). At the same time, the QPM gain for a given photon energy increases proportionally to the square of the laser wavelength (Fig. 24b):

$$f \sim \lambda^2 . \tag{77}$$

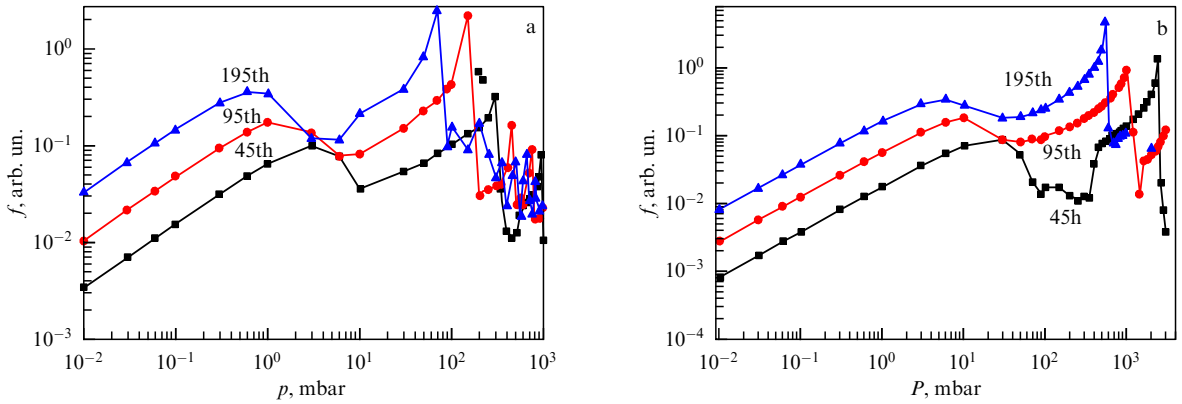

Figure 25. The QPM gain in the dependence of the gas pressure, calculated for the 45th (black curve with squares), 95th (red curve with dots), and 195th (blue curve with triangles) harmonics. Calculations were performed for $d = 100$ μm, (a) $\lambda = 800$ nm and (b) $\lambda = 6000$ nm [190].

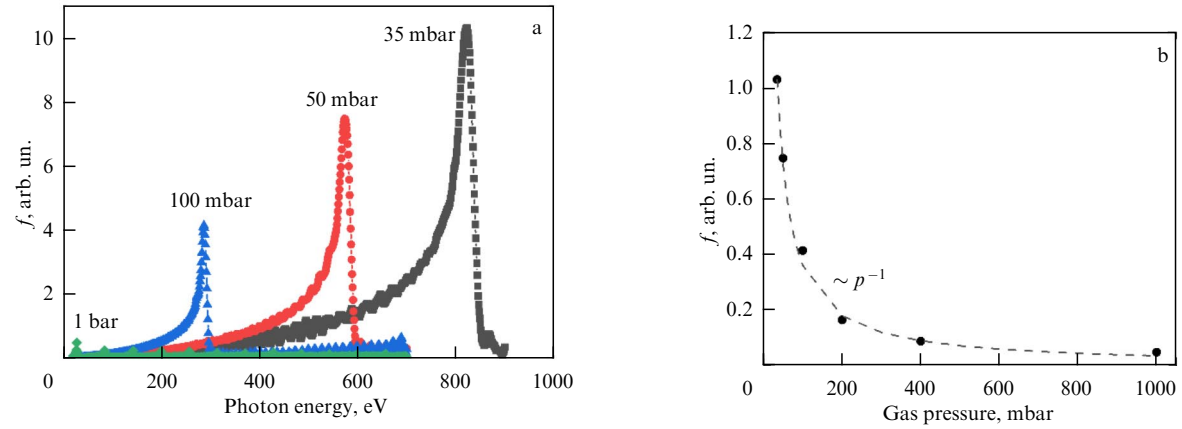

Figure 26. (a) Spectrum of the QPM gain, calculated for several values of gas pressure: $p = 35$ mbar (black curve with squares), 50 mbar (red curve with dots), 100 mbar (blue curve with triangles), 1 bar (green curve with diamonds). (b) The QPM gain in the dependence of the gas pressure. The dots show the results of the numerical study, the dashed line is the approximating curve. Gas jet width $d = 50$ μm, laser wavelength $\lambda = 800$ nm [190].

It appears that this is the most effective method of compensating for the decrease in radiation efficiency with increasing pump wavelength [61–63]. A comparative analysis of experimentally measured harmonic gain factors [188] located in the QPM region and generated in plasma plumes shows that when the wavelength of the laser source changes, the gain of the harmonic signal due to the QPM increases as $f_{\text{exp}} \sim \lambda^{2.44}$, which is close to the discovered theoretical dependence.

Another important control parameter of the problem is the pressure in the gas jets. To investigate the influence of this factor on the QPM gain, numerical studies of the generation efficiency of the 45th, 95th and 195th harmonics were carried out for different gas pressures from 0.01 mbar to 1 bar at a fixed value of the gas jet width ($d = 100$ μm) and for two wavelengths of the main component of the laser field: $\lambda = 800$ nm (Fig. 25a) and $\lambda = 6$ μm (Fig. 25b). It is evident that the dependences of the QPM gain on pressure have a multi-peak structure. The first peak (wider, in the region of low pressures) coincides with the peak of the unprofiled medium. The second peak corresponds to the conditions of the QPM. The pressure $p_{\text{opt,QPM}}$, at which this peak is observed, the wavelength λ of the laser radiation and the harmonic number H are related to each other as follows:

$$\frac{H}{\lambda} p_{\text{opt, QPM}} = \text{const}\,. \tag{78}$$

Thus, the position of the peak of the QPM gain changes inversely proportional to the pressure in the medium: by decreasing the pressure, it is possible to shift the peak of the QPM gain to the short-wavelength region of the spectrum. This can be explained by the fact that the coherence length is inversely proportional to the detuning of the wavevectors Δk, which for a plane wave is proportional to pH [191]. As a result, the QPM condition, the equality of the coherence length and the width of the gas jets, is realized for harmonics with a higher number at a lower gas pressure. At the same time, calculations show that, along with the shift of the peak of the QPM gain to the short-wavelength region, its amplitude also increases. This counterintuitive result (as the pressure decreases, the number of atoms that generate harmonics decreases) can be explained by the dependence of the refractive index on pressure: as the pressure decreases, the oscillation period of the harmonic generation efficiency [177] increases, which leads to an increase in the number of atoms generating radiation and interfering constructively.

The QPM gain f appears to be inversely proportional to the gas pressure p:

$$f \sim p^{-1}\,. \tag{79}$$

Indeed, as the results of numerical studies carried out for jets with $d = 50$ μm and shown in Fig. 26, with increasing pressure both the number of the amplified harmonic and the QPM gain decrease.

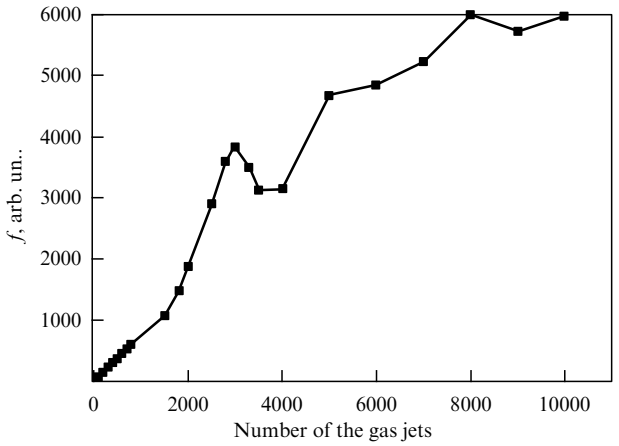

Figure 27. The QPM gain of the 195th harmonic in the dependence of the number of jets at $\lambda = 6$ μm, $d = 50$ μm, $p_{\text{opt,QPM}} = 1.1$ bar [166].

Although for the laser field parameters used in the numerical experiment (for a medium with $d = 50$ μm interacting with a dual-frequency laser field generated by the fundamental and second harmonics of a Ti:Sa laser), the QPM-enhanced harmonics lie outside the cutoff frequency [192]. The proposed optimization of the harmonic efficiency may be useful, since the position of the QPM-enhanced harmonics (in eV) does not depend on the laser wavelength (Fig. 24a), and this enhanced harmonic may be located before the cutoff frequency if, for example, the laser wavelength increases [193].

Finally, we will clarify the effect of the number of jets on the harmonic amplification efficiency with QPM. Numerical studies (at $\lambda = 6$ μm, 195th harmonic, $d = 50$ μm, $p_{\text{opt,QPM}} = 1.1$ bar) showed that changing the number of gas jets does not affect the number of the maximally amplified harmonic, but does affect the magnitude of the gain (Fig. 27). It is evident that with a small number of jets, the QPM gain is proportional to their number, since with an increase in this number, the total length of the medium and the number of atoms generating radiation increase. With a further increase in the number of jets, saturation occurs in the dependence.

Let us separately consider the influence of the QPM on the ellipticity of the generated harmonics. When a two-frequency (fundamental and second harmonic) laser field acts on a single atom, as shown in Fig. 28, the ellipticity of odd harmonics depends significantly on the time delay between the pulses acting on the atom and varies over a wide range from 0 to 0.3 (using the example of the generation of the 5th harmonic in an argon atom from a Cr:Forsterite laser source, laser wavelength $\lambda = 1.24$ μm, pulse duration 120 fs, intensity of the fundamental harmonic $I_1 \sim 10^{13}$ W cm^{-2}, intensity of the second one , angle between the polarization vectors of the components $\theta = \pi/4$), whereas the ellipticity of even harmonics remains low (for the 6th harmonic — less than 0.03).

Spatial profiling of the medium can change the ellipticity of the generated harmonics (Fig. 29a). When the components of a dual-frequency laser field act on the medium synchronously, with zero time delay, the ellipticities of both even and odd harmonics do not exceed 0.01–0.02, i.e., radiation close to linearly polarized is generated. To explore the possibility of increasing the contribution of elliptical radiation from individual atoms, we will calculate the responses of a profiled medium to a dual-frequency laser field with a 0.33 fs time delay between its components (see Fig. 29). It can be seen that for odd harmonics (5th), the calculated radiation ellipticity has increased significantly, while for even harmonics (6th), the ellipticity remains virtually unchanged. This is due to the low ellipticity of the even harmonics themselves, generated by individual atoms. It is important to note that, under QPM conditions, by adjusting the delay time between the components of a dual-frequency laser field, it is possible to obtain elliptically polarized harmonic radiation.

4. Nonlinear response of a medium as the atom response in the near-field

4.1 Analytical calculation of the nonlinear susceptibility of a medium

When studying the properties of harmonic radiation generated in dense gases and condensed media, the use of an interference model — that is, representing the total field as the sum of fields from different atoms — becomes difficult to implement for numerical experiments, as it requires highly extensive computations. The most convenient approach in this case is the concept of a continuous medium whose nonlinear properties

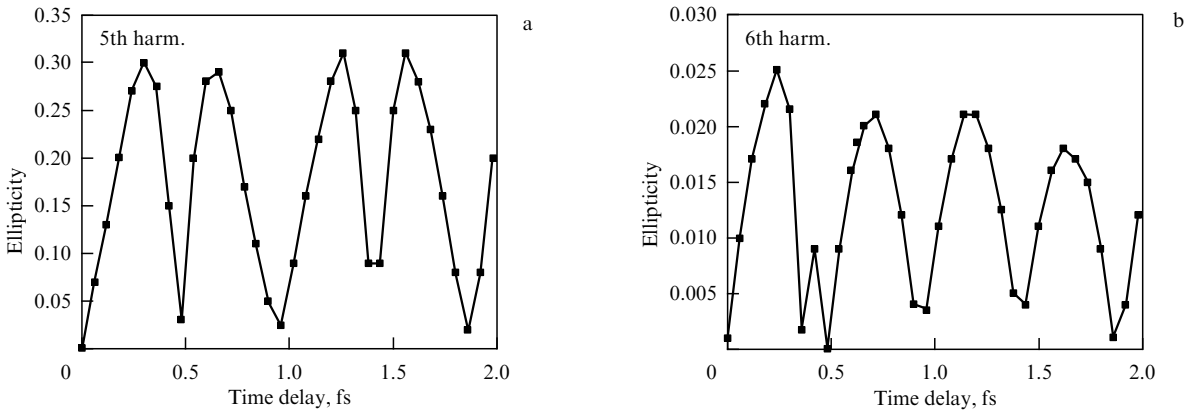

Figure 28. Ellipticity of (a) odd and (b) even harmonics generated by an argon atom, depending on the time delay between the components of a dual-frequency laser field: fundamental and second harmonics of a Cr:Forsterite laser, laser wavelength $\lambda = 1.24$ μm, pulse duration 120 fs, intensity of the fundamental harmonic $I_1 \sim 10^{13}$ W cm^{-2}, intensity of the second one $I_2 \sim 10^{12}$ W cm^{-2}, angle between the polarization vectors of the components $\theta = \pi/4$ [194].

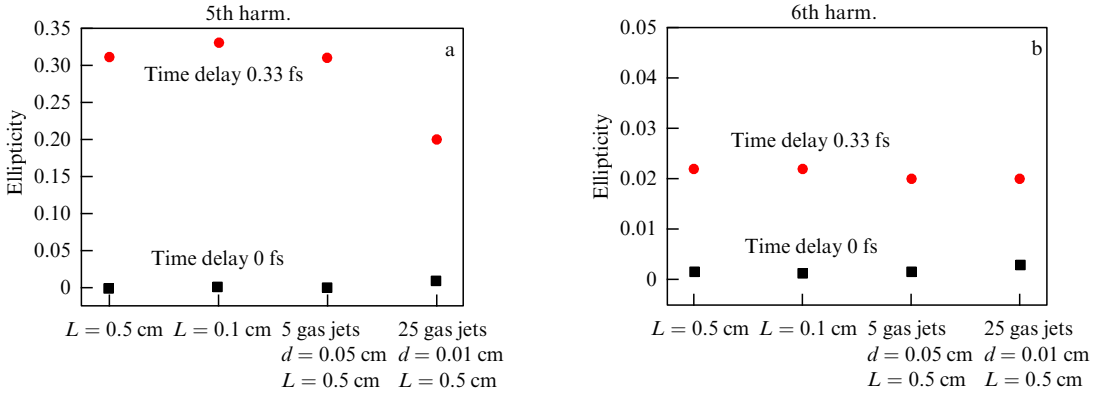

Figure 29. Ellipticity of (a) odd and (b) even harmonics generated by an argon atom for an extended and profiled medium and two time delays (0 fs — black squares, 0.33 fs — red dots) between the components of a two-frequency laser field: the fundamental and second harmonics of a Cr:Forsterite laser, wavelength $\lambda = 1.24$ μm, pulse duration 120 fs [194].

are characterized by nonlinear susceptibilities of several ranks. Using a nonperturbative approach, it becomes possible to analytically calculate the nonlinear susceptibility of a gas medium, which is the subject of this section.

The microscopic current $\mathbf{j}(\mathbf{r}, t)$, calculated using formula (45), based on the solution of system of equations (40) for the population amplitudes of energy levels, generates an electric field $\mathbf{E}_{\text{resp}}(\mathbf{r}, t)$ in the region of space outside the atom (in the Lorentz gauge and in the SI system of units):

$$\mathbf{E}_{\text{resp}}(\mathbf{r}, t) = -\frac{1}{4\pi\varepsilon_0 c^2}\int\left[\frac{\partial\mathbf{j}(\mathbf{r}', t')}{\partial t} - \mathbf{n}'\left(\frac{\partial\mathbf{j}(\mathbf{r}', t')}{\partial t}\mathbf{n}'\right)\right] \times \frac{\mathrm{d}V'}{|\mathbf{r}-\mathbf{r}'|} + \frac{1}{4\pi\varepsilon_0 c}\int\mathbf{n}'\big(\mathbf{j}(\mathbf{r}', t')\mathbf{n}'\big)\frac{\mathrm{d}V'}{|\mathbf{r}-\mathbf{r}'|^2} + \frac{1}{4\pi\varepsilon_0}\int\mathbf{n}'\rho(\mathbf{r}', t')\,\frac{\mathrm{d}V'}{|\mathbf{r}-\mathbf{r}'|^2}\,, \tag{80}$$

where $\mathbf{n}' = \mathbf{r}-\mathbf{r}'/|\mathbf{r}-\mathbf{r}'|$, $t' = t - |\mathbf{r}-\mathbf{r}'|/c$, $\rho(\mathbf{r}', t')$ is the electron density:

$$\rho\,(\mathbf{r}, t) = \psi^*(\mathbf{r}, t)\,\psi(\mathbf{r}, t\,) = \sum_{n,m} a_n^*(t)\,u_n^*(\mathbf{r})\,u_m(\mathbf{r})\,a_m(t)\,, \tag{81}$$

and the vector $\mathbf{r}$ is directed from the center of the atom to the point where the response field value is determined. Denote this vector as $\mathbf{r}_i$, and the radius vector of the atom's position as $\mathbf{R}_i$. The Fourier transform simplifies the calculation of the electric field:

$$\mathbf{E}_{\text{resp},\,i}(\mathbf{r}_i, \omega) = -\frac{\mathrm{i}\omega}{4\pi\varepsilon_0 c^2}\int\frac{\mathbf{j}(\mathbf{r}_i', \omega) - \mathbf{n}_i'\big(\mathbf{j}(\mathbf{r}_i', \omega)\,\mathbf{n}_i'\big)}{|\mathbf{r}_i - \mathbf{r}_i'|} \times \exp\left(\frac{\mathrm{i}\omega}{c}\,|\mathbf{r}_i - \mathbf{r}_i'|\right)\mathrm{d}^3\mathbf{r}_i' + \frac{1}{4\pi\varepsilon_0 c}\int\frac{\mathbf{n}_i'\big(\mathbf{j}(\mathbf{r}_i', \omega)\,\mathbf{n}_i'\big)}{|\mathbf{r}_i - \mathbf{r}_i'|^2}\exp\left(\frac{\mathrm{i}\omega}{c}|\mathbf{r}_i - \mathbf{r}_i'|\right)\mathrm{d}^3\mathbf{r}_i' + \frac{1}{4\pi\varepsilon_0}\int\frac{\mathbf{n}_i'\rho(\mathbf{r}_i', \omega)}{|\mathbf{r}_i - \mathbf{r}_i'|^2}\exp\left(\frac{\mathrm{i}\omega}{c}|\mathbf{r}_i - \mathbf{r}_i'|\right)\mathrm{d}^3\mathbf{r}_i'\,. \tag{82}$$

To calculate the susceptibility of a medium, it is necessary to sum the electric fields generated at a given point

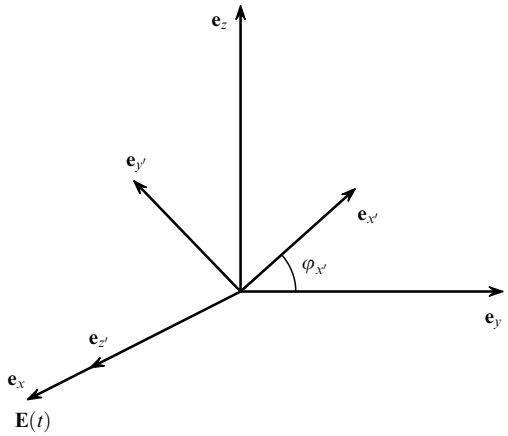

Figure 30. Selecting an atomic reference frame for calculating the atomic response to a laser field [195].

$\mathbf{r} = (r, \theta, \varphi)$ by all the atoms of a medium, and then average over these points. The value of the response field of an atom depends only on the position of the vector $\mathbf{r}_i$ in the atom's reference frame. Let us mentally transfer all the atoms to the origin of coordinates; then the vectors $\mathbf{r}_i$ will exactly coincide with the position of the atoms in space in the original picture. For the clarity of the subsequent presentation, we will align the direction of propagation of the laser field with the unit vector $\mathbf{e}_z$, the direction of polarization of the laser field with the unit vector $\mathbf{e}_x$, and we will denote the vectors $\mathbf{r} = (r, \theta, \varphi)$ by $\mathbf{r}_i$, position the atom's reference frame $\{\mathbf{e}_{x'}, \mathbf{e}_{y'}, \mathbf{e}_{z'}\}$ so that $\mathbf{e}_{z'} = \mathbf{e}_x$, and the unit vector $\mathbf{e}_{x'}$ is rotated the angle $\varphi_{x'}$ relative to $\mathbf{e}_y$ (Fig. 30). Then the averaged response field of the atoms of the medium will be the result of summing the field (82), firstly, over the vector $\mathbf{r} = (r, \theta, \varphi)$, and secondly, over the angle $\varphi_{x'}$:

$$\big\langle\mathbf{E}_{\text{resp}}(\omega)\big\rangle = n_{\text{at}}\int_{r_0}^{\infty} r^2\exp(-\gamma r)\,\mathrm{d}r\int_0^{\pi}\sin\theta\,\mathrm{d}\theta \times\int_0^{2\pi}\mathrm{d}\varphi\int_0^{2\pi}\frac{\mathrm{d}\varphi_{x'}}{2\pi}\,\mathbf{E}_{\text{resp}}(\mathbf{r}, \omega)\,, \tag{83}$$

where $n_{\text{at}} = p/k_{\text{B}}T$ is the concentration of atoms in the medium, p is the pressure of the gas medium, k_{B} is Boltzmann's constant, T is the temperature, $r_0 = \sqrt[3]{1/n_{\text{at}}}$ and is half the average distance between atoms. Since integration over r is performed over infinitely large limits,

the phase of the laser field $\exp(i\omega_0 z/c)$ must be taken into account in expression (83). The additional factor $\exp(-\gamma r)$ is due to the loss of coherence in the response fields of atoms located at large distances r, and the value of the parameter γ is then insignificant.

Expression (45) for the microscopic current density $\mathbf{j}(\mathbf{r}', \omega)$ contains an operator $\mathbf{p}$ that, in the dipole approximation, can be represented through the coordinate operator $\mathbf{r}'$: $u_l^*(\mathbf{r}')\,\mathbf{p}u_p(\mathbf{r}') = u_l^*(\mathbf{r}')(im_e/\hbar)(E_l - E_p)\,\mathbf{r}'u_p(\mathbf{r}')$. Therefore, the direction of the microscopic current density vector coincides with the direction of the radius vector $\mathbf{j}(\mathbf{r}', \omega) = \tilde{j}(\mathbf{r}', \omega)\mathbf{r}'$. We will average the response field over the variables $\varphi_{x'}$, φ, θ, r.

In the approximation $r' \ll c/\omega \sim \lambda$ and $r' \ll r$, retaining the terms up to the first power of r'/r only, one can obtain the following expressions included in (82):

$$\frac{\mathbf{r}' - \mathbf{n}'(\mathbf{r}'\mathbf{n}')}{|\mathbf{r} - \mathbf{r}'|} \exp\left(\frac{i\omega}{c}|\mathbf{r} - \mathbf{r}'|\right) \approx \exp\left(\frac{i\omega r}{c}\right)\left(\frac{\mathbf{r}'}{r} - \frac{\mathbf{r}(\mathbf{r}\mathbf{r}')}{r^3}\right) \overrightarrow{\int d\varphi \int d\varphi_{x'}} \frac{\mathbf{r}'\cos\theta'}{r} \exp\left(\frac{i\omega r}{c}\right)\left(1 - \frac{\sin^2\theta}{2}\right)\mathbf{e}_x, \tag{84a}$$

$$\frac{\mathbf{n}'(\mathbf{r}'\mathbf{n}')}{|\mathbf{r} - \mathbf{r}'|^2} \exp\left(\frac{i\omega}{c}|\mathbf{r} - \mathbf{r}'|\right) \approx \exp\left(\frac{i\omega r}{c}\right)\frac{\mathbf{r}(\mathbf{r}\mathbf{r}')}{r^4} \overrightarrow{\int d\varphi \int d\varphi_{x'}} \frac{\mathbf{r}'\cos\theta'}{r^2} \exp\left(\frac{i\omega r}{c}\right)\left(\frac{\sin^2\theta}{2}\right)\mathbf{e}_x, \tag{84b}$$

$$\frac{\mathbf{n}'}{|\mathbf{r} - \mathbf{r}'|^2} \exp\left(\frac{i\omega}{c}|\mathbf{r} - \mathbf{r}'|\right) \approx \frac{1}{r^2}\exp\left(\frac{i\omega r}{c}\right) \times \left[\frac{\mathbf{r}}{r} - \frac{\mathbf{r}'}{r} + \frac{\mathbf{r}(\mathbf{r}\mathbf{r}')}{r^3}\left(2 - \frac{i\omega r}{c}\right)\right] \overrightarrow{\int d\varphi \int d\varphi_{x'}} \frac{\mathbf{r}'\cos\theta'}{r^3} \times \exp\left(\frac{i\omega r}{c}\right)\left[-1 + \frac{\sin^2\theta}{2}\left(2 - \frac{i\omega r}{c}\right)\right]\mathbf{e}_x. \tag{84c}$$

Averaging over the angle θ is performed taking into account the spatial phase of the laser field $\exp(i\omega_0 z/c) = \exp(i\omega_0 r\cos\theta/c)$ along the direction of radiation propagation. Since the kth-order nonlinear susceptibility contains the laser field to the kth power, the phase factor will also be to this power. Then, to average the atomic response field over the angle θ, one can use the following expressions:

$$\int_0^\pi \sin\theta \exp(ib\cos\theta)\,d\theta = 2\frac{\sin b}{b}, \tag{85a}$$

$$\int_0^\pi \sin^3\theta \exp(ib\cos\theta)\,d\theta = \frac{4}{b^2}\left(\frac{\sin b}{b} - \cos b\right), \tag{85b}$$

$$b = \frac{k\omega_0 r}{c}. \tag{85c}$$

The averaged electric field $\langle \mathbf{E}_{\text{resp}}(\omega)\rangle$ is essentially the polarization $\mathbf{P}(\omega) = \varepsilon_0\langle \mathbf{E}_{\text{resp}}(\omega)\rangle$ of the medium, which determines the nonlinear susceptibility tensor of various orders:

$$\langle \mathbf{E}_{\text{resp}}(\omega)\rangle_S = \frac{1}{(\sqrt{2\pi})^{k-1}}\sum_{k=1}^{\infty}\int_{-\infty}^{+\infty} d\omega_1, \ldots, d\omega_{k-1} \times \chi^{(k)}_{S,S_1S_2\ldots S_k}(\omega, \omega_1, \ldots, \omega_{k-1})E_{S_1}(\omega - \omega_1) \times E_{S_2}(\omega_1 - \omega_2)\cdot\ldots\cdot E_{S_k}(\omega_{k-1}). \tag{86}$$

Note that such an of the medium's response in powers of the external field is, strictly speaking, only valid for low values of the external field strength. Therefore, when obtaining an analytical expansion of the current $\mathbf{j}(\mathbf{r}', \omega)$ in powers of the laser field, we will assume that the population of the excited states is small compared to the population of the ground state:

$$\begin{cases} a_0(t) = 1, \\ a_n(t) = 0,\ n > 0. \end{cases} \tag{87}$$

Expand the exponent in (45) into the series:

$$V_{nm}(t) = \sum_{k=0}^{\infty}\frac{1}{k!}\left(-\frac{iq}{\hbar c}\right)^k \int u_n^*(\mathbf{r}')\left(A(t)r'_{z'}\right)^k u_m(\mathbf{r}')\,d^3\mathbf{r}' = \sum_{k=0}^{\infty}\frac{1}{k!}\left(-\frac{iq}{\hbar c}\right)^k A^k(t)(r_x^k)_{nm}. \tag{88}$$

Consider the harmonic laser field $E(t) = E_a/2\,(\exp(i\omega_0 t) + \exp(-i\omega_0 t))$. Then the Fourier transform is $E(\omega) = (\sqrt{2\pi}/2)E_a(\delta(\omega - \omega_0) + \delta(\omega + \omega_0))$, and the vector potential and its kth power read the following:

$$A(t) = i\frac{c}{2\omega_0}E_a\left(\exp(i\omega_0 t) - \exp(-i\omega_0 t)\right),$$
$$A^k(t) = \left(i\frac{c}{2\omega_0}\right)^k E_a^k \sum_{k_1=0}^{k} C_k^{k_1}(-1)^{k_1}\exp\left(i(k - 2k_1)\omega_0 t\right). \tag{89}$$

Here and below $C_k^{k_1} = k!/(k_1!(k - k_1)!)$ is the number of combinations. When solving the system of equations (40) for the amplitudes of the energy level populations and calculating the microscopic current density (45), it is necessary to calculate factors of the form $V_{nl}^{-1}V_{pm}(t)$. In this case, the operator $\hat{V}$, by its definition, is unitary. Furthermore, as follows from the expansion (88), the matrix elements $(r_z^k)_{nm}$ are real and symmetric with respect to the permutation of indices. Then, taking into account (89), the factors $V_{nl}^{-1}V_{pm}(t)$ are reduced to the form:

$$V_{nl}^{-1}V_{pm}(t) = \sum_{k=0}^{\infty}\left(\frac{qE_a}{\hbar\omega_0}\right)^k \frac{1}{2^k}R^k_{nl,pm}\sum_{k_3=0}^{k} C_k^{k_3}(-1)^{k_3} \times \exp\left(i(k - 2k_3)\omega_0 t\right), \tag{90a}$$

$$R^k_{nl,pm} = \sum_{k_1}^{k}\frac{(-1)^{k_1}}{k_1!(k - k_1)!}(r_z^{k_1})_{nl}(r_z^{k-k_1})_{pm}. \tag{90b}$$

The matrix elements $R^k_{nl,pm}$ are real numbers and, by virtue of their structure, are antisymmetric with respect to permutations of pairs of indices nl and pm: $R^k_{nl,pm} = (-1)^k R^k_{pm,nl}$. Due to the symmetry of the matrix elements $(r_z^k)_{nm}$ with respect to permutations of indices, the matrix elements $R^k_{nl,pm}$ are symmetric with respect to permutations of indices within pairs of indices: $R^k_{nl,pm} = R^k_{ln,pm} = R^k_{nl,mp}$.

In the first order of smallness in a_n/a_0, assuming $a_0(t) \approx \exp(-iE_0 t/\hbar)$, the equations for the population dynamics of the levels, taking into account (89), are written as:

$$\frac{da_n}{dt} \approx \sum_m\left(-\frac{iE_m}{\hbar}\right)\sum_{k=0}^{\infty}\left(\frac{qE_a}{\hbar\omega_0}\right)^k \frac{R^k_{0m,m0}}{2^k}\sum_{k_1=0}^{k} C^{k_1}_{k_1=0}(-1)^{k_1} \times \exp\left(i(k - 2k_1)\omega_0 t\right)\exp\left(-\frac{iE_0 t}{\hbar}\right). \tag{90}$$

The solution of these equations is:

$$a_0(t) \approx \exp\left(-\frac{\mathrm{i}E_0 t}{\hbar}\right) + \sum_m \left(\frac{E_m}{\hbar\omega_0}\right) \sum_{k=1}^{\infty} \left(\frac{qE_a}{\hbar\omega_0}\right)^k \frac{R^k_{0m,m0}}{2^k} \times \sum_{k_1=0}^{k} C_k^{k_1} (-1)^{k_1} \frac{1-\exp\left(\mathrm{i}(k-2k_1-E_0/\hbar\omega_0)\omega_0 t\right)}{k-2k_1-E_0/\hbar\omega_0}\,, \tag{91a}$$

$$a_n(t)\big|_{n>0} \approx \sum_m \left(\frac{E_m}{\hbar\omega_0}\right) \sum_{k=1}^{\infty} \left(\frac{qE_a}{\hbar\omega_0}\right)^k \frac{R^k_{nm,m0}}{2^k} \times \sum_{k_1=0}^{k} C_k^{k_1} (-1)^{k_1} \frac{1-\exp\left(\mathrm{i}(k-2k_1-E_0/\hbar\omega_0)\omega_0 t\right)}{k-2k_1-E_0/\hbar\omega_0}\,, \tag{91b}$$

The conditions for the applicability of the presented approach follow from the form of solutions (91). In order for the population of all levels except the ground level to be negligible, it is necessary to require that $q\langle r_z\rangle E_a E_0/(\hbar\omega_0)^2 \ll 1$, where $q\langle r_z\rangle$ is the characteristic (maximum) value of the dipole moment of a pair of atomic levels, E_a is the laser field strength, E_0 is the energy of the ground level, $\hbar\omega_0$ and is the energy of a laser field quantum.

Substitute the population amplitudes (91) and the factor (90) into the expressions for the current density (45) and for the electron density (81). They are naturally broken down into three terms: (1) $n=m=0$ and $a_0(t) \approx \exp(-\mathrm{i}E_0 t/\hbar)$, (2) $n=m=0$ and $a_0(t)$ is calculated according to (91a), (3) $n=0$, $m\neq 0$ or $n\neq 0$, $m=0$, and $a_n(t)$, $a_m(t)$, is calculated according to (91b). Taking into account (82)–(86), one can obtain the final expression for the nonlinear susceptibility of an arbitrary order, which can be represented as a product of a numerical factor, factors B_{at} determined by the structure of the atomic levels, and factors B_r determined by averaging the responses of the atoms of the medium:

$$\chi^{(k)}(\omega) = \frac{n_{\mathrm{at}}}{4\pi\varepsilon_0}\left(\frac{qa_{\mathrm{B}}}{\hbar\omega_0}\right)^{k+1} \left(\mathrm{i}\mathrm{Ry} B^j_{\mathrm{at}} B^j_r(\omega,k) + \hbar\omega_0 B^{\rho}_{\mathrm{at}} B^{\rho}_r(\omega,k)\right), \tag{92}$$

where $\mathrm{Ry} = (m_e e^4)/2\hbar^2 = 2.18\times 10^{-18}$ J, $a_{\mathrm{B}} = 5.3\times 10^{-11}$ m is the Bohr radius, the term $B^j_{\mathrm{at}} B^j_r$ is due to the microscopic current, the term $B^{\rho}_{\mathrm{at}} B^{\rho}_r$ is due to the electron density. Moreover, B_{at} and B_r are dimensionless quantities, and the all matrix elements $R^k_{nl,pm}$ and $(r_z^k)_{nm}$ are expressed in units of a_{B}^k.

The factors B_{at} have the form:

$$B^{j,\rho}_{\mathrm{at}}(\omega,k) = B^{j,\rho(0)}_{\mathrm{at}}(\omega,k) + B^{j,\rho(1)}_{\mathrm{at}}(\omega,k)\,, \tag{93a}$$

$$B^{j(0)}_{\mathrm{at}}(\omega,k) = \sum_{lp} \frac{E_l - E_p}{\mathrm{Ry}} (r_z)_{lp} R^k_{0l,p0} \sum_{k_1=0}^{k} C_k^{k_1} (-1)^{k_1}\,, \quad \frac{\omega}{\omega_0} = k - 2k_1\,, \tag{93b}$$

$$B^{\rho(0)}_{\mathrm{at}}(\omega,k) = (r_z)_{00}\,, \quad \frac{\omega}{\omega_0} = 0\,, \tag{93c}$$

$$B^{j(1)}_{\mathrm{at}}(\omega,k) = \sum_{lp} \frac{E_l - E_p}{\mathrm{Ry}} (r_z)_{lp} \sum_m \frac{E_m}{\hbar\omega_0} \sum_{k_1=0}^{k-1} \sum_{k_3=0}^{k_1} \sum_{k_2=0}^{k-k_1} \times \frac{C_{k_1}^{k_3} C_{k-k_1}^{k_2} (-1)^{k_3+k_2}}{k-k_1-2k_2-E_0/\hbar\omega_0} \times \begin{cases} -\sum_n R^{k_1}_{0l,pn} R^{k-k_1}_{nm,m0}, & \frac{\omega}{\omega_0} = k-2k_3-2k_2 \\ -R^{k_1}_{0l,p0} R^{k-k_1}_{0m,m0} + (-1)^{k_1} \sum_{n>0} R^{k_1}_{0l,pn} R^{k-k_1}_{nm,m0}, & \\ \frac{\omega}{\omega_0} = -k+2k_1-2k_3+2k_2\,, & \end{cases} \tag{93d}$$

$$B^{\rho(1)}_{\mathrm{at}}(\omega,k) = \sum_m \frac{E_m}{\hbar\omega_0} \sum_{k_1=0}^{k-1} \frac{C_k^{k_1}(-1)^{k_1}}{k-2k_1-E_0/\hbar\omega_0} \times \left(-\sum_n R^k_{nm,m0}(r_z)_{n0}\right), \ \frac{\omega}{\omega_0} = \begin{matrix} k-2k_1 \\ -k+2k_1 \end{matrix}\,. \tag{93e}$$

The factor B_r have the form:

$$B^j_r(\omega,k) = 2\int_{x_0}^{\infty} \exp\left(\mathrm{i}\frac{\omega}{\omega_0}x\right) \exp(-\gamma x) \times \left[-\mathrm{i}\frac{\omega}{k\omega_0}\sin kx + \frac{1}{(kx)^2}\left(\frac{\sin kx}{kx} - \cos kx\right) \times \left(1 + \mathrm{i}\frac{\omega}{\omega_0}x\right)\right]\mathrm{d}x\,, \tag{94a}$$

$$B^{\rho}_r(\omega,k) = 2\int_{x_0}^{\infty} \frac{\exp\left(\mathrm{i}(\omega/\omega_0)x\right)}{x} \exp(-\gamma x) \times \left[-\frac{\sin kx}{kx} + \frac{1}{(kx)^2}\left(\frac{\sin kx}{kx} - \cos kx\right) \times \left(2 - \mathrm{i}\frac{\omega}{\omega_0}x\right)\right]\mathrm{d}x\,, \tag{94b}$$

where the parameter $x_0 = \omega_0/c\sqrt[3]{n_{\mathrm{at}}}$ is determined by half the average distance between atoms (since the average response field of atoms is determined at points equidistant from the atoms, so that the summation of the response fields begins with atoms located at a distance equal to half the average distance between atoms), and the factor $\exp(-\gamma r)$ is due to the loss of coherence in the response fields of atoms located at greater distances from the observation point.

Expression (92) for the nonlinear susceptibility of a gaseous medium has three notable features. First, it describes the nonlinear properties of the medium, not isolated atoms. Second, it contains an arbitrary order k and therefore allows for the calculation of nonlinear effects, quadratic in the laser field, cubic, etc. Third, it describes various nonlinear processes realized on a nonlinear susceptibility of a certain order, for example, the process $\omega = \omega_0 + \omega_0 + \omega_0 = 3\omega_0$ or $\omega = \omega_0 - \omega_0 + \omega_0 = \omega_0$ due to the nonlinear susceptibility $\chi^{(3)}$.

Let us once again emphasize the approximations within which expression (92) was derived. The long-wavelength approximation $r' \ll c/\omega \sim \lambda$ and the condition of sufficient rarefaction of the gas medium were used: $r' \ll r$, which can be reformulated as $r_0 = 1/\sqrt[3]{n_{\mathrm{at}}} \gg a_{\mathrm{B}}$. This condition is satisfied up to gas medium pressures $p \sim 1$ bar, when $k_0/a_{\mathrm{B}} \approx 70$ (at a temperature of 300 K). The second approximation is the condition of small excitation of atoms, such that the populations of all excited levels are small compared to the

population of the ground level. This condition is satisfied at $(q\langle r_z\rangle E_a E_0)/(\hbar\omega_0)^2 \ll 1$. For example, for a hydrogen atom, $E_0 = 13.6$ eV, with a laser wavelength of 1 μm (the photon energy is $\hbar\omega_0 \approx 1.2$ eV) and $\langle r_z\rangle \approx a_B = 5\times10^{-11}$ m, we obtain the condition for the laser field strength: $E_a \ll 2$ GV m^{-1}, which corresponds to an intensity of $I \ll 5\times10^{15}$ W m^{-2}. In the case of strong excitation of atoms by a laser field, including resonant excitation, an analytical expression for the nonlinear susceptibility is extremely difficult to obtain. However, in this case, numerical calculations of the level population dynamics and the spectrum of the averaged response field will allow one to isolate the value of the nonlinear susceptibility of the medium.

Point out one important feature of the obtained expression (92). As is well known, in a homogeneous medium with an inversion center, the signal of even harmonics should be zero. Direct calculation using formulas (92)–(94) for even k yields a zero signal at all frequencies $\omega = (k-n)\omega_0$, where $n \leqslant k$ is an even number. This agreement with the known analytical fact confirms the validity of the obtained expressions and can also serve as a measure of the accuracy of the numerical calculation of the nonlinear susceptibility of the medium. Indeed, to use expression (92), it is necessary to first calculate the matrix elements $R^k_{nl,pm}$ and $(r^k_z)_{nm}$, which depend significantly on the size and discretization of the spatial computational grid. The fact that the signal of even harmonics is zero can serve as a criterion for the sufficiency of the grid size and discretization.

4.2 Nonlinear susceptibility of and harmonic generation in argon gas

Consider argon as a gaseous medium. Choose a basis of hydrogen-like wavefunctions $u_{nlm}(r,\theta,\varphi)$ with level energies E_n (we neglect spin-orbit interactions, but take into account the incomplete screening of the nuclear charge by inner-shell electrons [167]):

$$u_{nlm}(r,\theta,\varphi) = \sqrt{\frac{(n-l-1)!}{2n(n+l)!}\left(\frac{2Z_{\text{eff}}}{na_B}\right)^3}\exp\left(-\frac{Z_{\text{eff}}r}{na_B}\right) \times\left(\frac{2Z_{\text{eff}}r}{na_B}\right)^l L^{2l+1}_{n-l-1}\left(\frac{2Z_{\text{eff}}r}{na_B}\right)Y_{lm}(\theta,\varphi), \quad (95)$$

$$E_n = -\frac{e^2}{8\pi\varepsilon_0 a_B}\left(\frac{Z_{\text{eff}}}{n}\right)^2, \quad (96)$$

where Z_{eff} is the effective charge of the remaining ion, $a_B = (4\pi\varepsilon_0\hbar^2)/m_e e^2$ is the Bohr radius, $L(x)$ is the generalized Laguerre polynomial, $Y_{lm}(\theta,\varphi)$ is the spherical function, n, l, m and are the principal, orbital, and magnetic quantum numbers, respectively. The value Z_{eff}/n can be determined from spectroscopic data on the energy levels of argon [168]. For the Ar atom, the values Z_{eff} are collected in Table.

Table. Effective charge of the Ar remaining ion, determined from spectroscopic data [168].

Level	Z_{eff}	Level	Z_{eff}	Level	Z_{eff}
3p	3.227	4f	1.005	5f	1.005
3d	1.123	5s	1.761	6s	1.559
4s	2.224	5p	1.545	6p	1.408
4p	1.830	5d	1.101	7s	1.445
4d	1.121				

Note that the energy levels are approximate and do not take into account fine and hyperfine level structure. Therefore, the electronic structure defined in this way should be considered a model, but one that approximates the actual structure.

The values of the nonlinear susceptibilities $\chi^{(3)}$, $\chi^{(5)}$ and $\chi^{(7)}$ for the processes of generation of the 3rd, 5th, and 7th harmonics, calculated using expression (92) under normal conditions (pressure of 1 bar and temperature of 300 K), are presented in Fig. 31 for the range of laser radiation wavelengths from the visible to the mid-infrared. Note that the resulting analytical expression (92) uses the assumption of small amplitudes of the populations of the excited levels and, thus, neglects the resonant transfer of population from one excited level to another.

Nonlinear susceptibilities increase with the laser wavelength and differ severalfold for different frequency combinations: $\chi^{(3)}(\omega_0):\chi^{(3)}(3\omega_0) \approx 3:1$, $\chi^{(5)}(\omega_0):\chi^{(5)}(3\omega_0):\chi^{(5)}(5\omega_0) \approx 10:5:1$, $\chi^{(7)}(\omega_0):\chi^{(7)}(3\omega_0):\chi^{(7)}(5\omega_0):\chi^{(7)}(7\omega_0) \approx 30:20:6:1$ regardless of the laser wavelength.

A signal of a particular harmonic is generated through several different channels. In the visible wavelength range, the dominant contribution at frequency $\omega = n\omega_0$ is made by the lowest-order susceptibility $\chi^{(n)}$. However, the contribution of higher-order susceptibilities is nonzero, although several units or tens of times smaller. Figure 32a shows the amplitude of the 3rd harmonic, normalized to the laser field amplitude, for generation using nonlinear susceptibilities of the 3rd, 5th, and 7th orders. These generation channels have significantly different dependences on the laser intensity. Therefore, at high laser radiation intensities, the efficiency

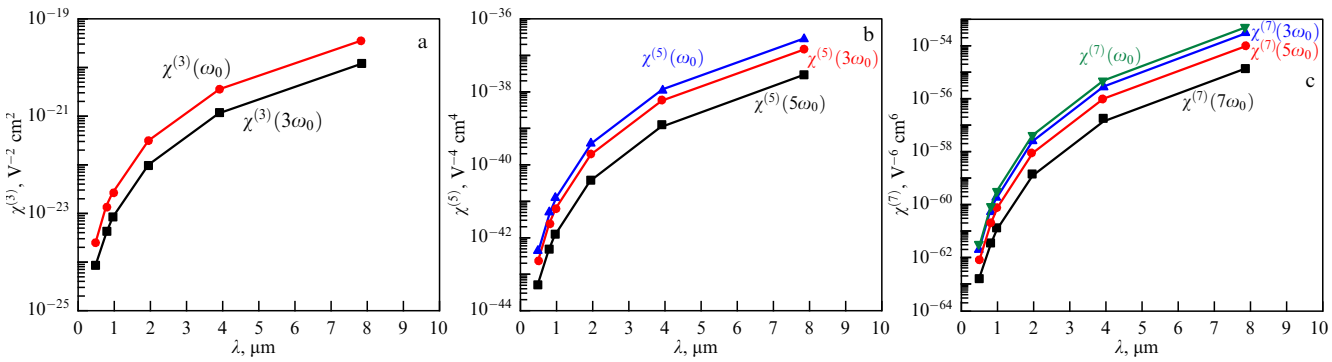

Figure 31. Nonlinear susceptibility of (a) the 3rd, (b) the 5th, and (c) the 7th orders in argon at the pressure of 1 bar and the temperature of 300 K [195].

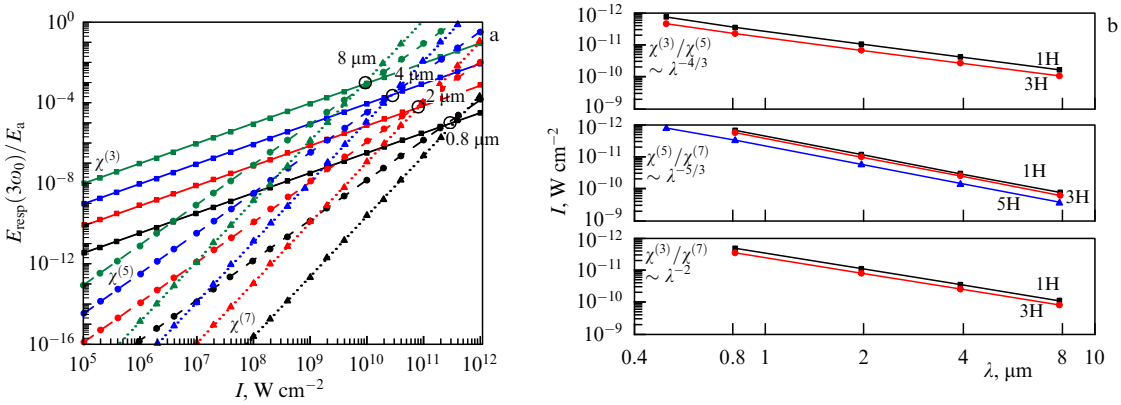

Figure 32. (a) The amplitude of the 3rd harmonic signal, normalized to the amplitude of the laser field, in argon at the pressure of 1 bar and the temperature of 300 K. The circles indicate the laser intensity at which the contribution of nonlinear susceptibilities of different orders to the 3rd harmonic signal becomes equal. (b) Such laser intensity as a function of wavelength [195].

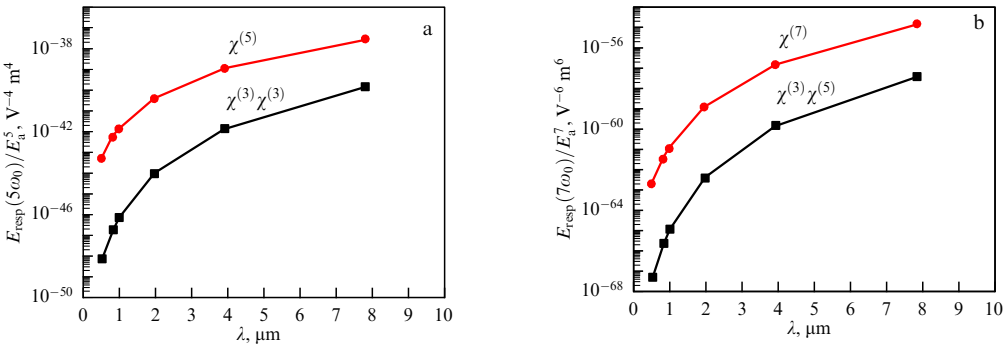

Figure 33. Generation efficiency of (a) the 5th and (b) the 7th harmonics in the direct channel (red curves) and in the cascade channel (black curves) [195].

of the 3rd harmonic generation via the 5th- and the 7th-order nonlinearities begins to exceed the efficiency of the generation channel via the 3rd-order nonlinearity (circles in Fig. 32a). This fact indicates the inconsistency of the series expansion of the medium polarization in powers of the laser field and the transition from the perturbative to the nonperturbative regime of harmonic generation. In the visible wavelength range, this occurs at laser radiation intensities $I > 1$ TW cm^{-2}, which is beyond the approximations used in deriving the analytical expression (92). However, an increase in the laser radiation wavelength leads to a decrease in the intensity of this transition. The same trend is manifested in the case of 1st and 5th harmonic generation. A detailed examination shows that the laser radiation intensity at which this transition occurs scales with wavelength as $\lambda^{-4/3}$ for channels $\chi^{(3)}/\chi^{(5)}$, as $\lambda^{-5/3}$ for channels $\chi^{(5)}/\chi^{(7)}$ and as λ^{-2} for channels $\chi^{(3)}/\chi^{(7)}$ (Fig. 32b). Thus, the shift of the wavelength to the mid-infrared range leads to the fact that even at low laser radiation intensities ($10^{10} - 10^{12}$ W cm^{-2}) the contributions of various nonlinear susceptibilities to the harmonic signal become comparable.

Figure 33 compares the efficiency of 5th and 7th harmonic generation for two different generation channels: the direct channel on $\chi^{(5)}$ and $\chi^{(7)}$, respectively, and the cascade channel on $\chi^{(3)}$ (Fig. 33a). For any wavelength used from 500 nm to 8 μm, the direct channel is significantly stronger (by 5–6 orders of magnitude in signal intensity) than the cascade channel. The vast majority of models of laser radiation propagation in a medium use only the nonlinear susceptibility $\chi^{(3)}$, and higher-order harmonics (greater than third) are generated via a cascade channel. However, the result obtained indicates that higher-order nonlinear susceptibilities cannot be omitted.

The approach proposed to calculating the nonlinear susceptibilities of a medium can be combined with experimental studies to identify promising gaseous media, including synthetic ones, with increased high-order harmonic generation efficiency and a broader generated spectrum.

5. Conclusion

This review describes a nonperturbative approach to studying the response of a single atom to an intense laser field, which allows for the calculation of radiation-matter interactions at the microscopic (quantum-mechanical) level. An interference model is described that, taking into account the specific interactions of radiation with atoms located in the medium, allows for the calculation of the parameters of the generated coherent radiation, taking into account both phase and quasi-phase matching. A method for calculating the values of nonlinear susceptibilities of arbitrary order in an extended gaseous medium is described in detail. The resulting analytical expressions can be used in modern programs for calculating the propagation of high-power laser radiation in matter. The influence of both the parameters of multicomponent arbitrarily polarized laser field and the parameters of the medium on the generation efficiency and polarization properties of the generated coherent short-wavelength radiation is analyzed.

Experimentally oriented theoretical calculations carried out using the described integrated approach showed good qualitative, and in some cases quantitative, agreement with the corresponding experimental results on the characteristics of harmonic generation in gases (Ar, Ne, Xe, $Xe + CO_2$) [77, 82, 165], in plasma (Ag, In) [163, 170, 189, 196, 197], in gas-cluster mixtures (Ar) [198], as well as on the generation of terahertz radiation (CO_2) [199].

The methods considered for controlling the properties of the generated radiation open up new possibilities in the creation of compact multispectral sources of coherent radiation for various applications: for the spectroscopy of macromolecular compounds; for the development of methods for real-time diagnostics of biological, pharmaceutical, and composite materials in medical centers and industries; for the creation of next-generation lithographic devices necessary for micro- and nanoelectronics; for the development of methods for conducting preliminary laboratory studies of new materials with the subsequent use of mega-science class facilities (synchrotron radiation sources, free-electron lasers); for the development of methods for generating attosecond laser pulses; and for the generation of 'seed' radiation in modern X-ray free-electron lasers, which allows for the improvement of both the energy and coherence properties of the generated radiation [200].

The authors are very grateful to professor A.V. Andreev for useful discussions of the results presented in the overview. This work was supported by the Russian Science Foundation (grant no. 24-22-00188, https://rscf.ru/project/24-22-00188/).

References

1. Akhmanov S A (Ed.) *Moshchnye Piko- i Femtosekundnye Lazernye Sistemy*: *Veshchestvo v Sverkhsil'nykh Svetovykh Polyakh* (High-Power Pico- and Femtosecond Laser Systems; Matter in Ultra-intense Light Fields) (Results of Science and Technology, Ser. Modern Problems of Laser Physics, Vol. 4) (Moscow: VINITI, 1991)
2. Borrego-Varillas R, Lucchini M, Nisoli M *Rep. Prog. Phys.* **85** 066401 (2022)
3. Hassan M Th *ACS Photonics* **11** 334 (2024)
4. Arkhipov R et al. *Sci. Rep.* **11** 1961 (2021)
5. Bloembergen N *Nelineinaya Optika* (Moscow: Mir, 1966); Translated from English: *Nonlinear Optics* (New York: W. A. Benjamin, 1965)
6. Belenov E M, Nazarkin A V *JETP Lett.* **51** 288 (1990); *Pis'ma Zh. Eksp. Teor. Fiz.* **51** 252 (1990)
7. Maimistov A I *Quantum Electron.* **30** 287 (2000); *Kvantovaya Elektron.* **30** 287 (2000)
8. Kozlov S A *Opt. Spectrosc.* **79** 267 (1995); *Opt. Spektrosk.* **79** 290 (1995)
9. Kamchatnov A M *Phys. Usp.* **64** 48 (2021); *Usp. Fiz. Nauk* **191** 52 (2021)
10. Rosanov N N, Arkhipov M V, Arkhipov P M *Phys. Usp.* **67** 1129 (2024); *Usp. Fiz. Nauk* **194** 1196 (2024)
11. Sazonov S V *JETP Lett.* **102** 834 (2015); *Pis'ma Zh. Eksp. Teor. Fiz.* **102** 951 (2015)
12. Delone N B, Krainov V P *Atom v Sil'nom Svetovom Pole* (Moscow: Energoatomizdat, 1984); Translated into English: *Atoms in Strong Light Fields* (Berlin: Springer-Verlag, 1995)
13. Fedorov M V *Elektron v Sil'nom Svetovom Pole* (Electron in Strong Light Fields) (Moscow: Nauka, 1991)
14. Koroteev N I, Shumai I L *Fizika Moshchnogo Lazernogo Izlucheniya* (Physics of High-Power Laser Radiation) (Moscow: Nauka, 1991)
15. Delone N B *Vzaimodeistvie Lazernogo Izlucheniya s Veshchestvom* (Interaction of Laser Radiation with Matter) (Moscow: Nauka, 1989)
16. Delone N B, Krainov V P *Osnovy Nelineinoi Optiki Atomarnykh Gazov* (Fundamentals of Nonlinear Optics of Atomic Gases) (Moscow: Nauka, 1986)
17. Il'inskii Yu A, Keldysh L V *Vzaimodeistvie Elektromagnitnogo Izlucheniya s Veshchestvom* (Moscow: Izd. MGU, 1989); Translated into English: *Electromagnetic Response of Material Media* (New York: Plenum Press, 1994)
18. Rapoport L P, Zon B A, Manakov N L *Teoriya Mnogofotonnykh Protsessov v Atomakh* (Theory of Multiphoton Processes in Atoms) (Moscow:Atomizdat, 1978)
19. Ganeev R A *Resonance Enhancement in Laser-Produced Plasmas*: *Concepts and Applications* (New York: John Wiley and Sons, 2018) DOI:10.1002/9781119472346
20. Ganeev R A *Frequency Conversion of Ultrashort Pulses in Extended Laser-Produced Plasmas* (Singapore: Springer, 2016) DOI:10.1007/978-981-10-0194-9
21. Ganeev R A *High-Order Harmonic Generation in Laser Plasma Plumes* (London: Imperial College Press, 2012)
22. Delone N B et al. *Sov. Phys. Usp.* **19** 711 (1976); *Usp. Fiz. Nauk* **120** 3 (1976)
23. Delone N B, Krainov V P *Phys. Usp.* **38** 1247 (1995); *Usp. Fiz. Nauk* **165** 1295 (1995)
24. Kim A V, Ryabkin M Yu, Sergeev A M *Phys. Usp.* **42** 54 (1999); *Usp. Fiz. Nauk* **169** 58 (1999)
25. Popov V S *Phys. Usp.* **47** 855 (1999); *Usp. Fiz. Nauk* **174** 921 (1999); Popov V S *Phys. Usp.* **42** 733 (1999); *Usp. Fiz. Nauk* **169** 819 (1999)
26. Platonenko V T, Strelkov V V *Quantum Electron.* **28** 564 (1998); *Kvantovaya Elektron.* **25** 582 (1998)
27. Zheltikov A M *Phys. Usp.* **60** 1087 (2017); *Usp. Fiz. Nauk* **187** 1169 (2017)
28. Löffler T et al. *Acta Phys. Polon. A* **107** 99 (2005)
29. Tzortzakis S et al. *Opt. Lett.* **27** 1944 (2002)
30. Bartel T et al. *Opt. Lett.* **30** 2805 (2005)
31. Andreeva V A et al. *Phys. Rev. Lett.* **116** 063902 (2016)
32. Ushakov A A et al. *Phys. Usp.* **67** 157 (2024); *Usp. Fiz. Nauk* **194** 169 (2024)
33. Yang S-H et al. *IEEE Trans. Terahertz Sci. Technol.* **4** 575 (2014)
34. Ponomarev D S et al. *Phys. Usp.* **67** 3 (2024); *Usp. Fiz. Nauk* **194** 2 (2024)
35. Zhang X C, Shkurinov A P, Zhang Y *Nature Photon.* **11** 16 (2017)
36. Kuchiev M Yu *JETP Lett.* **45** 404 (1987); *Pis'ma Zh. Eksp. Teor. Fiz.* **45** 319 (1987)
37. Corkum P B *Phys. Rev. Lett.* **71** 1994 (1993)
38. Platonenko V T *Quantum Electron.* **31** 55 (2001); *Kvantovaya Elektron.* **31** 55 (2001)
39. Schafer K J et al. *Phys. Rev. Lett.* **70** 1599 (1993)
40. Schötz J et al. *Phys. Rev. X* **10** 041011 (2020)
41. Ganeev R A *Phys. Usp.* **56** 772 (2013); *Usp. Fiz. Nauk* **183** 815 (2013)
42. Vampa G et al. *Opt. Express* **26** 12210 (2018)
43. Goulielmakis E, Brabec T *Nature Photon.* **16** 411 (2022)
44. Weissenbilder R et al. *Nature Rev. Phys.* **4** 713 (2022)
45. Ganeev R A *Appl. Phys. B* **129** 17 (2023)
46. Schütz G, Knülle M, Ebert H *Phys. Scr.* **1993** (T49A) 302 (1993) DOI:10.1088/0031-8949/1993/T49A/053
47. Stöhr J et al. *Science* **259** 658 (1993)
48. Eisebitt S et al. *Nature* **432** 885 (2004)
49. Burnett N H et al. *Appl. Phys. Lett.* **31** 172 (1977)
50. McLean E A et al. *Appl. Phys. Lett.* **31** 825 (1977)
51. Carman R L, Benjamin R F, Rhodes C K *Phys. Rev. A* **24** 2649 (1981)
52. Reitze D H et al. *Opt. Lett.* **29** 86 (2004)
53. Kazamias S et al. *Nature Phys.* **6** 927 (2010)
54. Fareed M A et al. *Phys. Rev. Lett.* **121** 023201 (2018)
55. Ganeev R A *Phys. Usp.* **52** 55 (2009); *Usp. Fiz. Nauk* **179** 65 (2009)
56. Ghimire S et al. *Nature Phys.* **7** 138 (2011)
57. Ghimire S, Reis D A *Nature Phys.* **15** 10 (2019)
58. Dromey B et al. *Nature Phys.* **2** 456 (2006)
59. Schweigert I V, Mukamel S *Phys. Rev. Lett.* **99** 163001 (2007)
60. Mitrofanov A V et al. *Opt. Lett.* **40** 2068 (2015)
61. Tate J et al. *Phys. Rev. Lett.* **98** 013901 (2007)
62. Frolov M V, Manakov N L, Starace A F *Phys. Rev. Lett.* **100** 173001 (2008)
63. Frolov M V et al. *Phys. Rev. A* **92** 023409 (2015)
64. Emelina A S, Emelin M Yu, Ryabikin M Yu *Phys. Rev. A* **93** 043802 (2016)
65. Taranukhin V D *Laser Phys.* **10** 330 (2000)
66. Walser M W et al. *Phys. Rev. Lett.* **85** 5082 (2000)

67. Chirilă C C et al. *Phys. Rev. A* **66** 063411 (2002)
68. Emelina A S, Emelin M Yu, Ryabikin M Yu *J. Opt. Soc. Am. B* **32** 2478 (2015)
69. Peng D et al. *Phys. Rev. A* **95** 033413 (2017)
70. Brunel F *J. Opt. Soc. Am. B* **7** 521 (1990)
71. Redkin P V, Kodirov M K, Ganeev R A *J. Opt. Soc. Am. B* **28** 165 (2011)
72. Laryushin I D, Romanov A A, Vvedenskii N V *Opt. Lett.* **50** 2207 (2025)
73. Salières P, L'Huillier A, Lewenstein M *Phys. Rev. Lett.* **74** 3776 (1995)
74. Balcou P et al. *Phys. Rev. A* **55** 3204 (1997)
75. Paul A et al. *Nature* **421** 51 (2003)
76. Willner A et al. *Phys. Rev. Lett.* **107** 175002 (2011)
77. Migal E A, Stremoukhov S Yu, Potemkin F V *Phys. Rev. A* **101** 021401 (2020)
78. Ciriolo A G et al. *J. Phys. Photon.* **2** 024005 (2020)
79. Seres J et al. *Nature Phys.* **3** 878 (2007)
80. Pirri A, Corsi C, Bellini M *Phys. Rev. A* **78** 011801 (2008)
81. Hareli L, Shoulga G, Bahabad A *J. Phys. B* **53** 233001 (2020)
82. Lambert G et al. *Nature Commun.* **6** 6167 (2015)
83. Willems F et al. *Phys. Rev. B* **92** 220405 (2015)
84. Alves C et al. *Phys. Rev. B* **100** 144421 (2019)
85. Antoine P et al. *Phys. Rev. A* **53** 1725 (1996)
86. Weihe F A, Bucksbaum P H *J. Opt. Soc. Am. B* **13** 157 (1996)
87. Shan B, Ghimire S, Chang Z *Phys. Rev. A* **69** 021404 (2004)
88. Zhang G P, George Th F *Phys. Rev. A* **74** 023811 (2006)
89. Liu C et al. *Phys. Rev. A* **97** 063412 (2018)
90. Flettner A et al. *Eur. Phys. J. D* **21** 115 (2002)
91. Möller M et al. *Phys. Rev. A* **86** 011401 (2012)
92. Li Y et al. *Opt. Express* **21** 4896 (2013)
93. Kakehata M et al. *Phys. Rev. A* **55** R861 (1997)
94. Ivanov M Yu, Brabec T, Burnett N *Phys. Rev. A* **54** 742 (1996)
95. Wang B et al. *Phys. Rev. A* **103** 053119 (2021)
96. Fleischer A et al. *Nature Photon.* **8** 543 (2014)
97. Ferré A et al. *Nature Photon.* **9** 93 (2015)
98. Lehmeier H J, Leupacher W, Penzkofer A *Opt. Commun.* **56** 67 (1985)
99. Shaw M J, Hooker C J, Wilson D C *Opt. Commun.* **103** 153 (1993)
100. Lundeen T, Hou S-Y, Nibler J W *J. Chem. Phys.* **79** 6301 (1983)
101. Akhmanov S A, Khokhlov R V *Problemy Nelineinoi Optiki* (*Elektromagnitnye Volny v Nelineinykh Dispergiruyushchikh Sredakh*) *1962–1963* (Problems of Nonlinear Optics (Electromagnetic Waves in Nonlinear Dispersive Media) 1962–1963) (Ser. Results of Science) (Moscow: VINITI AN SSSR, 1964)
102. Boyd R W *Nonlinear Optics* (Oxford: Academic Press, 2008)
103. Azarenkov A N et al. *Quantum Electron.* **23** 633 (1993); *Kvantovaya Electron.* **20** 733 (1993)
104. Dolgaleva K et al. *Phys. Rev. A* **92** 023809 (2015)
105. Tcypkin A et al. *Phys. Rev. Applied* **15** 054009 (2021)
106. Brée C, Demircan A, Steinmeyer G *Phys. Rev. A* **85** 033806 (2012)
107. Shelton D P *Phys. Rev. A* **36** 3032 (1987)
108. Bishop D M, Lam B *Phys. Rev. A* **37** 464 (1988)
109. Spott A, Jaroń-Becker A, Becker A *Phys. Rev. A* **90** 013426 (2014)
110. Becker W, Milošević D B *Laser Phys.* **19** 1621 (2009)
111. Kobe D H *Int. J. Quantum Chem.* **14** (S12) 73 (1978)
112. Han Y-C, Madsen L B *Phys. Rev. A* **81** 063430 (2010)
113. Gamow G *Z. Phys.* **51** 204 (1928)
114. Gurney R W, Condon E U *Nature* **122** 439 (1928)
115. Zener C *Proc. R. Soc. London A* **145** 523 (1934)
116. Keldysh L V *Sov. Phys. JETP* **6** 763 (1958); *Zh. Eksp. Teor. Fiz.* **33** 994 (1957)
117. Kane E O *J. Phys. Chem. Solids* **12** 181 (1960)
118. Bonch-Bruevich A M, Khodovoi V A *Sov. Phys. Usp.* **8** 1 (1965); *Usp. Fiz. Nauk* **85** 5 (1965)
119. Gladun A D, Barashev P P *Sov. Phys. Usp.* **12** 490 (1970); *Usp. Fiz. Nauk* **98** 493 (1969)
120. Keldysh L V *Sov. Phys. JETP* **20** 1307 (1965); *Zh. Eksp. Teor. Fiz.* **47** 1945 (1964); Keldysh L V *Phys. Usp.* **60** 1187 (2017); *Usp. Fiz. Nauk* **187** 1280 (2017)
121. Wolkow D M *Z. Phys.* **94** 250 (1935)
122. Xiong W, Chin S L *Sov. Phys. JETP* **72** 268 (1991); *Zh. Eksp. Teor. Fiz.* **99** 481 (1991)
123. Fittinghoff D N et al. *Phys. Rev. Lett.* **69** 2642 (1992)
124. Moshammer R et al. *Phys. Rev. Lett.* **84** 447 (2000)
125. Mohideen U et al. *Phys. Rev. Lett.* **71** 509 (1993)
126. Nikishov A I, Ritus V I *Sov. Phys. JETP* **23** 168 (1966); *Zh. Eksp. Teor. Fiz.* **50** 255 (1966)
127. Perelomov A M, Popov V S, Terent'ev M V *Sov. Phys. JETP* **23** 924 (1966); *Zh. Eksp. Teor. Fiz.* **50** 1393 (1966)
128. Perelomov A M, Popov V S, Terent'ev M V *Sov. Phys. JETP* **24** 207 (1967); *Zh. Eksp. Teor. Fiz.* **51** 309 (1966)
129. Perelomov A M, Popov V S *Sov. Phys. JETP* **25** 336 (1967); *Zh. Eksp. Teor. Fiz.* **52** 514 (1967)
130. Ammosov M V, Delone N B, Krainov V P *Sov. Phys. JETP* **64** 1191 (1986); *Zh. Eksp. Teor. Fiz.* **91** 2008 (1986)
131. Faisal F H M *J. Phys. B* **6** L89 (1973)
132. Reiss H R *Phys. Rev. A* **22** 1786 (1980)
133. Reiss H R *Prog. Quantum Electron.* **16** 1 (1992)
134. Karnakov B M, Mur V D, Popov V S *JETP Lett.* **88** 423 (2008); *Pis'ma Zh. Eksp. Teor. Fiz.* **88** 495 (2008); Karnakov B M et al. *Phys. Usp.* **58** 3 (2015); *Usp. Fiz. Nauk* **185** 3 (2015)
135. Gladkov S M, Koroteev N I *Sov. Phys. Usp.* **33** 554 (1990); *Usp. Fiz. Nauk* **160** (7) 105 (1990)
136. Strelkov S M et al. *Phys. Usp.* **59** 425 (2016); *Usp. Fiz. Nauk* **186** 449 (2016); Ryabikin M Yu, Emelin M Yu, Strelkov V V *Phys. Usp.* **66** 360 (2023); *Usp. Fiz. Nauk* **193** 382 (2023)
137. Lewenstein M et al. *Phys. Rev. A* **49** 2117 (1994)
138. Lewenstein M, Salières P, L'Huillier A *Phys. Rev. A* **52** 4747 (1995)
139. Gaarde M B et al. *Phys. Rev. A* **59** 1367 (1999)
140. Khokhlova M A, Strelkov V V *Phys. Rev. A* **93** 043416 (2016)
141. Becker W, Long S, McIver J K *Phys. Rev. A* **50** 1540 (1994)
142. Becker W et al. *Phys. Rev. A* **56** 645 (1997)
143. Strelkov V V *Phys. Rev. A* **74** 013405 (2006)
144. Salières P et al. *Science* **292** 902 (2001)
145. Strelkov V *Phys. Rev. Lett.* **104** 123901 (2010)
146. Kulander K C *Phys. Rev. A* **35** 445 (1987)
147. Kulander K C, Schafer K J, Krause J L *Phys. Rev. Lett.* **66** 2601 (1991)
148. Im K, Grobe R, Eberly J H *Phys. Rev. A* **49** 2853 (1994)
149. Gajda M, Piraux B, Rzażewski K *Phys. Rev. A* **50** 2528 (1994)
150. Telnov D A, Chu S-I *Phys. Rev. A* **71** 013408 (2005)
151. Le A-T et al. *J. Phys. B* **41** 081002 (2008)
152. Lagmago Kamta G, Bandrauk A D *Phys. Rev. A* **71** 053407 (2005)
153. Ivanov I A, Kheifets A S *Phys. Rev. A* **79** 053827 (2009)
154. He F, Ruiz C, Becker A *Phys. Rev. A* **75** 053407 (2007)
155. Clementi E, Roetti C *At. Data Nucl. Data Tables* **14** 177 (1974)
156. Bachau H et al. *Rep. Prog. Phys.* **64** 1815 (2001)
157. Cormier E, Lambropoulos P *J. Phys. B* **30** 77 (1997)
158. Chen S et al. *Phys. Rev. A* **86** 013410 (2012)
159. Javanainen J, Eberly J H, Su Q *Phys. Rev. A* **38** 3430 (1988)
160. Volkova E A et al. *J. Exp. Theor. Phys.* **102** 40 (2006); *Zh. Eksp. Teor. Fiz.* **129** 48 (2006)
161. Volkova E A, Popov A M, Tikhonova O V *J. Exp. Theor. Phys.* **86** 328 (1998); *Zh. Eksp. Teor. Fiz.* **113** 593 (1998)
162. Andreev A V, Stremoukhov S Yu, Shoutova O A *Eur. Phys. J. D* **66** 16 (2012)
163. Ganeev R A et al. *Eur. Phys. J. D* **74** 199 (2020)
164. Andreev A V, Stremoukhov S Yu *Phys. Rev. A* **87** 053416 (2013)
165. Stremoukhov S et al. *Phys. Rev. A* **94** 013855 (2016)
166. Stremoukhov S *J. Opt. Soc. Am. B* **39** 1203 (2022)
167. Landau L D, Lifshitz E M *Kvantovaya Mekhanika*: *Nerelyativistskaya Teoriya* (Moscow: Fizmatlit, 2002); Translated into English: *Quantum Mechanics. Non-Relativistic Theory* (Oxford: Pergamon Press, 1991)
168. Moore C E, Merrill P W *Partial Grotrian Diagrams of Astrophysical Interest* (Washington, DC: National Bureau of Standards, 1968)
169. Bethe H A, Salpeter E E *Quantum Mechanics of One- and Two-Electron Atoms* (Berlin: Academic Press, 1957) DOI:10.1007/978-3-662-12869-5
170. Andreev A V et al. *Eur. Phys. J. D* **67** 22 (2013)
171. Andreev A V, Stremoukhov S Y, Shoutova O A *J. Opt. Soc. of Am. B* **30** 1794 (2013)
172. Shafir D et al. *New J. Phys.* **12** 073032 (2010)
173. Popmintchev T et al. *Proc. Natl. Acad. Sci. USA* **106** 10516 (2009)
174. Stremoukhov S Yu, Yakovlev A A, Andreev A V *Laser Phys. Lett.* **17** 085405 (2020)

175. Mahieu B et al. *Phys. Rev. A* **97** 043857 (2018)
176. Andreev A V, Stremoukhov S Yu, Shutova O A *Opt. Spectrosc.* **112** 410 (2012); *Opt. Spektrosk.* **112** 454 (2012)
177. Stremoukhov S Yu, Andreev A V *Laser Phys.* **28** 035403 (2018)
178. Kolesik M, Moloney J V *Rep. Prog. Phys.* **77** 016401 (2014)
179. Börzsönyi Á et al. *Opt. Express* **18** 25847 (2010)
180. RefractiveIndex.INFO website, https://refractiveindex.info/
181. Lambert G et al. *Sci. Rep.* **5** 7786 (2015)
182. Ganeev R A et al. *Phys. Rev. A* **83** 063837 (2011)
183. Catoire F et al. *Phys. Rev. A* **94** 063401 (2016)
184. Carlström S et al. *New J. Phys.* **18** 123032 (2016)
185. Zaïr A et al. *Phys Rev. Lett.* **100** 143902 (2008)
186. Takahashi E et al. *J. Opt. Soc. Am. B* **20** 158 (2003)
187. Ganeev R A *J. Phys. B* **49** 095402 (2016)
188. Ganeev R A, Suzuki M, Kuroda H *Phys. Rev. A* **89** 033821 (2014)
189. Ganeev R A et al. *Appl. Sci.* **9** 1701 (2019)
190. Stremoukhov S *Atoms* **11** (7) 103 (2023)
191. Rumyantsev B V et al. *JETP Lett.* **115** 390 (2022); *Pis'ma Zh. Eksp. Teor. Fiz.* **115** 431 (2022)
192. Riedel D et al. *Rev. Sci. Instrum.* **72** 1977 (2001)
193. Popmintchev T et al. *Science* **336** 1287 (2012)
194. Stremoukhov S Yu *JETP Lett.* **121** 16 (2025); *Pis'ma Zh. Eksp. Teor. Fiz.* **121** 18 (2025)
195. Lvov K, Stremoukhov S *Opt. Lett.* **50** 3740 (2025)
196. Stremoukhov S Y, Ganeev R A, Andreev A V, in *X-Ray Lasers 2018. ICXRL 2018, Proc. of the 16th Intern. Conf. on X-Ray Lasers* (Springer Proc. in Physics, Vol. 241, Eds M Kozlová, J Nejdl) (Cham: Springer, 2020) p. 99, DOI:10.1007/978-3-030-35453-4_15
197. Stremoukhov S, Ganeev R, Andreev A *Eur. Phys. J. Web Conf.* **220** 01013 (2019)
198. Zhvaniya I A et al. *J. Phys. Conf. Ser.* **1692** 012017 (2020)
199. Andreev A V et al. *IEEE Trans. Terahertz Sci. Technol.* **10** 85 (2020)
200. Lambert G *Nature Phys.* **4** 296 (2008)